

ASSESSMENT OF CURRENT ACI 440.2R-08 DESIGN GUIDELINES
AND EVALUATION OF HOOP STRAIN IN
FRP CONFINED CONCRETE

by

Ana Daniela Ugartechea García, B.S.

A thesis submitted to the Graduate Council of
Texas State University in partial fulfillment
of the requirements for the degree of
Master of Science
with a Major in Technology
August 2014

Committee Members:

Kimberly G. Talley, Chair

Yoo-Jae Kim

Oswaldo Muñiz Solari

COPYRIGHT

by

Ana Daniela Ugartechea García

2014

FAIR USE AND AUTHOR'S PERMISSION STATEMENT

Fair Use

This work is protected by the Copyright Laws of the United States (Public Law 94-553, section 107). Consistent with fair use as defined in the Copyright Laws, brief quotations from this material are allowed with proper acknowledgment. Use of this material for financial gain without the author's express written permission is not allowed.

Duplication Permission

As the copyright holder of this work I, Ana Daniela Ugartechea García, refuse permission to copy in excess of the "Fair Use" exemption without my written permission.

DEDICATION

To my Mom and Dad.

For their endless love, support and encouragement

ACKNOWLEDGEMENTS

I would like to express my deepest appreciation to my advisor Dr. Kimberly Talley, for the continuous support on my Master's degree and research, for her patience, motivation, enthusiasm, and knowledge. Her guidance helped me in all the time of the research and writing of this thesis. I could not have imagined having a better advisor and mentor.

I would like to thank the rest of my committee, Dr. Yoo-Jae Kim and Dr. Osvaldo Muniz Solari, for their comments and questions which were very beneficial in the completion of my thesis. In addition, a big thank you to Dr. Austin Talley for his countless hours helping me program the NI DAQ.

Especially I would like to thank Andres Alvarez, who as a good friend, was always willing to help me and give his best suggestions. It would not have been possible to do this research without him. I would also like to give particular thanks to Juanito de Leon, Ben Orsak, Juan Gomez and Justin Dickey for their help in my project.

Technical assistance provided by Shane Arabie and Marcus Ickes is greatly acknowledge. Thanks to the Composites and Plastic Laboratory at Texas State University for donating the GFRP. I would also like to thank the administrative staff, Carla Collins and Sylvia Salinas.

Last but not least, I would like to thank my family. Mami and Papi thanks for giving me the strength and support to chase my dreams. Euge, Moni, Rebeca, Mama and Papa (who I know is up there watching me) deserve my wholehearted thanks as well.

TABLE OF CONTENTS

	Page
ACKNOWLEDGEMENTS.....	v
LIST OF TABLES.....	ix
LIST OF FIGURES.....	x
ABSTRACT.....	xiii
CHAPTER	
1 INTRODUCTION.....	1
1.1 Background.....	1
1.2 Research Motivations.....	3
1.3 Objectives and Scope.....	4
1.4 Limitations.....	4
1.5 Organization.....	5
2 LITERATURE REVIEW.....	6
2.1 Confined Concrete.....	6
2.2 ACI 440.2R-08 Design Guidelines.....	9
2.3 Previous Research on FRP-Confined Concrete.....	11
2.3.1 Lam and Teng 2003.....	11
2.3.2 Lam and Teng 2009.....	12
2.3.3 Realfonzo and Napoli 2011.....	13
2.3.4 Ozbakkaloglu and Lim 2013.....	13
2.3.5 Hoop Strain in FRP Confined Concrete.....	14
2.4 Summary.....	15
3 METHODOLOGY OF ACI 440.2R-08 DESIGN GUIDELINE EVALUATION...	16
3.1 Introduction.....	16
3.2 Database Development.....	16
3.3 Design Guidelines.....	17
3.4 Comparison of Test Results to Design Guideline Predictions.....	18
3.4.1 Maximum Confined Concrete Compressive Strength, f'_{cc}	18
3.4.2 Maximum Confinement Pressure, fl	19

3.5 Recommendation Development.....	22
4 EXPERIMENTAL PROGRAM OF FRP-CONFINED CONCRETE CYLINDERS	23
4.1 Introduction	23
4.2 Material Properties of Concrete and FRP Composites	23
4.2.1 Concrete	23
4.2.2 FRP Composites.....	24
4.3 FRP Wrapping Schemes	25
4.4 Test Specimens.....	26
4.5 Procedure for Wrapping GFRP-Confined Concrete Cylinders.....	27
4.6 FRP-Confined Concrete Cylinder Test	33
5 DISCUSSION OF RESULTS ACI 440.2R-08 DESIGN GUIDELINE EVALUATION.....	36
5.1 Introduction	36
5.2 GFRP-Confined Concrete	36
5.2.1 Evaluation of Current Design Recommendations for f'_{cc}	36
5.2.2 Evaluation of the Maximum Confinement Pressure.....	37
5.2.3 Development of Revised Equation	40
5.2.4 Verification of Revised Equation.....	41
5.3 CFRP-Confined Concrete	44
5.3.1 Evaluation of Current Design Recommendations for f'_{cc}	44
5.3.2 Evaluation of the Maximum Confinement Pressure.....	46
5.3.3 Development of Revised Equation	48
5.3.4 Verification of Revised Equation.....	50
5.4 Summary of Results	52
6 DISCUSSION OF RESULTS FRP-CONFINED CONCRETE CYLINDERS.....	53
6.1 Introduction	53
6.2 GFRP-Confined Concrete Cylinders with One Layer	54
6.2.1 One layer GFRP Bidirectional	54
6.2.2 One layer GFRP Multidirectional.....	55
6.2.3 Summary of GFRP-Confined Concrete Cylinder with One Layer.....	56
6.3 GFRP-Confined Concrete Cylinders with Two Layers	57
6.3.1 Two layer GFRP Bidirectional	57
6.3.2 Two layer GFRP Multidirectional	64
6.3.3 Summary of GFRP-Confined Concrete Cylinders with Two Layers	76
6.4 GFRP-Confined Concrete Cylinders with Three Layers	76

6.4.1 Three layer GFRP Bidirectional	77
6.4.2 Three layer GFRP Multidirectional	83
6.4.3 Summary of GFRP-Confined Concrete Cylinders with Three Layers	93
6.5 Summary of FRP-Confined Concrete Cylinder Results	94
7 CONCLUSIONS AND RECOMMENDATIONS.....	96
7.1 Summary of Research	96
7.1.1 Evaluation of ACI Design Guidelines	96
7.1.2 Evaluation of FRP-Confined Concrete Cylinders.....	98
7.2 Conclusions	99
7.3 Recommendations for Future Work.....	100
REFERENCES	102

LIST OF TABLES

Table	Page
4.1 Properties of bidirectional fiber	24
4.2 Properties of multidirectional fiber	25
4.3 Epoxy-Resin Mechanical Properties (635 Thin Epoxy Resin)*	25
4.4 Details of Test Specimens.....	27
5.1 New factors and percent conservative values	43
5.2 Modified reduction factors and percent conservative values.....	44
5.3 New factors and percent conservative values	49
5.4 Modified reduction factors and percent conservative values.....	49
6.1 Compressive test results.....	54

LIST OF FIGURES

Figure	Page
2.1 Axial stress-strain curve for FRP-confined concrete (Lam and Teng, 2003).....	7
2.2 Definition of ductility factor (Cui, 2009).....	8
2.3 Normalized axial stress-strain behavior of confined concrete (Spoelstra and Monti, 1999).....	9
3.1 Measured f'_{cc} versus predicted f'_{cc} for GFRP-confined specimens using current design guidelines.....	19
3.2 Measured fl versus predicted fl for GFRP-confined specimens using current design guidelines.....	20
3.3 Measured fl unfactorized versus predicted fl for GFRP-confined specimens using current design guidelines.....	21
3.4 Measured fl versus predicted fl for GFRP-confined specimens using current design guidelines.....	22
4.1 Glass fibers.....	24
4.2 Typical GFRP-confined concrete cylinder schemes.....	26
4.3 Preparation of epoxy resin.....	28
4.4 Saturation of GFRP sheet with the epoxy resin.....	28
4.5 Wrapping cylinder with one GFRP layer.....	29
4.6 Cylinder with one GFRP layer and strain gages.....	30
4.7 Application of strain gage with petroleum jelly and wax paper.....	31
4.8 Cylinder with two GFRP layers and strain gages on the first layer.....	32
4.9 Cylinder with three GFRP layers and respective strain gages.....	33
4.10 Typical GFRP-confined concrete cylinder test setup.....	34

4.11 NI cDAQ-9174 with two modules (NI 9219 and NI 9235).....	35
5.1 Measured f'_{cc} versus predicted f'_{cc} for GFRP-confined specimens using current design guidelines	37
5.2 Measured f_l versus predicted f_l for GFRP-confined specimens using current design guidelines	38
5.3 Measured f_l versus predicted f_l for GFRP-confined specimens using current design guidelines	39
5.4 Measured f_l unfactorized versus predicted f_l for GFRP-confined specimens using current design guidelines	40
5.5 Measured f'_{cc} versus new predicted f'_{cc} for GFRP-confined specimens using revised Equation	41
5.6 Measured f'_{cc} versus predicted f'_{cc} for CFRP-confined specimens using current design guidelines	45
5.7 Measured f_l versus predicted f_l for CFRP-confined specimens using current design guidelines	46
5.8 Measured f_l versus predicted f_l for CFRP-confined specimens using current design guidelines	48
5.9 Measured f'_{cc} versus new predicted f'_{cc} for CFRP-confined specimens using revised Equation	50
5.10 Measured f_l unfactorized versus predicted f_l for GFRP-confined specimens using current design guidelines	51
6.1 Axial Stress versus hoop strain for specimen B2C3L1M.....	55
6.2 B2C3L1M failure mode.....	56
6.3 Axial Stress versus hoop strain for specimen B1C2L2B.....	57
6.4 Axial Stress versus hoop strain for specimen B1C2L2B separated by location.....	59
6.5 B1C2L2B failure mode.....	61
6.6 Axial Stress versus hoop strain for specimen B1C3L2B.....	62

6.7 Axial Stress versus hoop strain for specimen B1C3L2B separated by location.....	63
6.8 Axial Stress versus hoop strain for specimen B2C1L2M.....	65
6.9 B2C1L2M failure mode.....	66
6.10 Axial Stress versus hoop strain for specimen B2C1L2M separated by location.....	67
6.11 Axial Stress versus hoop strain for specimen B2C2L2M.....	69
6.12 B2C2L2M failure mode.....	69
6.13 Axial Stress versus hoop strain for specimen B2C2L2M separated by location.....	71
6.14 Axial Stress versus hoop strain for specimen B2C3L2M.....	73
6.15 B2C3L2M failure mode.....	73
6.16 Axial Stress versus hoop strain for specimen B2C3L2M separated by location.....	74
6.17 Axial Stress versus hoop strain for specimen B1C1L3B.....	77
6.18 Axial Stress versus hoop strain for specimen B1C1L3B separated by location.....	79
6.19 Axial Stress versus hoop strain for specimen B1C3L3B.....	81
6.20 Axial Stress versus hoop strain for specimen B1C3L3B separated by location.....	82
6.21 Axial Stress versus hoop strain for specimen B2C1L3M.....	84
6.22 Axial Stress versus hoop strain for specimen B2C1L3M separated by location.....	85
6.23 Axial Stress versus hoop strain for specimen B2C2L3M.....	87
6.24 Axial Stress versus hoop strain for specimen B2C2L3M separated by location.....	88
6.25 Axial Stress versus hoop strain for specimen B1C3L2B.....	90
6.26 Axial Stress versus hoop strain for specimen B1C3L2B separated by location.....	91

ABSTRACT

Strengthening concrete structures with fiber reinforced polymers (FRP) is becoming increasingly common in construction practice. The currently available design guideline for FRP confined concrete is the ACI 440.2R-08 model for predicting the maximum confined compressive strength. These formulas are based on a modest test dataset of carbon fiber reinforced polymers (CFRP) and a small test dataset of glass fiber reinforced polymers (GFRP) wrapped specimens. This investigation reviewed a meta-analysis of published testing data from CFRP and GFRP-wrapped plain concrete specimens to evaluate the performance of the design guidelines. The results from 694 compression tests are compared to the predicted maximum confined compressive strength following the ACI 440.2R-08 design formulas. The investigation showed that for CFRP-wrapped plain concrete specimens the design formulas work reasonably well, 82% of the values are conservative. However for the GFRP-wrapped specimens, it was found that one third of the tested specimens had capacities that were less than the design guidelines' prediction. Therefore the current design formula is unconservative for the design of GFRP-wrapped specimens. In order to suggest a conservative design formula, a variation of the existing formula for calculating the confined compressive strength of a GFRP-wrapped specimen is presented. Also, a variation was made for CFRP-confined concrete specimens to make the formula more conservative. Additionally, an investigation of the transfer of strain between FRP layers in FRP confined concrete specimens was completed. Glass fibers were applied to plain concrete specimens, with the number of

layers ranging from one to three layers. Strain gages were placed on every layer to perform an analysis of the hoop strains under load. The results showed that the different layers of a GFRP wrap on a specimen do not receive the same amount of strain for the same axial compressive load on the cylinder. This inequality could be a possible explanation for why FRP jackets do not achieve the same tensile strength as the results from tensile coupon tests.

CHAPTER 1

INTRODUCTION

1.1 Background

Since their introduction in the 1970s, fiber reinforced polymers (FRP) composites have become an important part of civil engineering structures either to repair/retrofit old structures or as part of a new building (Hollaway, 2010). Throughout the following forty years, a great amount of investigation was conducted on the behavior of FRP-wrapped concrete columns, and it has been proven numerous times that FRP is an effective strengthening material for concrete members (Nanni & Bradford, 1995; Xiao & Wu, 2000; Berthet, Ferrier, & Hamelin, 2005).

ACI 440.2R-08 serves as the current guideline for designing externally bonded FRP systems for strengthening concrete structures. Its model for determining the maximum confined concrete compressive strength is based on the model developed by Lam and Teng (2003) with the inclusion of a reduction factor (ACI, 2014). When Lam and Teng (2003) developed this model the database available at the time was small. Seventy-six total specimens were considered and only nine of them were glass fiber reinforced polymers (GFRP) confined specimens versus sixty-seven carbon fiber reinforced polymers (CFRP) confined specimens. At the time, the authors suggested that more tests of GFRP specimens should be added to verify the model (Lam & Teng, 2003). A few years later Teng et al. (2009) refined their model by focusing on the hoop tensile strain reached at failure of the FRP system while using a different database than in 2003. This database included forty-eight total specimens with eighteen of those being GFRP-confined specimens and the balance CFRP-confined specimens (Teng, Jiang, Lam, &

Luo, 2009). This 2009 database, however, was still small compared to all the currently existing data.

In 2011, Realfonzo and Napoli (2011) created a large database of FRP-wrapped concrete cylinders to evaluate the FRP strain efficiency factor and to estimate the confined compressive strength. As well, Ozbakkaloglu and Lim (2013) presented an extensive database in 2013 that covered the majority of the studies that have been published to date: 832 test results from 99 experimental studies. Of these test results, 167 were for GFRP-confined specimens and 476 for CFRP-confined specimens. These databases, along with the addition of other test results provided 204 GFRP and 490 CFRP-confined test specimens used by the author to assess the current FRP design guidelines for both GFRP and CFRP confined plain concrete (Karbhari & Gao, 1997; Karbhari & Howie, 1997; Harries, Kestner, Pessiki, Sause, & Ricles, 1998; Toutanji & Balaguru, 1998; Arduini, Di Tommaso, Manfroni, Ferrari, & Romagnolo, 1999; Toutanji, 1999; Karbhari, Rivera, & Dutta, 2000; Karbhari, 2002; Harries & Kharel, 2003; Faella, Realfonzo, & Salerno, 2004; Lin & Liao, 2004; Modarelli, Micelli, & Manni, 2005; Li, 2006; Wu, Wu, Lu, & Ando, 2006; Sadeguiyan, Shekari, & Mousavi, 2008; Ramezaniyanpour & Gharachorlou, 2009; Chastre & Silva, 2010; Gharachorlou & Ramezaniyanpour, 2010; Bouchelaghem, Bezazi & Scarpa, 2011; Ozbakkaloglu & Akin, 2012; Micelli & Modarelli, 2013).

The ultimate strain is an important part of the ACI 440.2R-08 design formula to predict the ultimate compressive strength of FRP confined concrete. As mentioned earlier, while some investigation has been conducted to evaluate the strain efficiency factor, there is still more research needed in this area. Therefore, this thesis also includes

a preliminary evaluation of how the FRP wrap shared strain among its different number of layers. Further, there is currently no research that evaluates how strain is shared between FRP layers, which could beneficially contribute to the understanding of the FRP confined concrete system and lead to a better design formula.

1.2 Research Motivations

The currently design guidelines were originally based on a small group of GFRP- and CFRP-confined concrete test results. An evaluation of the existing design guidelines for determining the maximum confined concrete compressive strength has never been attempted with a large database. Therefore, by using a large database of test results to evaluate the current design guidelines this thesis contributes to enhanced design safety.

There is considerable variation in the test results that evaluate the strain efficiency factor, which has been attributed to the different procedures used to test the specimens or to placement of the strain gauges of the FRP's overlapping zone. This research project also investigated the interaction of strain between FRP layers to increase the understanding of the FRP confined concrete systems and potentially identify the source of some test result variation.

In summary, an assessment of the performance of the current design guidelines for determining the maximum confined concrete compressive strength with a large and comprehensive database was needed in order to verify the safety and conservativeness of the current design guidelines for this type of system. It was also an important contribution to the field of knowledge to evaluate the hoop strain between layers in FRP-confined concrete systems in order to better understand a cause of variation in specimen

performance. This understanding may lead to a more accurate strain efficiency factor and help future researchers in developing an improved design model for FRP-confined concrete.

1.3 Objectives and Scope

The objectives of this research are as follows:

1. Evaluate the safety of the current ACI 440.2R-08 design guidelines for predicting the maximum confined concrete compressive strength by comparing the guidelines' predictions to an extensive database for GFRP- and CFRP-confined concrete cylinder specimens test results and suggest refinements as needed.
2. Understand a cause of variation in FRP-confined concrete test results by looking at how the layers of FRP share or transfer hoop strain.

1.4 Limitations

For the ACI 440.2R-08 design evaluation the database only included specimens that had diameters ranging from 1.85 in to 16 in (47mm to 406.4mm) and unconfined concrete strengths ranging from 0.90 ksi to 25 ksi (6.2 Mpa to 169.79 Mpa). Only plain concrete cylinders that had a minimum confinement ratio of 0.08 and aspect ratios from two to five were used. Additionally, only specimens with glass or carbon fibers wrapped in the hoop direction were considered; the number of GFRP layers ranged from one to fifteen layers and for CFRP it ranged from one to twelve layers.

For the hoop strain share between FRP layers, only GFRP-confined concrete specimens were considered. The design unconfined concrete strength was of 4000 psi.

Only two types of GFRP were used: bidirectional or multidirectional. The study focused on the share of strain between GFRP layers, thus an analysis of the strain efficiency factor was not provided. The number of GFRP layers ranged from one to three layers and for each type of GFRP arrangement only three specimens were tested. Additionally, only three strain gages were provided for each GFRP layer.

1.5 Organization

Chapter 2 discusses the literature review of both current ACI 440.2R-08 design guidelines and previous studies of hoop strain in FRP-confined concrete. Chapter 3 describes the procedure for evaluating the safety of the current ACI 440.2R-08 design guidelines and Chapter 4 covers the experimental program procedure carried out on GFRP-confined concrete cylinders to evaluate the hoop strain. An analysis and discussion of the design guideline investigation and FRP-confined cylinders test results are given in Chapter 5 and Chapter 6, respectively. Finally, Chapter 7 provides a summary of this study, including major conclusions and recommendations for future study.

CHAPTER 2

LITERATURE REVIEW

2.1 Confined Concrete

Fiber reinforced polymer (FRP) composites are generally made of carbon, glass or aramid fibers embedded in a resin matrix made of epoxy, polyester or vinylester resins. In 1999, the construction sector was the world's largest consumer of polymer composites representing 35% of the global market (Weaver, 1999). Recently, FRPs have been increasingly used for structural load bearing applications especially for rehabilitation and retrofit of existing civil structures and, to a lesser extent, in new civil structures e.g. as a replacement for steel in reinforced concrete (ACI, 2014).

In the area of rehabilitation and retrofit of existing civil structures, the traditionally used methods included concrete jackets or external steel sheets designed to improve structural properties such as strength and ductility (Julio, Branco, & Silva, 2003; Moghaddam & Samadi, 2009). In the last decade, FRP jackets have been successfully used for retrofitting concrete columns (Saadatmanesh, Ehsani, & Li, 1994). In the case of FRP-confined concrete, the FRP is bonded externally to the structure in the form of laminates or sheets (ACI, 2014).

FRP jackets on concrete columns provide passive confinement. Therefore, the system activates only when the lateral expansion of the concrete is resisted by the confining FRP jacket. The confining pressure provided by the FRP jacket depends highly on the relationship between the axial stress applied to the composite system and the subsequently induced lateral strain in the FRP jacket. As the hoop strain increases under load, the passive confining stress also keeps increasing with the expansion of concrete

due to the linear elastic properties of the FRP. As shown in Figure 2.1, while the composite system is acting in the linear elastic region of the stress-strain curve, the confining effect is small since the lateral expansion is small. However, once the system is in the plastic portion of the stress-strain curve (Figure 2.1), the stress-strain response is dominated by the behavior of the confining jacket that resists the lateral expansion establishing a multi-axial state of stress in the core concrete. The FRP jacket behaves linearly elastic up to the final failure and exerts a growing confining pressure on the concrete core. Lam and Teng (2003) believed that the best way to describe the bilinear stress-strain curve of FRP-confined concrete was to use a modified parabola for the elastic behavior and a straight line for the plastic behavior.

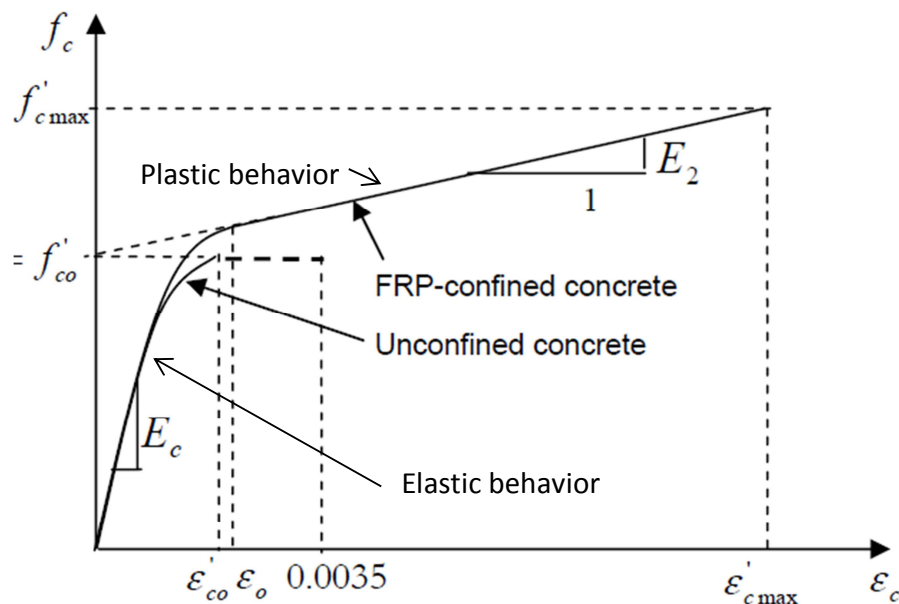


Figure 2.1 Axial stress-strain curve for FRP-confined concrete

(Lam and Teng, 2003)

The passive confinement of the FRP jacket results in a considerably increased strength and ductility of concrete when loaded axially. Ductility is very important in the design of concrete structures, as defined by Gunes, Lau, Tuakta and Büyüköztürk (2013)

is “the ability to undergo inelastic deformation before failure” (p. 916). An increase in ductility reduces the dynamic load demand and makes it possible to design safe economic structures for seismic areas. This increase in ductility of FRP-confined concrete is obtained due to the large deformations that the FRP jacket can undertake, resulting in high hoop strain values corresponding to the rupture of the FRP jacket and to the maximum confined concrete stress (Cui and Sheikh, 2010). This phenomenon is illustrated on Figure 2.2 corresponding to the ductility factor expression:

$$\mu_{cu} = \varepsilon_{cu} / \varepsilon_1 \quad \text{Equation 2.1}$$

where

ε_{cu} = hoop strain corresponding to rupture of FRP jacket

ε_1 = hoop strain corresponding to the maximum confined concrete stress on the initial tangent E_t

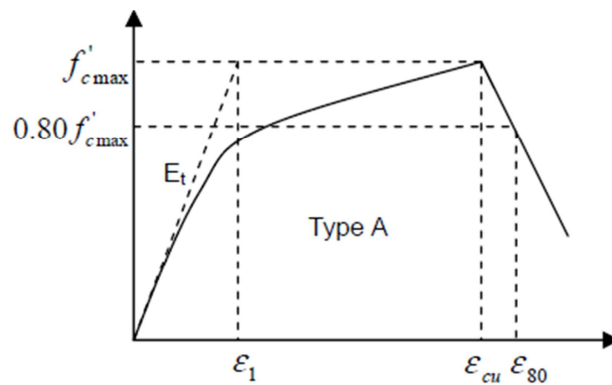


Figure 2.2 Definition of ductility factor

(Cui, 2009)

The qualitative difference between steel, GFRP and CFRP confinement is illustrated in Figure 2.3. This illustration is of stress-strain curves for the same confinement ratio using these three materials. Steel-confined concrete normally experiences a constant lateral confining pressure before it reaches a maximum stress,

after which, it follows the yielding of steel and a gradual post-peak descending branch. To contrast, CFRP- and GFRP-confined concrete displays a distinct bilinear response with a sharp softening and a transition zone at the level of its unconfined concrete strength. The confining pressure always increases with the lateral strain of concrete because FRP does not yield as steel does. Therefore, the stiffness of FRP confined specimens stabilize at a constant value until reaching the ultimate strength. This plastic stiffness is significantly affected by the concrete and FRP properties due to the passive nature of FRP-confined concrete system. By increasing the number of FRP layers or the FRP's modulus of elasticity, the system's plastic stiffness increases which is graphically represented by a steeper slope on the stress-strain curve.

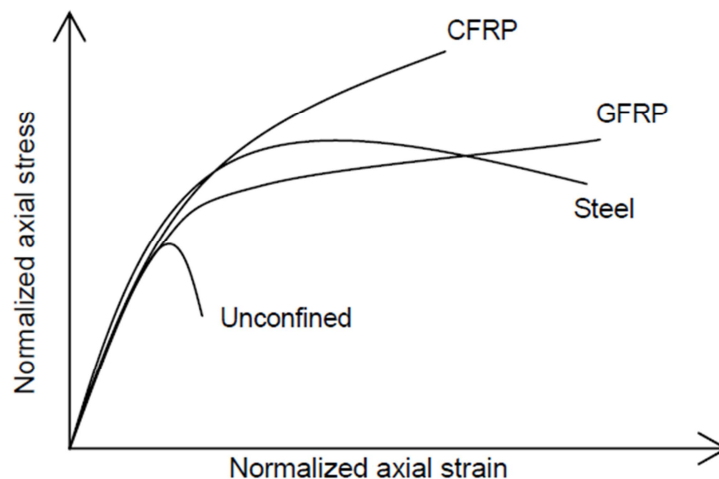


Figure 2.3 Normalized axial stress-strain behavior of confined concrete
(Spoelstra and Monti, 1999)

2.2 ACI 440.2R-08 Design Guidelines

The American Concrete Institute (ACI) is a technical society that is the internationally recognized authority on concrete technology. The ACI's most widely

known publication is ACI 318-11: Building Code Requirements for Structural Concrete, a widely adopted model code for concrete design (ACI, 2013).

ACI 440.2R-08 is ACI's current guideline for designing externally bonded FRP systems for strengthening concrete structures (ACI, 2013). Its model for determining the maximum confined concrete compressive strength, f'_{cc} , is based on the design-oriented stress-strain model for FRP-confined concrete developed by Lam and Teng (2003) with the inclusion of a reduction factor. When Lam and Teng developed this model the available database was small and only seventy-six total specimens of GFRP- and CFRP-confined specimens were considered. Of those seventy-six specimens, only nine GFRP-confined specimens were used and the balance were CFRP-confined specimens. Lam and Teng (2003) suggested that more test data of GFRP specimens should be added to verify the design guidelines.

The formulas for the maximum confined concrete compressive strength, f'_{cc} , and the maximum confinement pressure, f_l , defined by the ACI 440.2R-08 (2013) are:

$$f'_{cc} = f'_c + \psi_f 3.3 \kappa_a f_l \quad \text{Equation 2.2}$$

$$f_l = \frac{2E_f n t_f \varepsilon_{fe}}{D} \quad \text{Equation 2.3}$$

where:

ψ_f = reduction factor of 0.95

κ_a = efficiency factor depending on the geometry of the section: for circular sections κ_a is 1.0

E_f = tensile modulus of elasticity of FRP, MPa (psi)

n = number of plies of FRP reinforcement

t_f = nominal thickness of one ply of FRP reinforcement, mm (in.)

D = diameter of concrete cylinder, mm (in.)

In Eq. (2) the effective strain level in the FRP at failure ε_{fe} is defined as

$$\varepsilon_{fe} = \kappa_{\varepsilon} \varepsilon_{fu} \quad \text{Equation 2.4}$$

where κ_{ε} is the strain efficiency factor due to the premature failure of the FRP jacket and ε_{fu} the design rupture strain of the FRP reinforcement, mm/mm (in./in.). As directed by the ACI 440.2R-08 (2008) design guidelines, the κ_{ε} was taken as 0.55.

2.3 Previous Research on FRP-Confined Concrete

As Lam and Teng's paper that established the design guidelines explicitly called for more research to evaluate the accuracy of the formulas, the author sought out the existing literature examining FRP-confined compressive strength design formulas, ultimate axial strain, hoop strain and stress-strain models. The subsequent papers in this section looked at various aspects of FRP behavior, even some of them proposed new predictive models for FRP-confined concrete or re-calibrated the existing models but did not evaluate the safety of the current ACI 440.2R-08 design guidelines. Each paper that published useable FRP-confined specimen test results is discussed.

2.3.1 *Lam and Teng 2003*

In 2003, Lam and Teng develop a design-oriented stress-strain model that is now used in the current ACI 440.2R-08. The FRP-confined concrete cylinders that were used for developing this model had the FRP fibers wrap mainly in the hoop direction. As stated by Lam and Teng, the model captured all the important characteristics of FRP-confined concrete including the hoop strains, the ultimate axial strain, and the amount of FRP

needed for compressive strength increase. Previous models assumed that the hoop rupture strain occurred when the FRP jacket reached the tensile strength from coupon tests. However that is not what happens, as failure usually occurs at a lower value. Therefore this model was corrected based on the actual hoop rupture strain. They also indicated that the confinement ratio (f_t/f'_c) of FRP-confined concrete needs to be at least 0.07 to be sufficiently confined. If not, the FRP-confined concrete did not achieve compressive strengths considerably above the unconfined concrete strength. Lam and Teng suggested that their model could be used directly in design. They also suggested that there was room for improvement using a larger database. This model only used normal strength concrete cylinders and it may not be appropriate for high strength concrete (Lam & Teng, 2003). As such, this study looked at Lam and Teng's design formula with a large database.

2.3.2 Lam and Teng 2009

In 2009, Teng et al. (2009) refined their first model while focusing on the hoop tensile strain reached at failure of the FRP system. At that time, the researchers used a different database than the one they used in 2003 but it was still small; with only forty-eight specimens. They presented two modified versions of their original model. The first updated the ultimate axial strain and compressive strength Equations, and the second one focused on the stress-strain curves with a descending branch. The first refinement had a design-oriented approach and the second one an analysis-oriented approach. They made an important observation regarding measurements hoop strain specifically that hoop strain readings in the overlapping zone are lower than those measure somewhere else in

the specimen and should be excluded. They also concluded that their 2003 model overestimated the ultimate strain of concrete confined with a large amount of FRP and the compressive strength of concrete confined with a small amount of FRP (not sufficiently confined, below the 0.07 confinement ratio).

2.3.3 Realfonzo and Napoli 2011

In 2011, Realfonzo assembled a large database of 465 FRP-wrapped concrete cylinders to evaluate the FRP strain efficiency factor and to estimate the confined compressive strength. They focused on data that had an unconfined concrete strength equal or below 5800 psi (40 MPa). Additionally, they proposed a new design strength model for FRP-confined concrete but still trying to model the average behavior. They did not evaluate the efficacy of the current design guidelines, their new model fit the average behavior of FRP confined specimens but it did not predict a lower bound to the data.

2.3.4 Ozbakkaloglu and Lim 2013

Ozbakkaloglu and Lim (2013) presented an extensive database that covers the majority of the studies that have been published to the present: 3042 test results from 253 experimental studies. They developed a new design-oriented model that has a better fit with the test results from the database compared to existing models. They observed that there was a variation in the average FRP efficiency factor depending on the type of fiber, therefore suggesting that a different κ_{ϵ} value needs to be set for GFRP and CFRP. Also they observed that the variability in the instrumentation arrangement of the test contributes to scatter in the database.

2.3.5 Hoop Strain in FRP Confined Concrete

The ultimate strength and ultimate strain of FRP-confined concrete depends greatly on the confining pressure that is provided by the FRP jacket. In the past it was assumed that the confining pressure of the FRP jacket was equal to the tensile strength obtained by the FRP tensile coupon tests (Toutanji and Balaguru, 1998; Saafi, Toutanji, & Li, 1999). But as mentioned before, later research suggested that the tensile strength of FRP cannot be reached in FRP-confined concrete because the hoop strains readings of FRP jackets from compression tests were considerably smaller than the ones obtained in the coupon tests (Xiao & Wu, 2000; Shahawy, Mirmiran, & Beitelman, 2000).

Li et. al showed in their research that the distribution of FRP hoop strains varied around the circumference of the FRP-confined concrete cylinder (2012). In the overlapping zone, which is the zone where the FRP layer ends and an extension of the FRP fabric overlaps itself to secure the wrap, the hoop strains are lower than the strains measured in all other zone (Li et al., 2012).

Numerous studies on the strain efficiency factor, κ_ϵ , hypothesized that the premature failure of the FRP system (Pessiki et al., 2001) is probably due to the multiaxial state of stress to which the FRP system is subjected compared to the pure axial tension to which the FRP is subjected when tested in coupon tests (ACI, 2013).

Throughout the studies of κ_ϵ there has been a wide range of variation between test results. This variation could be caused by the different procedures used to test the specimens or by placing the strain gauges on the overlapping (Karbhari & Howie, 1997; Pessiki et al., 2001; Campione & Miraglia, 2003; Harries & Carey, 2003).

The κ_ε is key to developing an accurate design formula for FRP-confined concrete systems because the FRP ultimate tensile strength is usually not reached at the failure of the confined concrete system. Therefore, analyzing the share or transfer of hoop strain between different numbers of FRP layers will add valuable knowledge to what is currently known about and will represent a step forward in creating a better design formula.

2.4 Summary

The experimental research of confined concrete with FRP wraps was relatively limited during the development of current design guidelines and an evaluation of these existing design guidelines for determining the maximum confined concrete compressive strength has never been attempted with a large database. Therefore, using a robust database for evaluating the design guidelines with tests results is of great importance for the maintenance of public safety. Further, analyzing the behavior of the hoop strain between FRP layers of confined concrete has never been attempted and this information will be an excellent source for better understating of the behavior of FRP confined concrete, which could lead to the refinements of predictive design models.

CHAPTER 3

METHODOLOGY OF ACI 440.2R-08 DESIGN GUIDELINE EVALUATION

3.1 Introduction

The author compiled an extensive database of GFRP and CFRP wrapped specimens to evaluate the effectiveness of the current ACI design guideline formula. The test results in the database were then compared with the predictions made by these guidelines.

3.2 Database Development

This study's final database included test results from a wide variety of specimens. The database from Ozbakkaloglu and Lim (2013) was incorporated, although the results from specimens confined by concrete-filled GFRP and CFRP tubes were excluded because their behavior from GFRP- and CFRP-wrapped specimens differ (Saafi, Toutanji, & Li, 1999). Additionally, published test results that were not reported in Ozbakkaloglu and Lim were added to the database (Karbhari & Gao, 1997; Karbhari & Howie, 1997; Harries, Kestner, Pessiki, Sause, & Ricles, 1998; Toutanji & Balaguru, 1998; Arduini, Di Tommaso, Manfroni, Ferrari, & Romagnolo, 1999; Toutanji, 1999; Karbhari, Rivera, & Dutta, 2000; Karbhari, 2002; Harries & Kharel, 2003; Faella, Realfonzo, & Salerno, 2004; Lin & Liao, 2004; Modarelli, Micelli, & Manni, 2005; Li, 2006; Wu, Wu, Lu, & Ando, 2006; Sadeguiyan, Shekari, & Mousavi, 2008; Ramezaniapour & Gharachorlou, 2009; Chastre & Silva, 2010; Gharachorlou & Ramezaniapour, 2010; Bouchelaghem, Bezazi & Scarpa, 2011; Ozbakkaloglu & Akin, 2012; Micelli & Modarelli, 2013).

The new database had a total of 204 test results for GFRP-confined concrete cylinders from 47 different publications and 490 test results for CFRP-confined concrete cylinders from 58 different publications. The database used for this investigation has a total of 694 test results from 105 different studies as assembled from an extensive literature review. These specimens have diameters ranging from 1.85 in to 16 in (47mm to 406.4mm) and unconfined concrete strengths ranging from 0.90 ksi to 25 ksi (6.2 Mpa to 169.79 Mpa). ACI 440.2R-08 states that the design guidelines can be used only with non-slender, normal weight concrete members (ACI, 2014). Therefore, only specimens with aspect ratios from two to five were used. The number of GFRP layers ranged from one to fifteen layers and for CFRP it ranged from one to twelve layers. Only specimens with glass or carbon fibers wrapped in the hoop direction were considered. Since the purpose of the study was to evaluate the efficiency of the design guidelines in safely predicting the capacity of concrete confined with GFRP and CFRP wraps, only plain concrete cylinders that had a minimum confinement ratio were considered. The minimum confinement ratio, which is defined as the ratio of the maximum confining pressure due to the FRP jacket to the unconfined concrete strength (f_l/f'_c), was 0.08 as required by the ACI 440.2R-08 design guidelines (ACI, 2014).

3.3 Design Guidelines

In order to compare the confined compressive strength from the test results of the database with the predicted confined compressive strength given by the ACI design guidelines, the formulas for the maximum confined concrete compressive strength, f'_{cc} , and the maximum confinement pressure, f_l , defined by the ACI 440.2R-08 (ACI 2014)

were used to predict f'_{cc} for all of the test results. These design formulas were discussed in Chapter 2 and, for the reader's reference, they are repeated here:

$$f'_{cc} = f'_c + \psi_f 3.3 \kappa_a f_l \quad \text{Equation 3.1}$$

$$f_l = \frac{2E_f n t_f \varepsilon_{fe}}{D} \quad \text{Equation 3.2}$$

where:

ψ_f = reduction factor of 0.95

κ_a = efficiency factor depending on the geometry of the section: for circular sections κ_a is 1.0

E_f = tensile modulus of elasticity of FRP, MPa (psi)

n = number of plies of FRP reinforcement

t_f = nominal thickness of one ply of FRP reinforcement, mm (in.)

D = diameter of concrete cylinder, mm (in.)

In Eq. (2) the effective strain level in the FRP at failure ε_{fe} is defined as

$$\varepsilon_{fe} = \kappa_\varepsilon \varepsilon_{fu} \quad \text{Equation 3.3}$$

where κ_ε is the strain efficiency factor due to the premature failure of the FRP jacket and ε_{fu} the design rupture strain of the FRP reinforcement, in./in. (mm/mm). As directed by the ACI 440.2R-08 design guidelines, the κ_ε was taken as 0.55 (ACI, 2014).

3.4 Comparison of Test Results to Design Guideline Predictions

3.4.1 Maximum confined Concrete Compressive Strength, f'_{cc}

To evaluate the effectiveness of the model, the measured confined concrete strengths, $f'_{cc \text{ measured}}$, of the database were compared with the predicted confined concrete strengths, $f'_{cc \text{ predicted}}$, calculated by the current ACI 440.2R-08 guidelines described in

the preceding section. For the f'_{cc} comparison, the $f'_{cc \text{ measured}}$ was plotted against the $f'_{cc \text{ predicted}}$ as shown in Figure 3.1. In this figure, only GFRP-confined specimens are plotted to show the procedure. A one-to-one relation line was added in order to make an evaluation. The values that fell below the line were unconservative for the design as they represented test results with capacities overestimated by current the design guidelines.

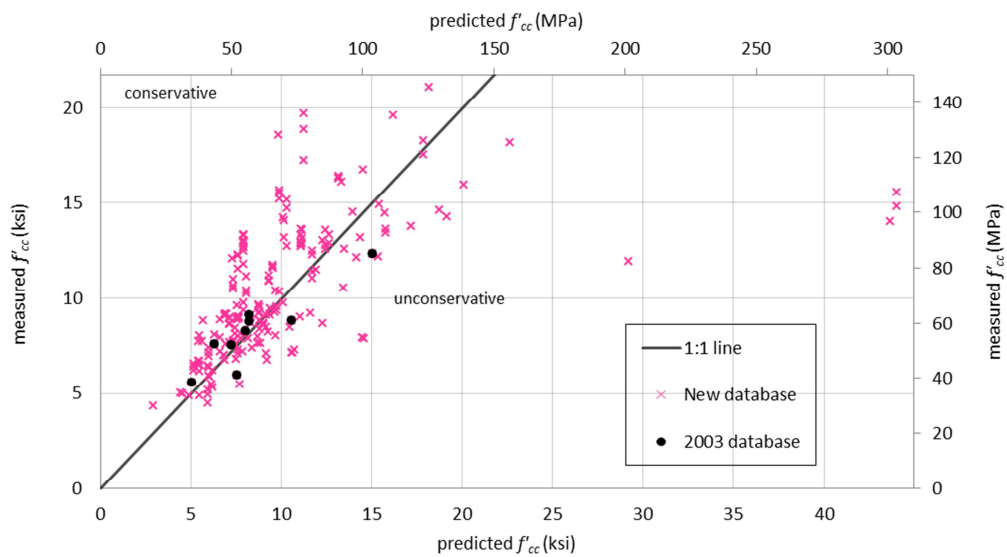


Figure 3.1 Measured f'_{cc} versus predicted f'_{cc} for GFRP-confined specimens using current design guidelines

3.4.2 Maximum Confinement Pressure, f_l

As one of the most important factors in accurately predicting f'_{cc} is the predicted maximum confinement pressure, $f_l \text{ predicted}$, an assessment of Equation 3.2 was also conducted. This assessment was completed by comparing the $f_l \text{ predicted}$ from Equation 3.2 with the $f_l \text{ measured}$. The $f_l \text{ measured}$ was calculated by isolating the confinement contribution of Equation 3.1, which was accomplished by subtracting the unconfined

concrete strength, f'_c measured, from the measured confined concrete strength,

f'_{cc} measured:

$$f_l \text{ measured} = f'_{cc} \text{ measured} - f'_c \text{ measured} \quad \text{Equation 3.4}$$

Is very important to note that Equation 3.1 only represents the contribution of the FRP confinement to the overall confined concrete specimen, it also has a reduction factor ψ_f of 0.95, an efficiency factor κ_a of 1 for circular sections, and 3.3 factor that the author did not isolate and are being lumped into Equation 3.4.

For the f_l comparison, the f_l measured was plotted against the f_l predicted. Figure 3.2 shows an example of this comparison using GFRP-confined specimens. For the evaluation of f_l , a one-to-one line was added to perceive which values were unconservative. The values below the line were overestimated by the design formula and thus were unconservative.

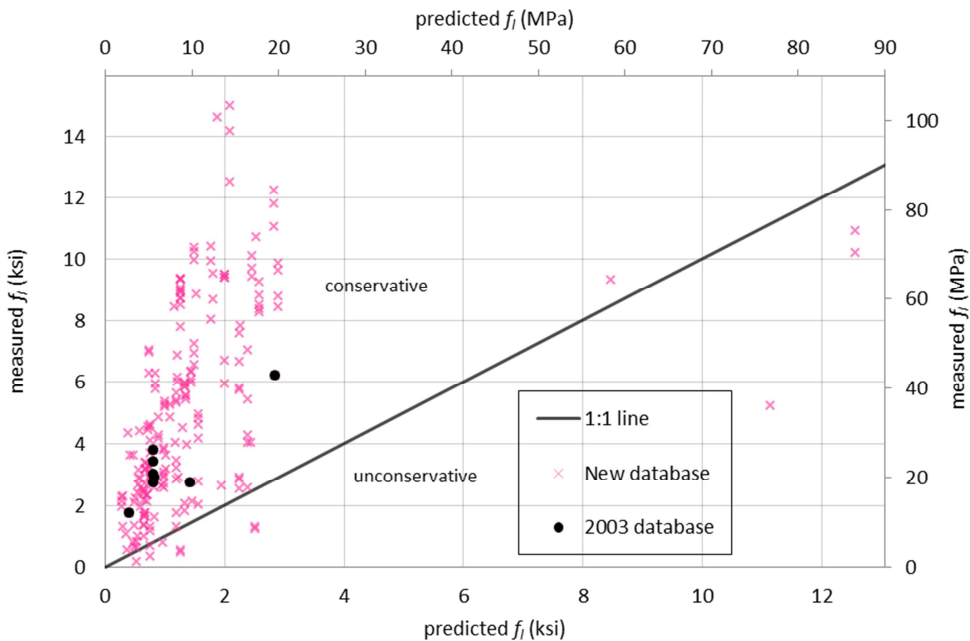


Figure 3.2 Measured f_l versus predicted f_l for GFRP-confined specimens using current design guidelines

Additionally the author isolated the reduction factor ψ_f of 0.95, the efficiency factor κ_a of 1 for circular sections, and the 3.3 factor confinement contribution of Equation 3.1 from Equation 3.4 to observe only the contribution of the FRP confinement to the confined concrete specimen without factors. The Equation for this procedure was:

$$f_l \text{ measured unfactorized} = \frac{f'_{cc} \text{ measured} - f'_c \text{ measured}}{0.95 * 1 * 3.3} \quad \text{Equation 3.5}$$

For the f_l unfactorized comparison, the $f_l \text{ measured unfactorized}$ was plotted against the $f_l \text{ predicted}$. Figure 3.3 shows an example of this comparison using GFRP-confined specimens. For the evaluation of f_l , a one-to-one line was added to perceive which values were unconservative. The values below the line were overestimated by the design formula and thus were unconservative.

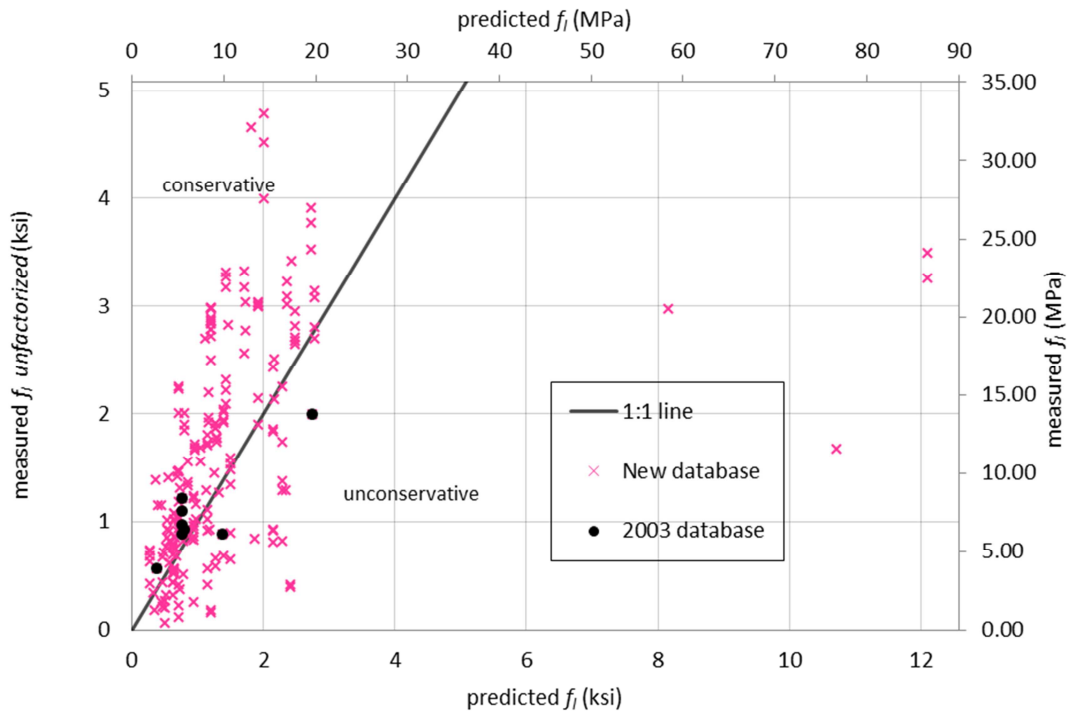


Figure 3.3 Measured f_l unfactorized versus predicted f_l for GFRP-confined specimens using current design guidelines

3.5 Recommendation Development

A 1-to-3.3 line was added to Figure 3.4 to observe how many data points remained conservative when the 3.3 factor of Equation 3.1 was added. After this comparison was made, a variation of the existing formula was created to suggest a more conservative design guideline for GFRP-wrapped specimens. This recommendation was developed by iterating values for the 3.3 factor of Equation 3.1 until a more conservative relationship was identified. The reduction factor of 0.95 and the efficiency factor of 1.0 remained unchanged. The same procedure was used for CFRP-wrapped specimens.

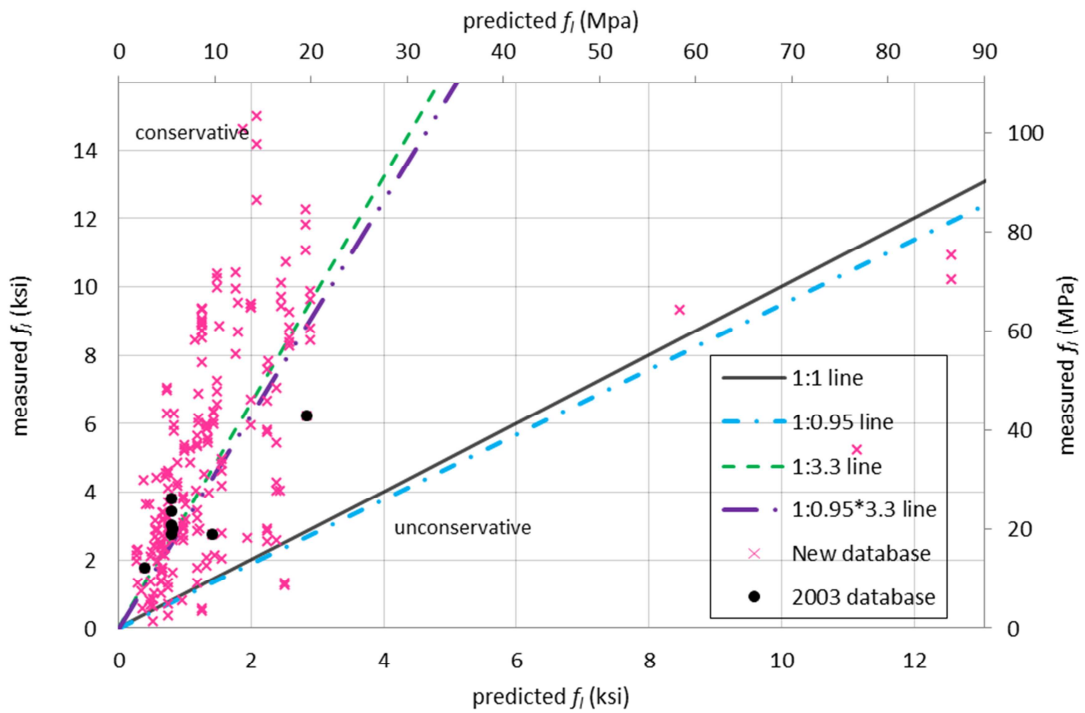


Figure 3.4 Measured f_l versus predicted f_l for GFRP-confined specimens using current design guidelines

CHAPTER 4

EXPERIMENTAL PROGRAM OF FRP-CONFINED CONCRETE CYLINDERS

4.1 Introduction

This chapter describes the experimental methods and testing procedures followed to explore how the different layers of a multi-layer FRP repair share or transfer hoop strain. Section 4.2 describes the material properties of concrete and FRP composites, section 4.3 describes the FRP wrapping schemes, section 4.4 the test specimens, section 4.5 the procedure for wrapping GFRP-confined concrete cylinders, and section 4.6 the FRP-confined concrete cylinder test.

4.2 Material Properties of Concrete and FRP Composites

This section describes the material mechanical properties of concrete and FRP composites used in this study. Section 4.2.1 describes the concrete properties, and section 4.2.2 the FRP composites.

4.2.1 Concrete

The concrete cylinders were cast at the Construction and Concrete Laboratory at Texas State University. The cylinders were made by casting plain concrete in cylindrical plastic molds that were 6 in. in diameter by 12 in tall. The standard ASTM C192 was followed in the fabrication. Two batches with a design compressive strength of 4000 psi were made in December 2013, and twelve 6x12 in cylinders were cast from each batch. These cylinders were cured for at least 28 days prior to the application of the FRP jacket.

Three cylinders per batch were tested on the 28th day after casting, using ASTM C39 to determine the compressive strength.

4.2.2 FRP Composites

Two glass fiber-reinforced polymer (GFRP) composite systems were used, in combination with an epoxy resin matrix. Both GFRP composite systems were donated by the Composites and Plastic Laboratory at Texas State University. The first GFRP material was bidirectional material, as pictured in Figure 4.1(a), and the second GFRP material was multidirectional, as pictured in Figure 4.1(b).

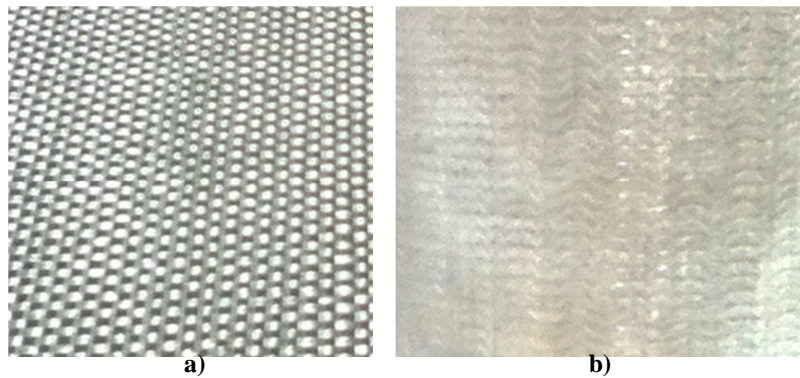


Figure 4.1 Glass fibers. (a) Bidirectional. (b) Multidirectional.

The results from the coupon tests for the bidirectional fiber are shown in Table 4.1 and the results from the coupon tests for the multidirectional fiber are shown in Table 4.2.

Table 4.1 Properties of bidirectional fiber

BIDIRECTIONAL FIBER						
	1	2	3	4	5	AVERAGE
Ultimate Tensile Strength	213.90	226.47	227.14	220.32	224.58	222.48
Modulus (Gpa)	15.292	16.028	40.973	17.882	14.302	20.90
%E	1.75%	1.87%	1.43%	1.78%	1.94%	1.75%

Table 4.2 Properties of multidirectional fiber

MULTIDIRECTIONAL FIBER						
	1	2	3	4	5	AVERAGE
Ultimate Tensile Strength	305.57	284.84	297.28	287.51	300.30	295.10
Modulus (Gpa)	19.654	22.871	18.62	20.45	27.737	21.87
%E	2.06%	2.01%	2.14%	1.72%	1.90%	1.97%

The 635 Thin Epoxy Resin system with a 3:1 ratio medium hardener from US Composites was used, the mechanical properties of the epoxy resin are shown in Table 4.3.

Table 4.3 Epoxy-Resin Mechanical Properties (635 Thin Epoxy Resin)*

Heat Deflection Temperature (°F)	135-145
Tensile Strength (psi)	9,000-10,000
Flexural Modulus (psi x 10 ⁻⁵)	4.7-5.2
Elongation at break (%)	2-3
Viscosity (cps)	600

*Supplied by the manufacturer

4.3 FRP Wrapping Schemes

In order to examine the effects of strain in the FRP based upon the number of layers, each cylinder was wrapped with a different number of layers: one, two, or three layers. For each number of layers and type of GFRP used. Three specimens were made. Thus, there were 6 specimens types constructed.

FRP-confined concrete cylinders with an epoxy-resin matrix were made by wrapping each layer with an overlap of about 6 in. Additionally, in every layer three strain gages were applied. Figure 4.2 shows the different wrapping schemes.

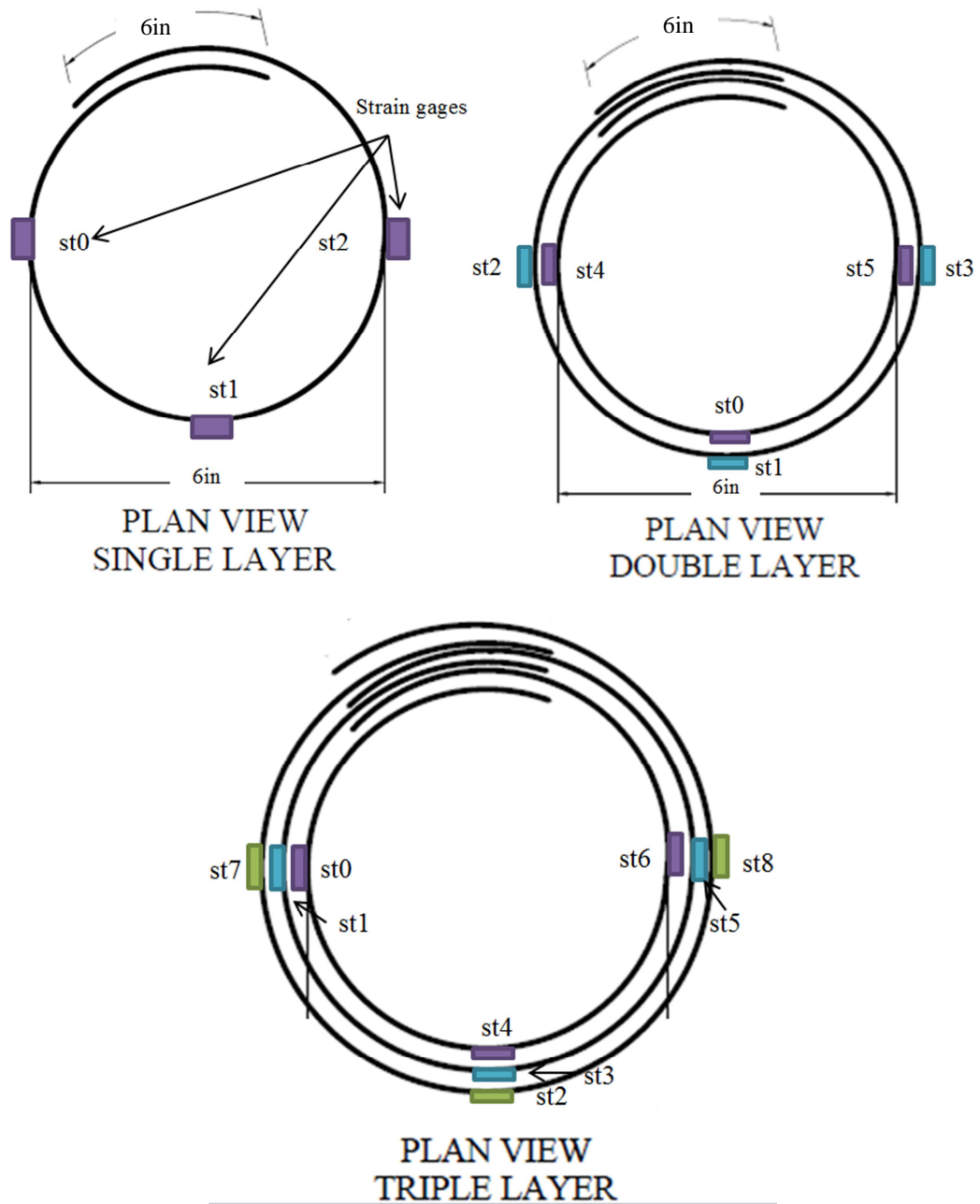


Figure 4.2 Typical GFRP-confined concrete cylinder schemes

4.4 Test Specimens

A total of 24 specimens were used for the experimental program. Table 4.4 Details of Test Specimens gives the details of the specimens. The letter B stands for the batch

(either one or two), letter C for the cylinder (either one, two or three) and L for the number of layers (one, two or three layers). Cylinders that do not contain a letter L are the control cylinders.

Table 4.4 Details of Test Specimens

Spec.	Treatment
B1C1	Control
B1C2	Control
B1C3	Control
B2C1	Control
B2C2	Control
B2C3	Control
B1C1L1B	1 layer GFRP bidirectional
B1C2L1B	1 layer GFRP bidirectional
B1C3L1B	1 layer GFRP bidirectional
B2C1L1M	1 layer GFRP multidirectional
B2C2L1M	1 layer GFRP multidirectional
B2C3L1M	1 layer GFRP multidirectional
B1C1L2B	2 layers GFRP bidirectional
B1C2L2B	2 layers GFRP bidirectional
B1C3L2B	2 layers GFRP bidirectional
B2C1L2M	2 layers GFRP multidirectional
B2C2L2M	2 layers GFRP multidirectional
B2C3L2M	2 layers GFRP multidirectional
B1C1L3B	3 layers GFRP bidirectional
B1C2L3B	3 layers GFRP bidirectional
B1C3L3B	3 layers GFRP bidirectional
B2C1L3M	3 layers GFRP multidirectional
B2C2L3M	3 layers GFRP multidirectional
B1C3L3M	3 layers GFRP multidirectional

4.5 Procedure for Wrapping GFRP-Confined Concrete Cylinders

The GFRP-confined concrete specimens were strengthened with bidirectional or multidirectional GFRP wraps according to the following procedure. First the 635 Thin Epoxy Resin System was prepared according to the manufacturer's directions. Figure 4.3

Preparation of epoxy resin (a) shows the two parts of the epoxy system and (b) the mixed epoxy resin.

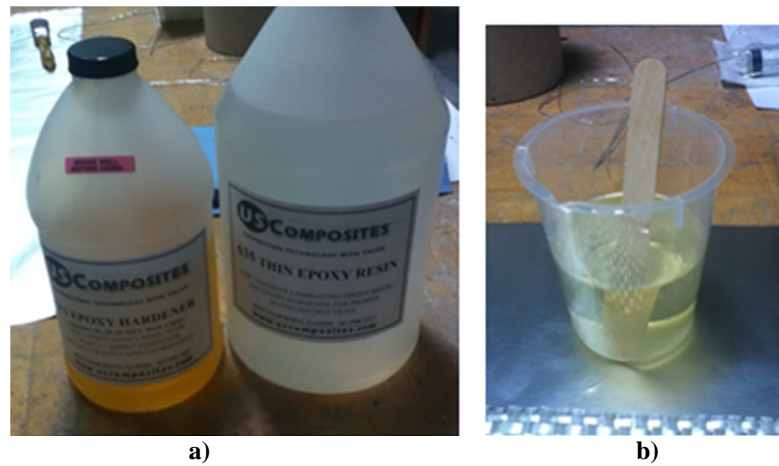


Figure 4.3 Preparation of epoxy resin.

(a) two parts of the epoxy system. (b) mixed epoxy resin.

Each GFRP sheet was saturated in the epoxy prior to being wrapped around the cylinder as shown in Figure 4.4. Figure 4.4 a) shows the preparation of the GFRP sheet and b) the saturation of the GFRP sheet.

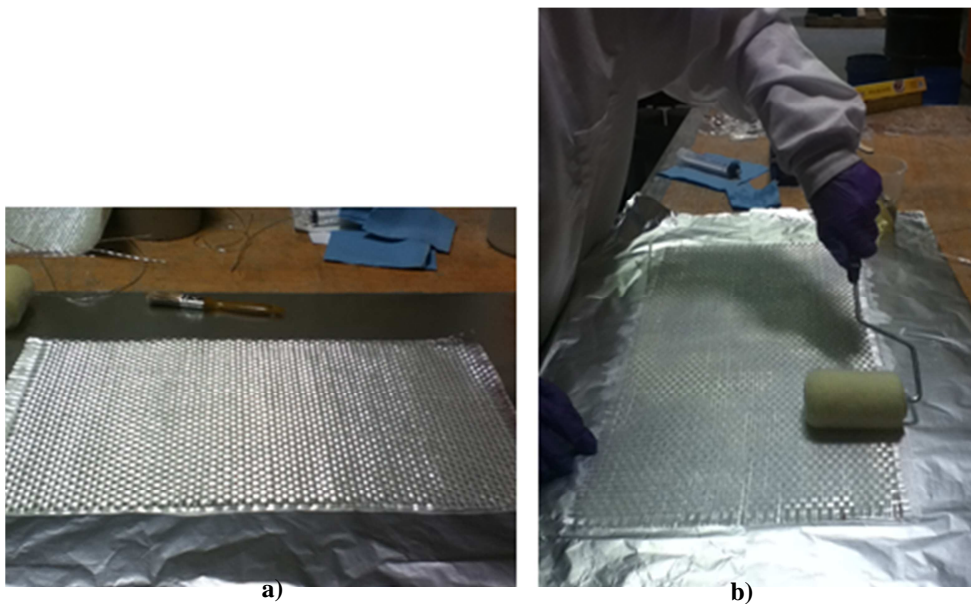


Figure 4.4 Saturation of GFRP sheet with the epoxy resin. (a) Preparation of GFRP sheet. (b)

Saturation of GFRP sheet.

The composite was then wrapped around the cylinder with the majority of the fiber orientation in the circumferential direction with an overlap length of 6 in. Figure 4.5 (a) show the process for wrapping the cylinder with one GFRP layer and (b) shows the finish GFRP-confined concrete cylinder with one layer.



a)



b)

Figure 4.5 Wrapping cylinder with one GFRP layer. (a) Wrapping the cylinder. (b) Cylinder wrapped with one GFRP layer.

For cylinders that only had one layer, the epoxy was allowed to cure and then the strain gages FLA-6-11 from Tokyo Sokki Kenkyujo were applied according to the scheme shown in section 4.3. Figure 4.6 is a picture of a specimen with one layer of FRP and strain gages applied.



Figure 4.6 Cylinder with one GFRP layer and strain gages

For cylinders that had two or three layers, additional precautions were taken to protect the strain gages on lower layers of FRP. The first set of strain gages were applied according to the scheme shown in section 4.3 and illustrated in Figure 4.2 after placing the first GFRP layer. These strain gages were covered by a layer of petroleum jelly and a small sheet of wax paper to avoid bonding to the layer that was going to be placed on top. Figure 4.7 shows a protected strain gage.



Figure 4.7 Application of strain gage with petroleum jelly and wax paper

Next, the second GFRP sheet was prepared as previously described and applied to the cylinder. This layer had to be applied carefully so that the cables from the strain gages of the previous layer could pass through the FRP fabric. Figure 4.8 shows a concrete cylinder confined with two GFRP layers and strain gages on the first layer.



Figure 4.8 Cylinder with two GFRP layers and strain gages on the first layer

For cylinders that had two layers, the epoxy was allowed to cure and then the strain gages from the second layer were applied according to the scheme in section 4.3. The gages for the second layer were applied in the locations shown in section 4.3, similar to the ones in layer one, but in a different vertical location so that they would not be over each other.

Similarly for cylinders that had three layers, the strain gages on the second GFRP sheet were applied according to Figure 4.2. These strain gages were placed and protected following the same procedure described above and then the third GFRP sheet was applied while passing all of the strain gages cables through the GFRP fabric. The epoxy was allowed to cure and then the strain gages for the third layer were applied according to the

scheme in section 4.3. Figure 4.9 shows a confined concrete cylinder with three GFRP layers and respective strain gages.

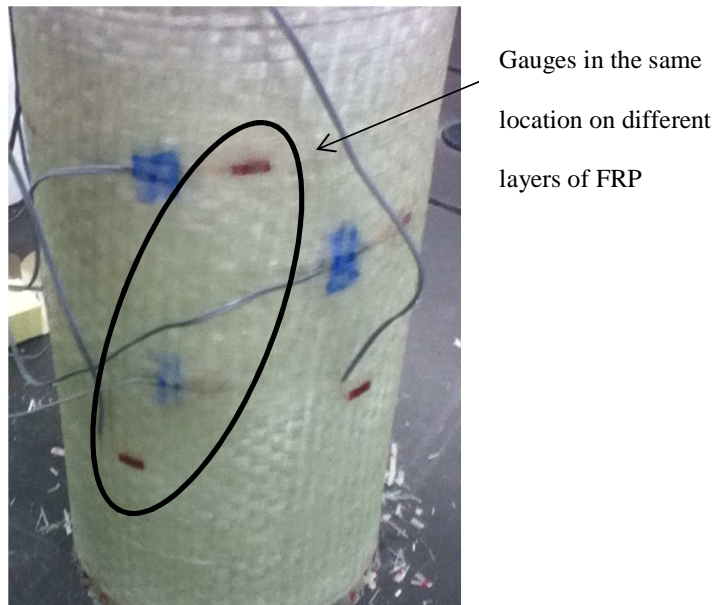


Figure 4.9 Cylinder with three GFRP layers and respective strain gages

According to the supplier, approximately 90% of the epoxy strength is gained in the first twenty-four hours. The epoxy was allowed to cure for at least 5 days to gain full strength before testing.

4.6 FRP-Confined Concrete Cylinder Test

ASTM C39 was adopted to determine the confined compressive strength and hoop strain of the GFRP-confined concrete cylinders because no testing specification specific to FRP confined specimens has been established. The GFRP-confined concrete cylinders were tested in compression using a Test Mark CM-4000 series as shown in Figure 4.10. To record the strain data, the strain gages were connected to a NI cDAQ-9174 with two modules (NI 9219 and NI 9235) as shown in Figure 4.11. The compressive load was

acquired using WinCom. Both data acquisition systems were synchronized to record data every 0.5 seconds.



Figure 4.10 Typical GFRP-confined concrete cylinder test setup



Figure 4.11 NI cDAQ-9174 with two modules (NI 9219 and NI 9235)

CHAPTER 5
DISCUSSION OF RESULTS ACI 440.2R-08 DESIGN
GUIDELINE EVALUATION

5.1 Introduction

As previously mentioned in Chapter 3, the procedure for evaluating the ACI 440.2R-08 design guidelines for GFRP- and CFRP-confined concrete was the same. But in this chapter the discussion of the results was separated for GFRP- and CFRP-confined concrete because the analyses of the design guidelines lead to different results depending on the type of FRP.

5.2 GFRP-Confined Concrete

5.2.1 Evaluation of Current Design Recommendations for f'_{cc}

When the $f'_{cc \text{ predicted}}$ was compared to the $f'_{cc \text{ measured}}$, 71 specimens out of 204 were found to be unconservative. As shown in Figure 5.1, the test results that fell below the 1:1 line are unconservative because the $f'_{cc \text{ predicted}}$ was greater than the $f'_{cc \text{ measured}}$. This situation means that for 35% of the total database, the design guidelines overestimated the capacity of the specimen. While the current design guidelines may provide an acceptable average approximation of GFRP-confined concrete behavior for the purpose of modeling average behavior, a more conservative design formula is in the interest of public safety in structural design. Structural designers need a conservative design formula in order to determine the safest, most efficient, and

appropriate solution when strengthening or repairing a concrete structure. If the design formula is overestimating the measured results, then the structural design is going to be overestimated which may lead to safety issues and legal problems.

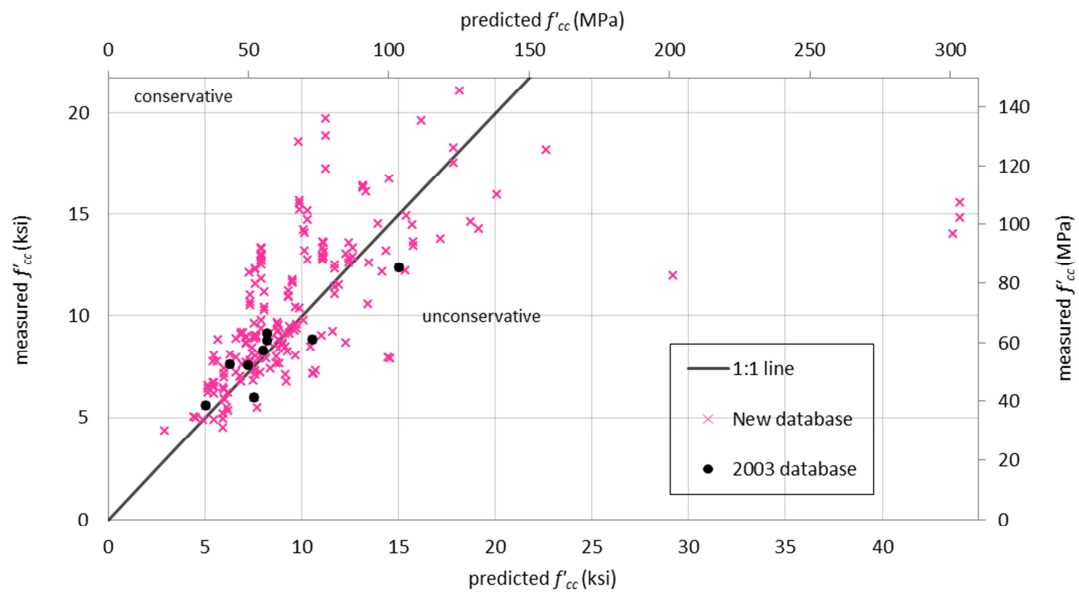


Figure 5.1 Measured f'_{cc} versus predicted f'_{cc} for GFRP-confined specimens using current design guidelines

5.2.2 Evaluation of the Maximum Confinement Pressure

To better understand why the ACI 440.2R-08 design guidelines were so frequently unconservative for GFRP-confined specimens, the predicted and measured f_l , $f_{l \text{ predicted}}$ and $f_{l \text{ measured}}$ respectively, were plotted against each other in Figure 5.2. The term $f_{l \text{ measured}}$ represents the confinement contribution to the composite strength of Equation 3.1.

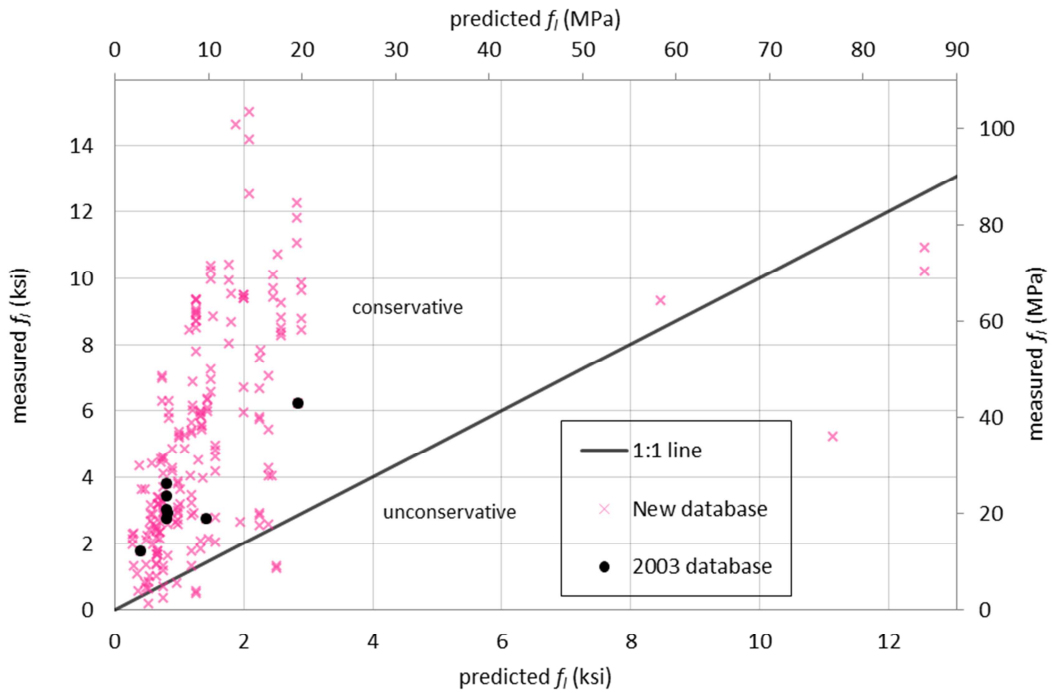


Figure 5.2 Measured f_l versus predicted f_l for GFRP-confined specimens using current design guidelines

In this figure, all values that are above the one-to-one line are conservative. This figure shows that the confinement pressure predicted by Equation 3.2 for a GFRP-confined specimen, $f_{l \text{ predicted}}$, is a fairly conservative estimate of the confinement contribution to f'_{cc} when considering a one-to-one relationship, as 94% of the unfactored f_l predictions are conservative.

Although the unfactored f_l , as predicted by Equation 3.2, was shown to be a conservative estimate of the confinement contribution to f'_{cc} for this dataset, Equation 3.1 modifies f_l with several factors: a reduction factor, ψ_f , of 0.95; a geometry-dependent efficiency factor, κ_a , which was 1.0 for a circular section; and a factor of 3.3. It can be observed in Figure 5.3 that there is no significant difference between the 1 to 1 line and the 1 to 0.95 line, which takes into consideration the reduction factor and the efficiency

factor, as the same percentage of specimens remain on the conservative side of either line. However, when considering the impact of the 3.3 factor in Equation 3.1 a large number of the cases moved to the unconservative side, as shown by the 1:3.3 line in Figure 5.3. Even when considering the reduction factor and the efficiency factor, as seen on the 1 to 0.95×3.3 line, a large number of specimens remain unconservative. From this unconservative shift, it was concluded that Equation 3.1's overestimation of f'_{cc} for GFRP-confined concrete resulted from the 3.3 factor.

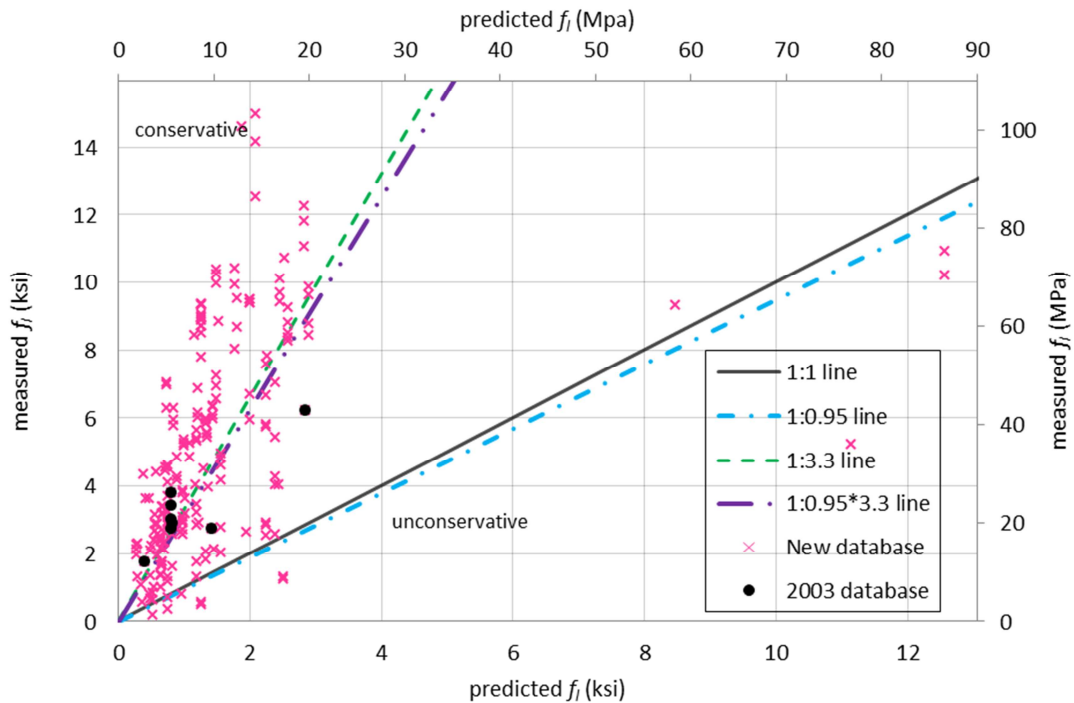


Figure 5.3 Measured f_l versus predicted f_l for GFRP-confined specimens using current design guidelines

Additionally, the author isolated the measured f_l to remove all the factors affecting the result and compared it with the predicted f_l . This comparison can be observed in Figure 5.4. It can be observed that even if the all the factors are removed, the formula is still unconservative.

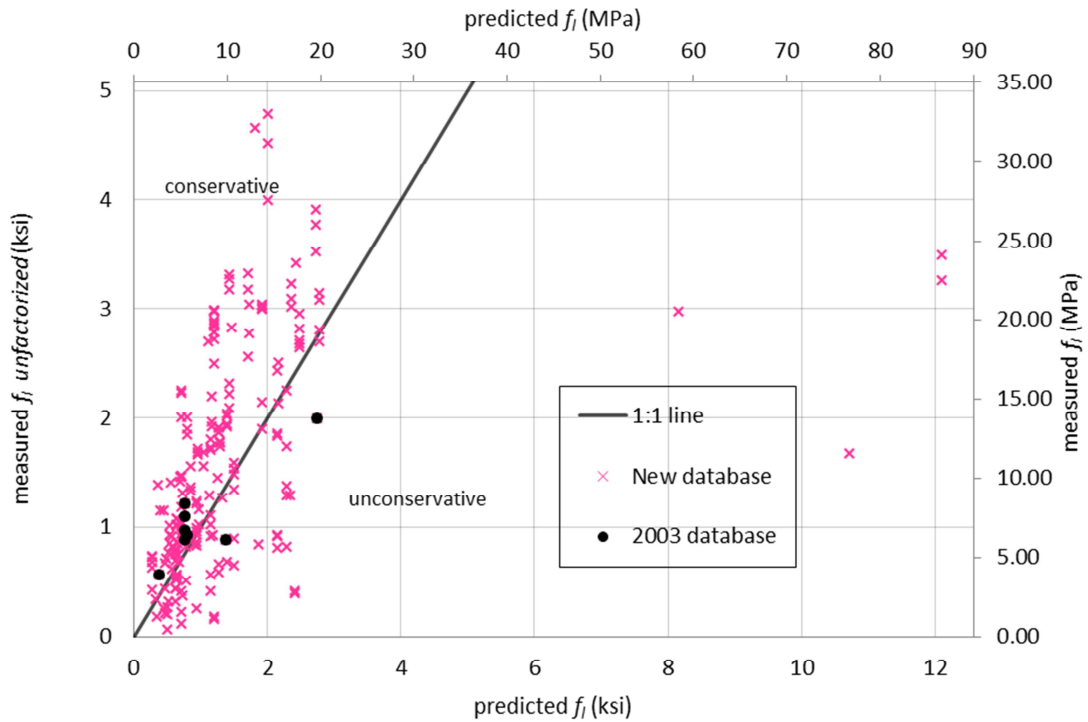


Figure 5.4 Measured f_l unfactorized versus predicted f_l for GFRP-confined specimens using current design guidelines

5.2.3 Development of Revised Equation

In order to make Equation 3.1 more conservative for use in structural design, the 3.3 factor was modified. As discussed in the previous section, the 3.3 factor was targeted because it has the greatest influence in generating unconservative results in f'_{cc} . When a value of 1.0 was considered in lieu of 3.3, most of the specimen results fell in the conservative side. The suggested new Equation for confined concrete compressive strength is:

$$f'_{cc} = f'_c + \psi_f \kappa_a f_l \quad \text{Equation 5.1}$$

5.2.4 Verification of Revised Equation

In Figure 5.5 f'_{cc} measured is plotted versus f'_{cc} predicted new from Equation 5.1.

In addition, a one-to-one line is added to evaluate the conservativeness of the new formula. As with the other figures, values above the line are conservative and values below the line were overestimated by the new Equation. As 94% of the values using f'_{cc} predicted new were conservative, it can be observed that Equation 5.1 is a more appropriate model for predicting the design strength of GFRP confined concrete cylinders than the current design guideline, Equation 3.1.

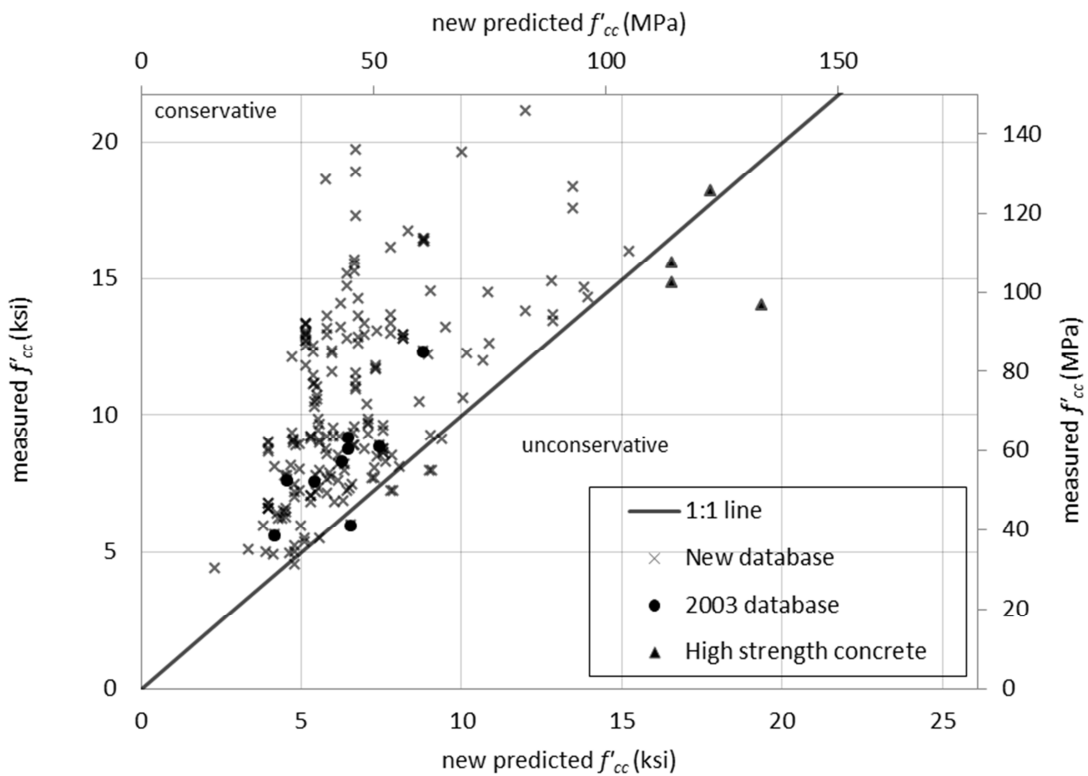


Figure 5.5 Measured f'_{cc} versus new predicted f'_{cc} for GFRP-confined specimens using revised Equation

With Equation 5.1, most of the data points fall in the conservative side and only 6% of the test specimens were overestimated versus with the original Equation, Equation 3.1, when 35% of the results were overestimated. Similarly, the percent error of the unconservative results greatly reduced with the revised Equation. The unconservative percent error ranged from 20% to 210% with Equation 3.1 and with the revised Equation, Equation 5.1, the unconservative percent error ranged from 0.34% to 38%. Thus, the new Equation both reduces the number of unconservative values and the magnitude of unconservativeness versus the current design guidelines.

The remaining discrepancies could be due to multiple factors. For the three data points that are on the top right of Figure 5.5 the formula may be overestimating the confined compression strength for high strength concrete. Almusallam (2009) observed that normal strength concrete has a greater percentage increase in confined compressive strength than high strength concrete. As such, this formula may not be appropriate for high strength concrete. According to the ACI, high strength concrete has unconfined compressive strength values over 6000 psi (ACI, 2014). If the high strength concrete specimens are ignored, the unconservative percent error ranged from 20% to 84% with Equation 3.1 and from 0.34% to 15% for the revised Equation, Equation 5.1.

While the lay-up procedure, in situ effects, quality control and/or placing the strain gauges at the overlap region of the GFRP jacket (Toutanji, 1999; Li, 2006; Micelli & Modarelli, 2013) have been cited as common sources of test data variation, a reduction factor of 0.34 in lieu of the current 0.95, would result in a conservative prediction of all the remaining 6% test specimens that are on the unconservative side of Figure 5.5. Such a reduction factor, however, seems excessive for such a small percentage of unconservative

values. The design professional must make the call as to their comfort level with a 4% chance of overestimating the capacity of GFRP-confined concrete if high strength concretes are excluded pending further research. As observed in Figure 5.5, the revised Equation 5.1, is more conservative for the design of GFRP-confined concrete than the current design guidelines.

Table 5.1 shows different factors and their respective percentage of conservative values. This table was added so that the designer can select the conservativeness that the design professional wants to achieve. The author believes a factor of 1 is the safest design.

Table 5.1 New factors and percent conservative values

Factor	% conservative values
3.3	65
3	72
2.5	78
2	82
1.75	85
1.5	89
1.25	92
1	94

Also the author gives another option for designing. If the design professional does not want to modify the Equation from the ACI design guideline, the designer can add a modified reduction factor for the entire Equation. Table 5.2 shows the different modified reduction factors and % of conservative values.

Table 5.2 Modified reduction factors and percent conservative values

Modified Reduction Factor	% conservative values
0.85	86
0.8	90
0.75	94
0.7	96
0.6	97
0.5	98
0.4	99
0.3	100

The author feels comfortable with a modified reduction factor of 0.75 because that gives around the same percentage of conservative values as in Equation 5.1. The proposed Equation with the modified reduction factor of 0.75 is:

$$f'_{cc} = \mathbf{0.75}(f'_c + 3.3\psi_f\kappa_a f_l) \quad \text{Equation 5.2}$$

5.3 CFRP-Confined Concrete

5.3.1 Evaluation of Current Design Recommendations for f'_{cc}

When the f'_{cc} predicted was compared to the f'_{cc} measured, 87 specimens out of 490 were found to be unconservative. Figure 5.6 shows the measured f'_{cc} plotted against the predicted f'_{cc} . As before, the test results that fell below the 1:1 line in Figure 5.6 are unconservative because the f'_{cc} predicted is greater than the f'_{cc} measured. This situation means that for 18% of the total database, the design guidelines overestimated the capacity of the specimen.

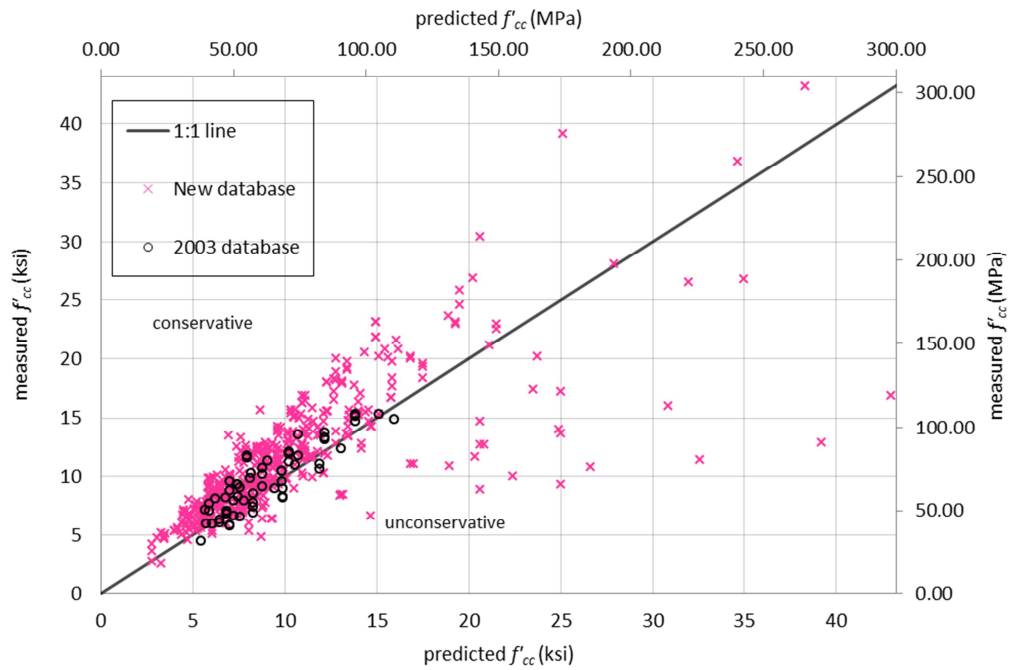


Figure 5.6 Measured f'_{cc} versus predicted f'_{cc} for CFRP-confined specimens using current design guidelines

As mentioned in section 5.2 for GFRP-confined concrete, the current design guidelines may provide an acceptable average approximation of CFRP-confined concrete behavior for the purpose of modeling average behavior but in structural design a more conservative design formula is in the interest of public safety.

5.3.2 Evaluation of the Maximum Confinement Pressure

To better understand why the ACI 440.2R-08 design guidelines were unconservative for more than one-in-six CFRP-confined specimens, the predicted and measured f_l , f_l predicted and f_l measured respectively, were plotted against each other in Figure 5.7. The f_l measured is showing the confinement contribution to the composite strength of Equation 3.1 as defined in Equation 3.4

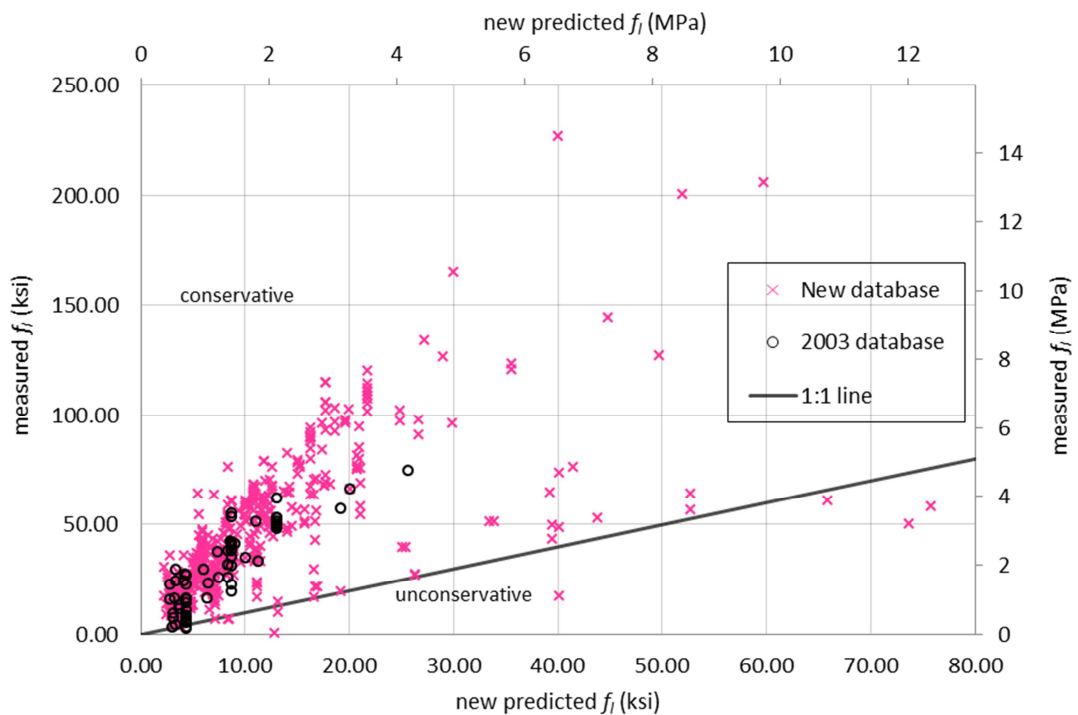


Figure 5.7 Measured f_l versus predicted f_l for CFRP-confined specimens using current design guidelines

In Figure 5.7, all values that are above the one-to-one line are conservative. This figure shows that the confinement pressure predicted by Equation 3.2 for a CFRP-confined specimen, f_l predicted, is a fairly conservative estimate of the confinement contribution to f'_{cc} when considering a one-to-one relationship, as 98% of the unfactored f_l predictions are conservative. This correlation was similar to the same comparison with

GFRP specimens, which had f_l predicted conservatively for 94% of the specimens.

Therefore, Equation 3.2 for f_l appears to be a good predictor of the confinement portion of f'_{cc} for both CFRP and GFRP.

As mentioned before in Chapter 3 and section 5.2.2, Equation 3.1 takes into account several factors: a reduction factor, ψ_f , of 0.95; a geometry-dependent efficiency factor, κ_a , which was 1.0 for a circular section; and a factor of 3.3. It can be observed in Figure 5.8 that there is no significant difference between the 1 to 1 line and the 1 to 0.95 line, which takes into consideration the reduction factor and the efficiency factor. When considering the impact of the 3.3 factor in Equation 3.1, a large number of the results moved to the unconservative side as shown in Figure 5.8 by the 1:3.3 line. Even when considering the reduction factor and the efficiency factor, as seen on the 1 to 0.95*3.3 line, a large number of specimens remain unconservative. From this unconservative shift, it was concluded that Equation 3.1's overestimation of f'_{cc} for CFRP-confined concrete resulted from including the 3.3 factor.

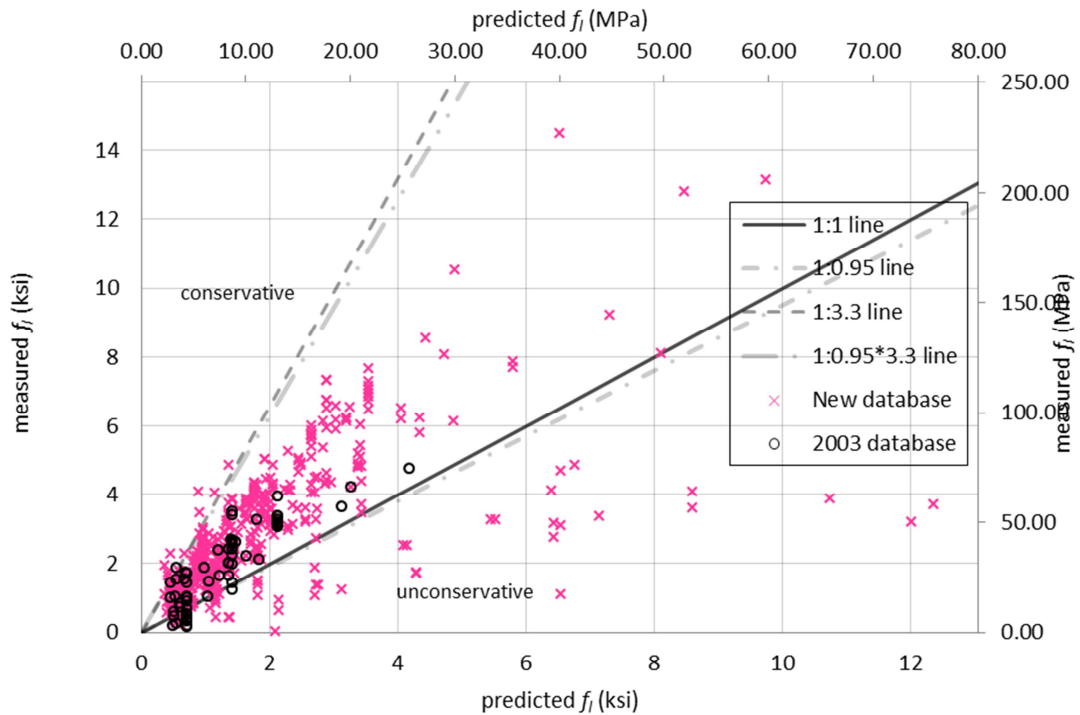


Figure 5.8 Measured f_l versus predicted f_l for CFRP-confined specimens using current design guidelines

5.3.3 Development of Revised Equation

In order to make Equation 3.1 more conservative for use in structural design, the 3.3 factor was modified. As discussed in the previous section, the 3.3 factor was targeted because it had the greatest influence in generating unconservative results in f'_{cc} . When a value of 1.75 was considered in lieu of 3.3, most of the results fell in the conservative side. The suggested new Equation for confined concrete compressive strength is:

$$f'_{cc} = f'_c + \psi_f 1.75 \kappa_a f_l \quad \text{Equation 5.3}$$

Additionally, the author has added Table 5.3 with different factors and their respective percentage of conservative values so that the design professional can use a

factor that meets his needs and comfort level. With a level of 1, almost 100% of the specimens have a conservative prediction but this may be excessive.

Table 5.3 New factors and percent conservative values

Factor	% conservative values
3.3	82
3	86
2.5	91
2	92
1.75	93
1.5	95
1.25	97
1	98

Also, as in the section for GFRP, the author added Table 5.4 Modified reduction factors and percent conservative values to give to the design professional the option of not modifying the formula and just add a modified reduction factor. The author believes a modified reduction factor of 0.80 is enough to make the ACI design formula conservative.

Table 5.4 Modified reduction factors and percent conservative values

Modified reduction factor	% conservative values
0.85	93
0.8	94
0.75	94
0.7	95
0.6	97
0.5	98
0.4	99
0.3	100

The proposed Equation with the modified reduction factor of 0.80 is:

$$f'_{cc} = 0.80(f'_c + 3.3\psi_f\kappa_a f_l) \quad \text{Equation 5.4}$$

5.3.4 Verification of Revised Equation

In Figure 5.9 f'_{cc} measured is plotted versus f'_{cc} predicted new from Equation 5.3. In addition, a one-to-one line was added to evaluate the conservativeness of the new formula. As with the other figures, values above the line were conservative and values below the line were overestimated by the new Equation. As 93% of the values using f'_{cc} predicted new were conservative, it can be observed that Equation 5.3 is a more appropriate model for predicting the design strength of CFRP-confined concrete cylinders than the current design guideline, Equation 3.1.

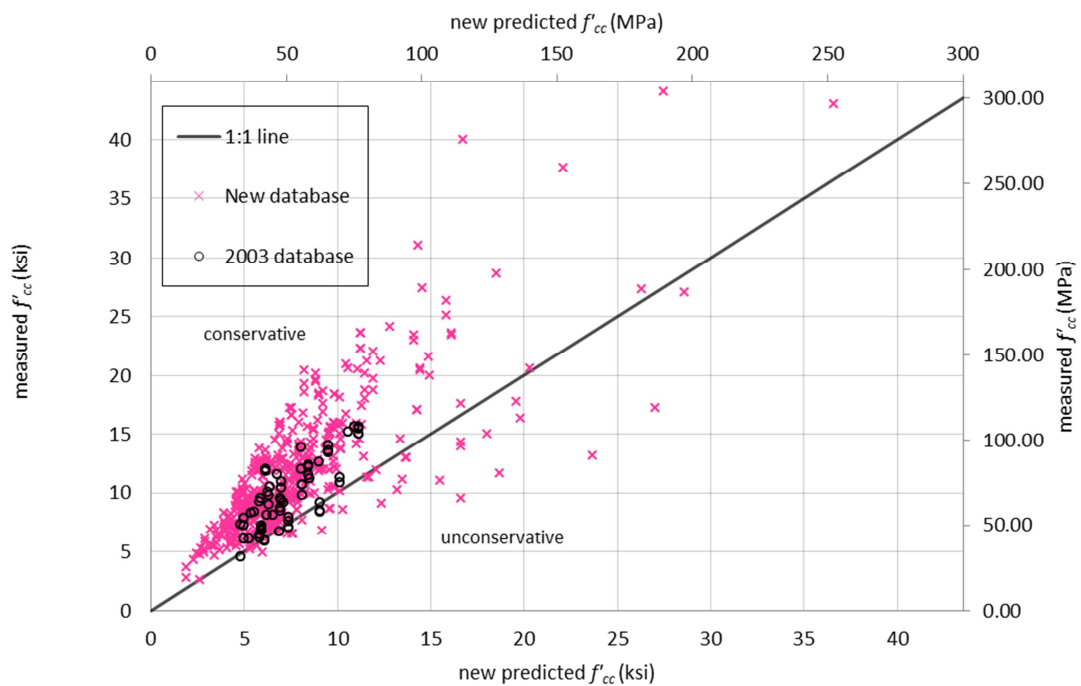


Figure 5.9 Measured f'_{cc} versus new predicted f'_{cc} for CFRP-confined specimens using revised Equation

With Equation 5.3 most of the data points fell in the conservative side and only 7% of the test specimens were overestimated versus the original Equation, Equation 3.1, when 18% of the results were overestimated. Similarly, the percent error ranged from 14% to 199% with Equation 3.1 and with the revised Equation, Equation 5.3, the unconservative percent error ranged from 1% to 80%. Thus, the new Equation both reduces the number of unconservative values and the magnitude of unconservativeness versus the current design guidelines.

Additionally, the author isolated the measured f_l to remove all the factors affecting the result and compared it with the predicted f_l . This comparison can be observed in Figure 5.10. It can be observed that even if all the factors are removed, the formula is still unconservative.

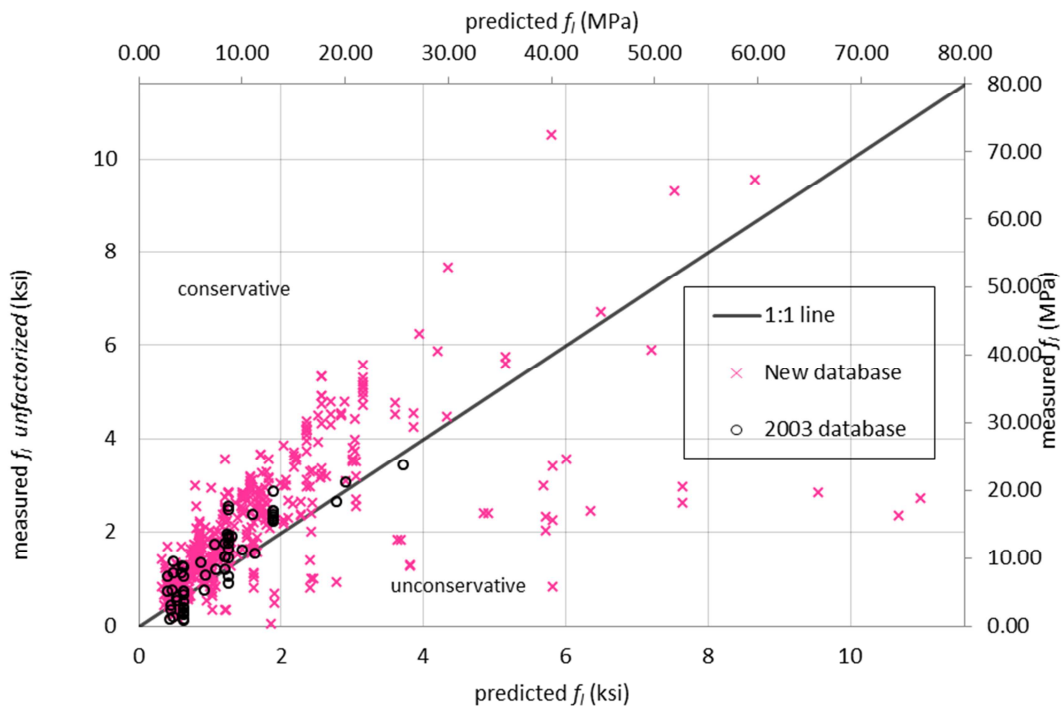


Figure 5.10 Measured f_l unfactorized versus predicted f_l for CFRP-confined specimens using current design guidelines

5.4 Summary of Results

In this chapter an evaluation of the ACI 440.2R-08 design guidelines was made. The $f'_{cc \text{ predicted}}$ was compared to the $f'_{cc \text{ measured}}$ and it was found that 71 out of 204 or 35% of GFRP-confined specimens were unconservative and 87 out of 490 or 18% of CFRP-confined specimens were unconservative.

Additionally, $f_l \text{ predicted}$ and $f_l \text{ measured}$ were plotted against each other to better understand why the ACI 440.2R-08 design guidelines were so frequently unconservative. From this analysis it was found that $f_l \text{ predicted}$ is a fairly conservative estimate of the confinement contribution to f'_{cc} . For GFRP-confined specimens 94% of the unfactored f_l predictions are conservative and 98% for CFRP-confined specimens. From the later it was concluded that the unconservativeness of Equation 3.1, for both GFRP- and CFRP-confined specimens, relies on the 3.3 factor. New confined compressive strength Equations were made for GFRP- and CFRP-confined specimens to make the design of FRP confined concrete specimens safer.

CHAPTER 6

DISCUSSION OF RESULTS FRP-CONFINED CONCRETE CYLINDERS

6.1 Introduction

The GFRP-confined specimens were tested in axial compression to obtain FRP strain values during confinement. This chapter discusses the results from the evaluation of how strain is shared between GFRP layers in GFRP-confined concrete cylinders. The measured 28 day compressive strengths of unconfined concrete for batch 1 and batch 2 were 3950 psi and 4170 psi, respectively. Table 6.1 shows the compressive test results for the control specimens and the confined specimens. Section 6.2 describes the GFRP-confined concrete cylinders with one layer, subdividing them in GFRP bidirectional and GFRP multidirectional (Section 6.2.1 and Section 6.2.2 respectively). Section 6.3 describes the GFRP-confined concrete cylinders with two layers, subdividing them in GFRP bidirectional and GFRP multidirectional (Section 6.3.1 and Section 6.3.2 respectively). Finally, Section 6.4 describes the GFRP-confined concrete cylinders with three layers, subdividing them in GFRP bidirectional and GFRP multidirectional (Section 6.4.1 and Section 6.4.2 respectively).

Table 6.1 Compressive test results

Spec.	Treatment	f'_c measured (psi)	f'_{cc} measured (psi)
B1C1	Control	3890	
B1C2	Control	3950	
B1C3	Control	4010	
B2C1	Control	4300	
B2C2	Control	4120	
B2C3	Control	4090	
B1C1L1B	1 layer GFRP bidirectional	3950	4375
B1C2L1B	1 layer GFRP bidirectional	3950	4780
B1C3L1B	1 layer GFRP bidirectional	3950	4322
B2C1L1M	1 layer GFRP multidirectional	4170	5259
B2C2L1M	1 layer GFRP multidirectional	4170	5208
B2C3L1M	1 layer GFRP multidirectional	4170	5240
B1C1L2B	2 layers GFRP bidirectional	3950	4354
B1C2L2B	2 layers GFRP bidirectional	3950	4176
B1C3L2B	2 layers GFRP bidirectional	3950	4586
B2C1L2M	2 layers GFRP multidirectional	4170	4751
B2C2L2M	2 layers GFRP multidirectional	4170	4902
B2C3L2M	2 layers GFRP multidirectional	4170	5157
B1C1L3B	3 layers GFRP bidirectional	3950	5025
B1C2L3B	3 layers GFRP bidirectional	3950	5352
B1C3L3B	3 layers GFRP bidirectional	3950	5401
B2C1L3M	3 layers GFRP multidirectional	4170	6376
B2C2L3M	3 layers GFRP multidirectional	4170	6530
B2C3L3M	3 layers GFRP multidirectional	4170	5861

6.2 GFRP-Confined Concrete Cylinders with One Layer

The specimens in this section were not needed for the study of how different layers of GFRP share strain but they were used to debug the Data Acquisition (DAQ) system.

6.2.1 One layer GFRP Bidirectional

As explained earlier, the results from the specimens tested in this group were discarded because the author was calibrating the DAQ system. The maximum loads

reached at failure for B1C1L1B, B1C2L1B and B1C3L1B were 4375 psi, 4780 psi, and 4322 psi respectively.

6.2.2 One layer GFRP Multidirectional

The maximum load values for B2C1L1M and B2C2L1M were 5259 and 5208 respectively, these cylinders were also used to debug the DAQ system. Figure 6.1 shows the axial stress versus the hoop strain for specimen B2C3L1M, where the sign convention used is that compressive stress and hoop strain are positive. It can be observed from Figure 6.1 that the specimen initially behaved linear elastically as expected for a confined cylinder. Then, as the hoop strain increased, microcracking of the concrete core or damage accumulated turned into a nonlinear elastic response. Finally, the plastic linear hoop stress-strain response was controlled by the lateral restraint of the GFRP jacket and failure occurred when the ultimate radial strain of the GFRP-confined concrete was reached.

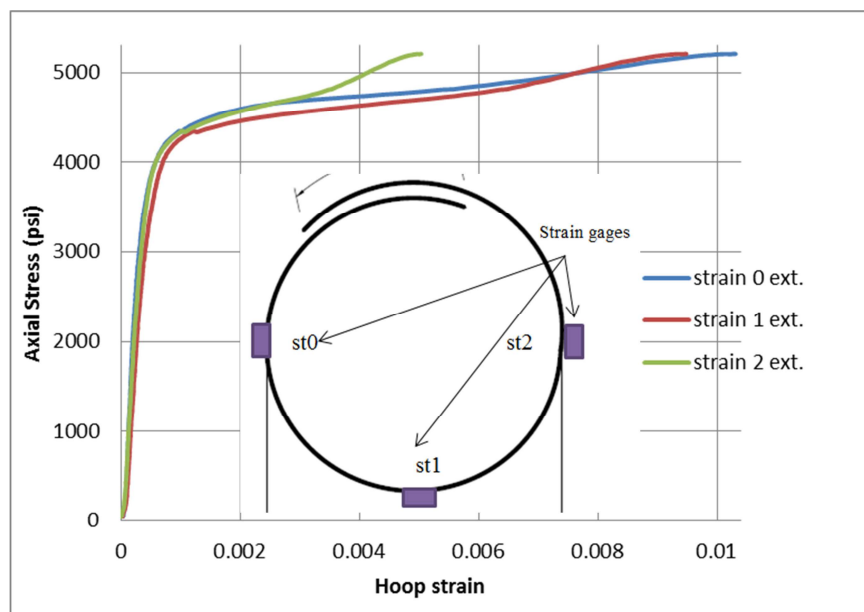


Figure 6.1 Axial Stress versus hoop strain for specimen B2C3L1M

Figure 6.2 shows the GFRP failure of B2C3L1M. In Figure 6.2 also shows that the gage “strain 2” was located in the failure area. This proximity to the failure explains why in Figure 6.1 the values of the measured strain 2 stop at around 0.005 of the hoop strain. Also around 0.003 of the strain, strain 2 stopped sharing strain equally compared to the other two strains and took a small amount of additional strain to take it to failure. The measured strain 0 and strain 1 showed a similar response, sharing strain almost equally.



Figure 6.2 B2C3L1M failure mode

6.2.3 Summary of GFRP-Confined Concrete Cylinder with One Layer

Specimens confined with one layer helped to calibrate the DAQ system. Additionally specimen B2C3L1M showed that the specimens were appropriately confined because the stress-strain curve showed the typical stress-strain curve for FRP-confined specimens.

6.3 GFRP-Confined Concrete Cylinders with Two Layers

Three cylinders of each type of GFRP (bidirectional and multidirectional) were tested while monitoring hoop strain and axial load. The results from specimen B1C1L2B were discarded due calibration of the DAQ system.

6.3.1 Two layer GFRP Bidirectional

6.3.1.1 B1C2L2B

Specimen B1C2L2B axial stress versus hoop strain is shown in Figure 6.3. It can be observed that all the strains, except for strain 1 ext. 180°, show a similar behavior up to the unconfined concrete strength, then the shape of the curves change indicating that the FRP layers were not sharing the strain uniformly when the confinement was activated.

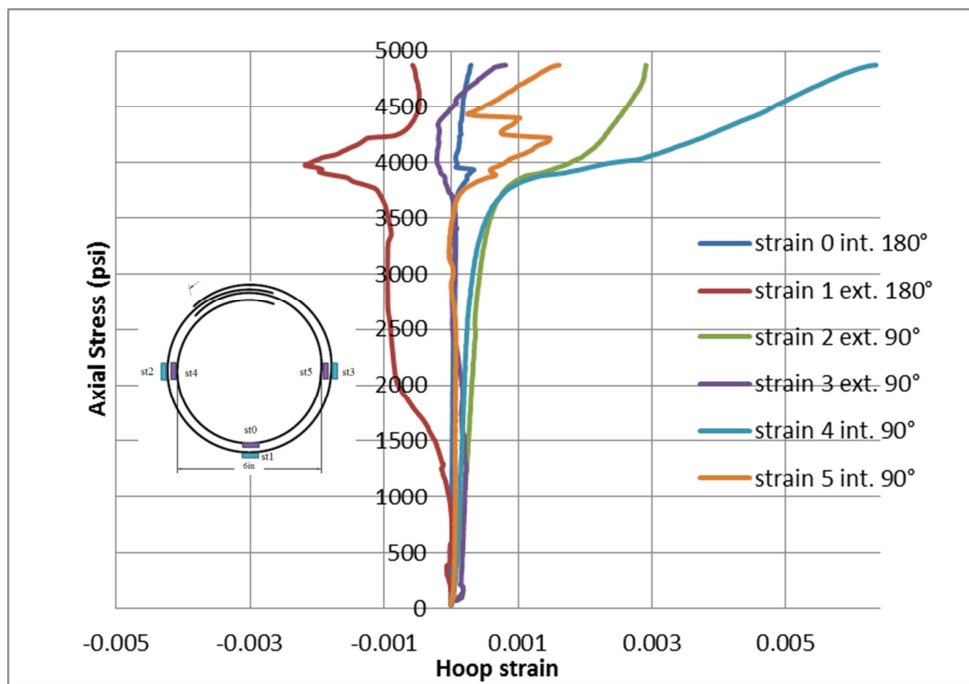
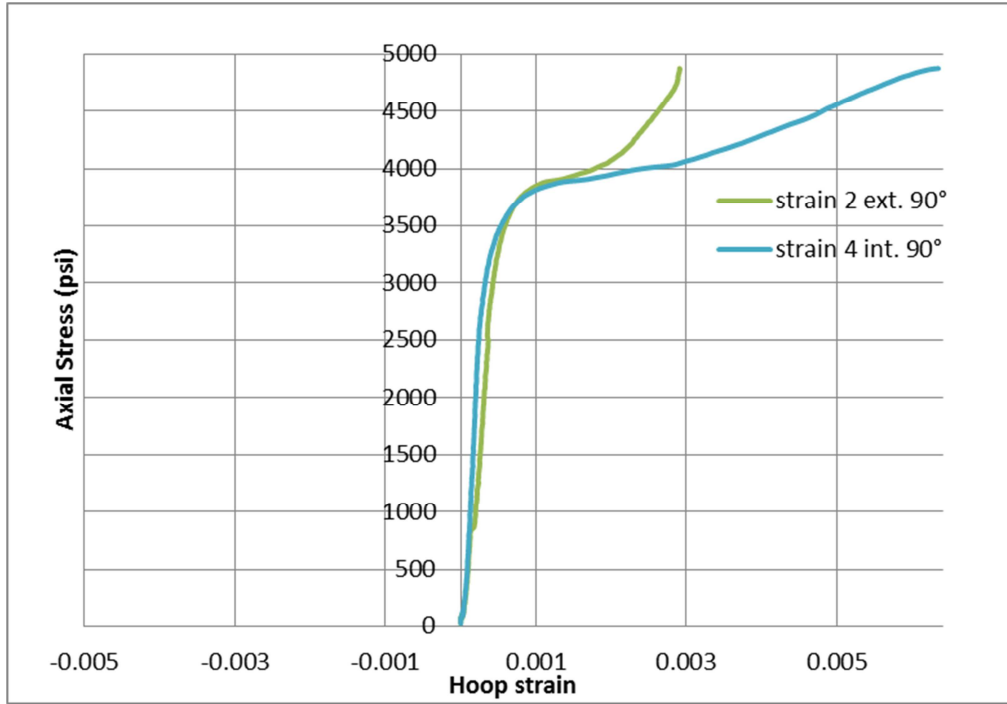


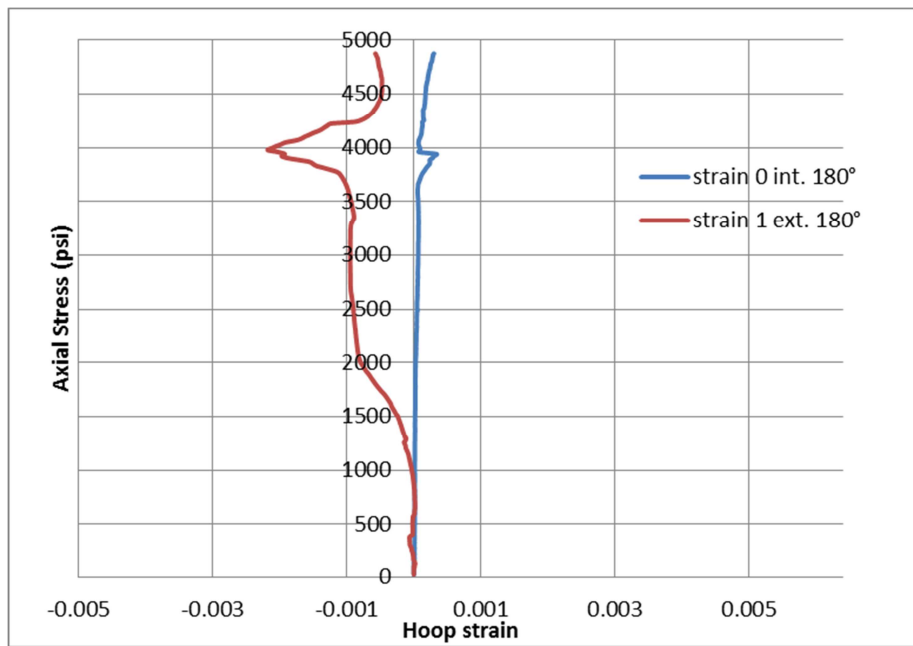
Figure 6.3 Axial Stress versus hoop strain for specimen B1C2L2B

Figure 6.4 shows the values of hoop stress versus hoop strain separated by location. In Figure 6.4(a) the axial stress versus the hoop strain measured by the gages located on the left side of the GFRP lap are shown. The strain values have similar values and shape until the unconfined compressive strength of the concrete is achieved. After that, the gage located in the exterior (outer layer) measured less strain compared to the gage located in the interior (inner layer). A similar phenomenon occurred in strain gages 0 and 1 as shown in Figure 6.4(b), the exterior layer received less strain than the interior layer. It is also important to note that strain gage 1 had negative strain values, suggesting that it received compressive strain. As strain gage 1 was located near one of the failures of the GFRP confined system its proximity to the failure location could account for this unexpected reading.

In Figure 6.4(c) the trend is repeated where both strains showed similar behavior until the concrete's unconfined strength was reached, and then the exterior strain gage (strain 3) measured less strain than on the interior layer (strain 5).



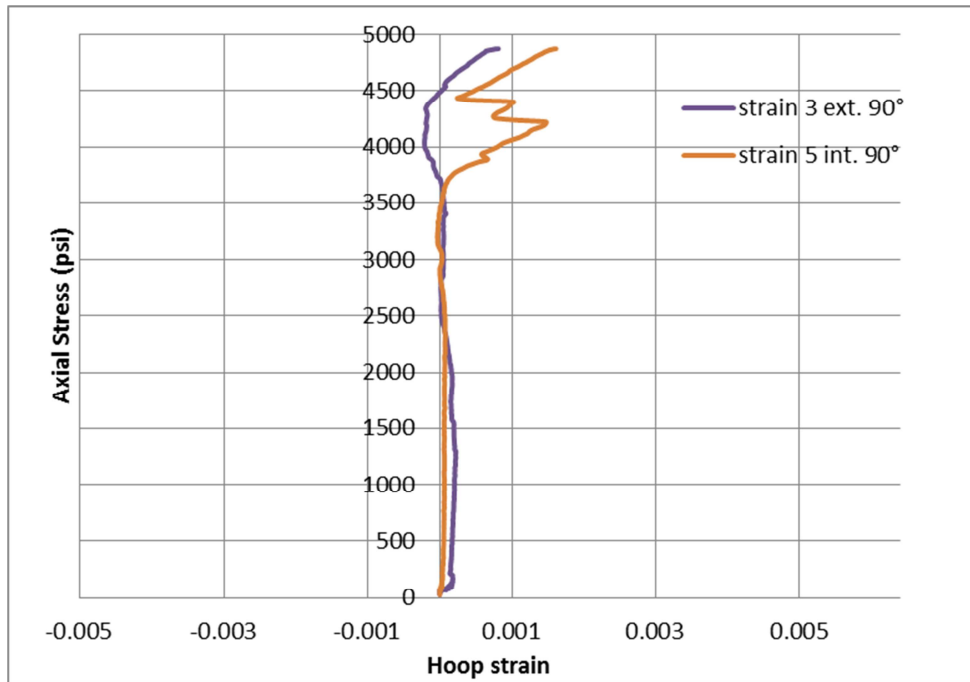
(a)



(b)

Figure 6.4 Axial Stress versus hoop strain for specimen B1C2L2B separated by location.

(a) left 90°. (b) middle 180°. (c) right 90°.



(c)

Figure 6.4 Continued

Figure 6.5 shows the failure mode of B1C2L2B from the right 90° side (near strain gage 5 and strain gage 3). Strain gages 0, 1, 2, 3, and 5 were all located near or over the failure, the FRP jacket broke all around the specimen in a hoop shape. Strain gage 4 was the only strain that was not near a failure and hence the one that exhibit greater strain values. Even though strain gage 2 is located in the same area as strain gage 4 they are at different heights, exhibiting different hoop strain values.



Figure 6.5 B1C2L2B failure mode

6.3.1.2 B1C3L2B

Results from specimen B1C3L2B are shown in Figure 6.6. Strain gage 2 (ext. 90°) was damaged during testing and therefore values from that gauge are not shown here. As observed for the preceding specimen, the strain values are similar until the unconfined compressive strength of the specimen is achieved. Again, these differences in strains while the confinement is engaged show that the GFRP is not sharing strain uniformly around the wrap.

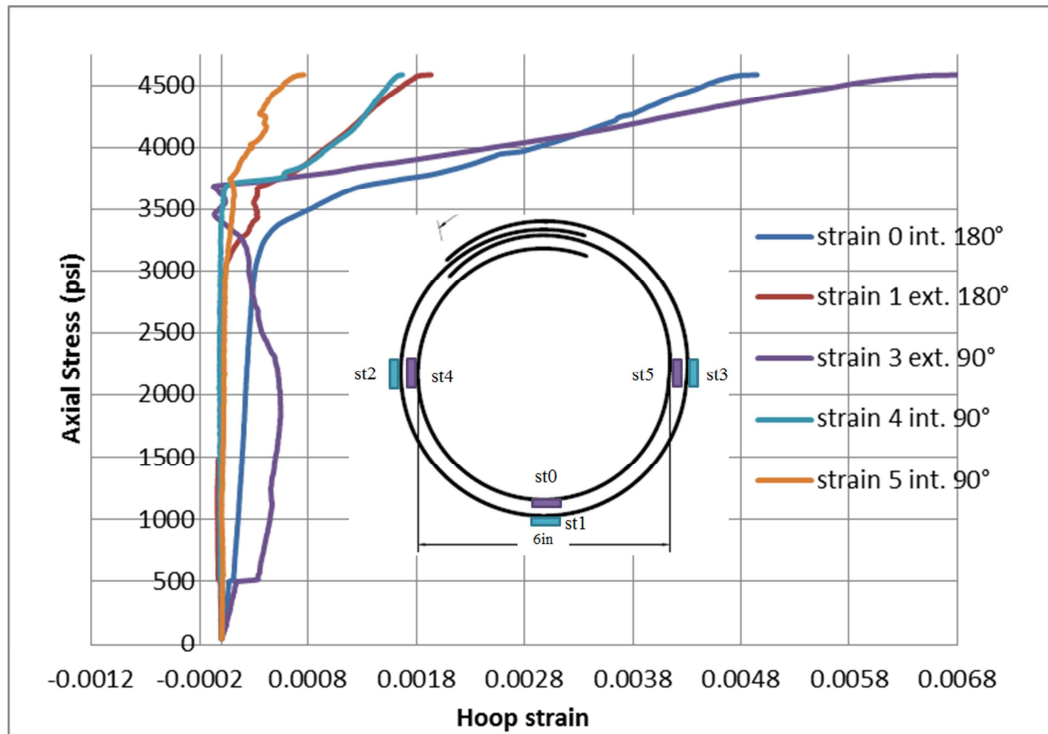
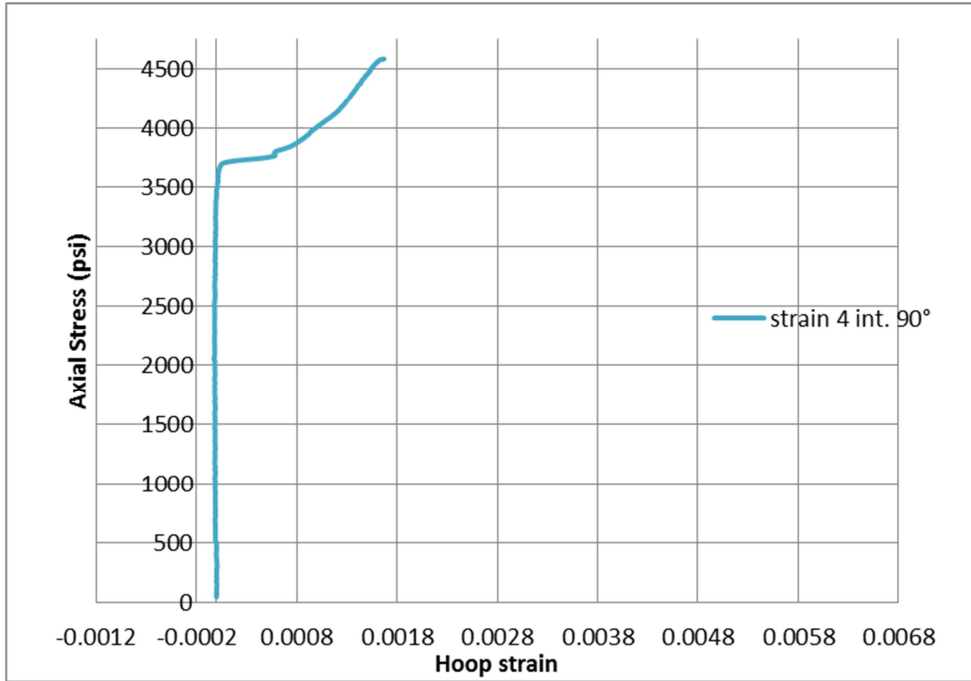
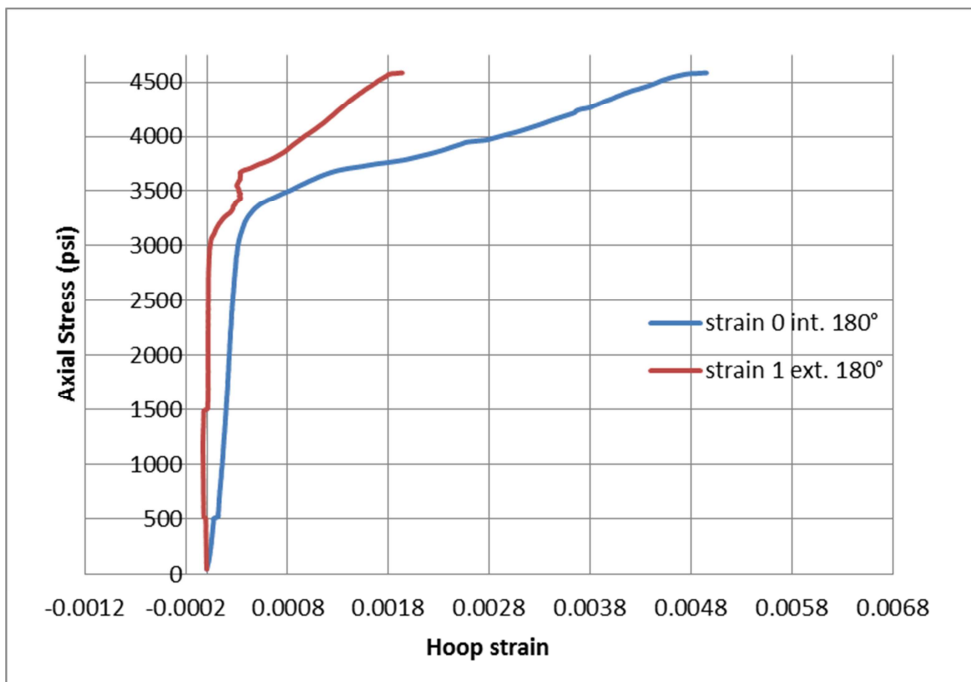


Figure 6.6 Axial Stress versus hoop strain for specimen B1C3L2B

Figure 6.7 shows the values of axial stress versus hoop strain separated by location. In Figure 6.7(a) the axial stress versus the hoop strain of the strains located in the left side are shown. Strain 2 was omitted due to damage. Figure 6.7(b) shows the strain values opposite from the overlap region. Strain gages 0 and 1 exhibited similar behavior as the one mentioned in Figure 6.4(a). Also, the exterior strain gage (strain 1) recorded lower strain values than the interior strain gage (strain 0), suggesting again that the interior layer is subjected to more strain than the exterior layer. But in Figure 6.7(c) the trend is flipped showing the exterior strain gage (strain 3) receiving more strain than the interior layer (strain 5). However, this strain gage (strain 5) does not have the typical stress-strain curve. This exception to the trend may be due to the fact that strain gage 5 was located near the failure of the composite specimen.



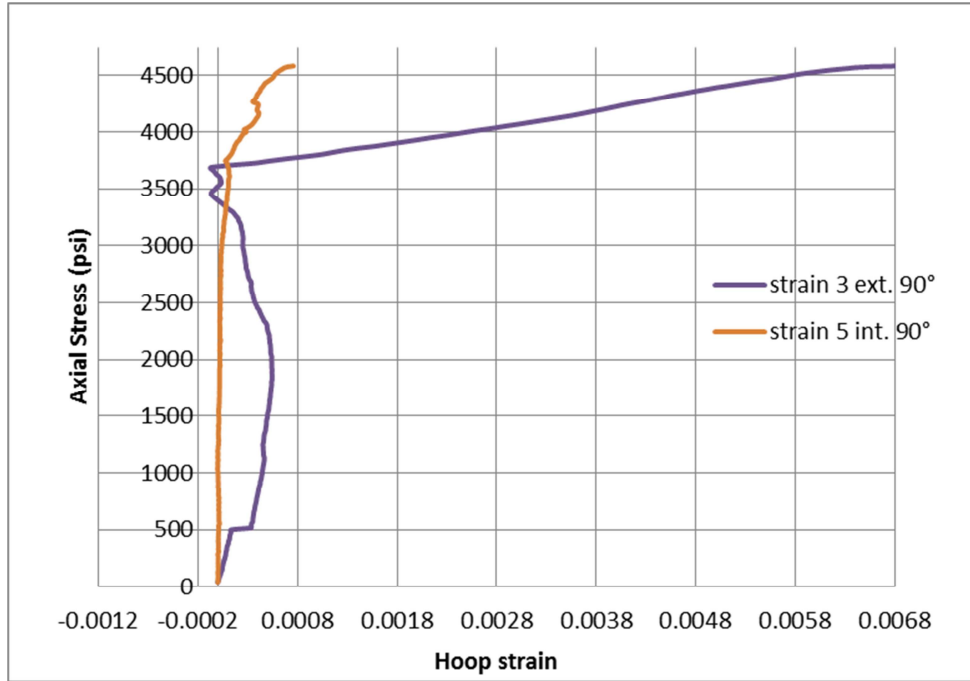
(a)



(b)

Figure 6.7 Axial Stress versus hoop strain for specimen B1C3L2B separated by location.

(a) left 90°. (b) middle 180°. (c) right 90°.



(c)

Figure 6.7 Continued

6.3.2 Two layer GFRP Multidirectional

6.3.2.1 B2C1L2M

Specimen B2C1L2M axial stress versus hoop strain is shown in Figure 6.8. It can be observed that all the strains gages, except for strain 3 ext. 90°, recorded a similar behavior up to the unconfined concrete strength. Once the confinement activated, the curves' shapes changed because these strain gage locations measured lower or greater strain values relative to each other because strain is not shared uniformly around the FRP jacket. The negative behavior of strain gage 3, which was the exception to the typical behavior, may be attributed to the fact that it was in the failure area. Figure 6.9 shows the failure location of this specimen. Note that strain gage 3 is not pictured because it was in the ruptured surface and thus popped out of the specimen at the end of the test. Gages 2,

4, and 5 engaged at around 3300 psi and gages 0, 1, and 3 at around 3700 psi. Gage 5 (interior) engaged before gage 3 (exterior) suggesting that the interior layer receives more strain at the beginning of the test.

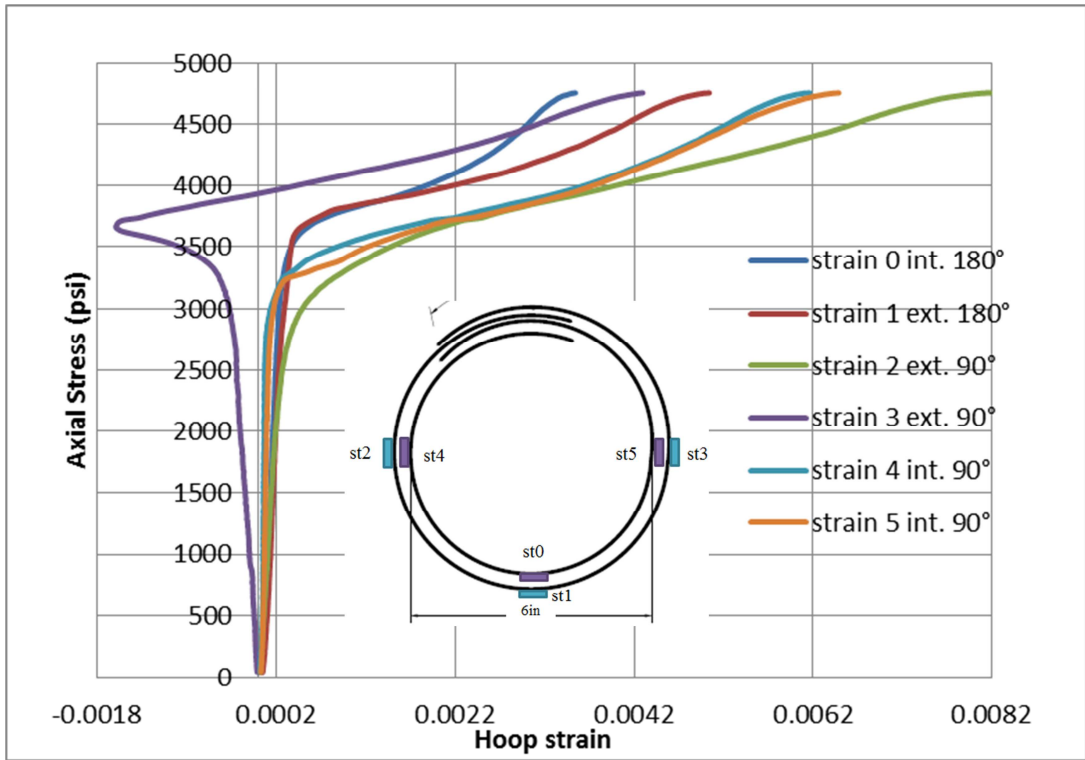


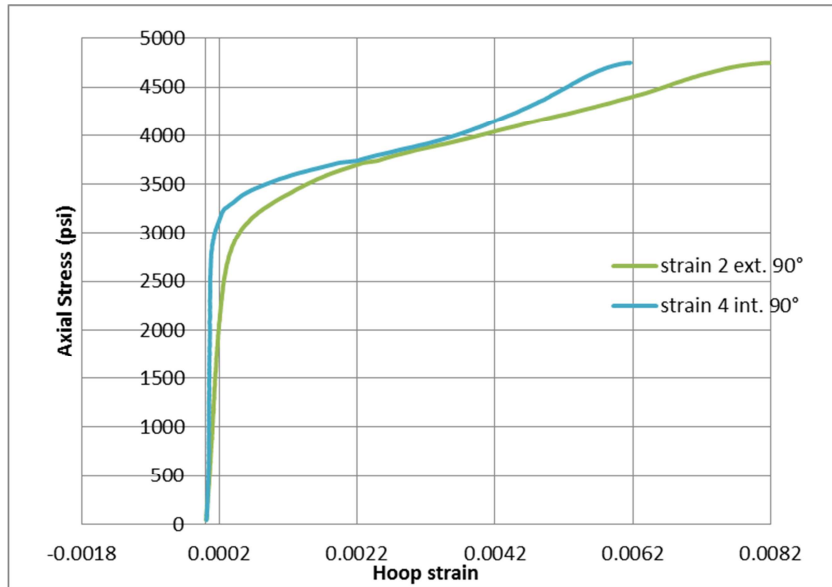
Figure 6.8 Axial Stress versus hoop strain for specimen B2C1L2M



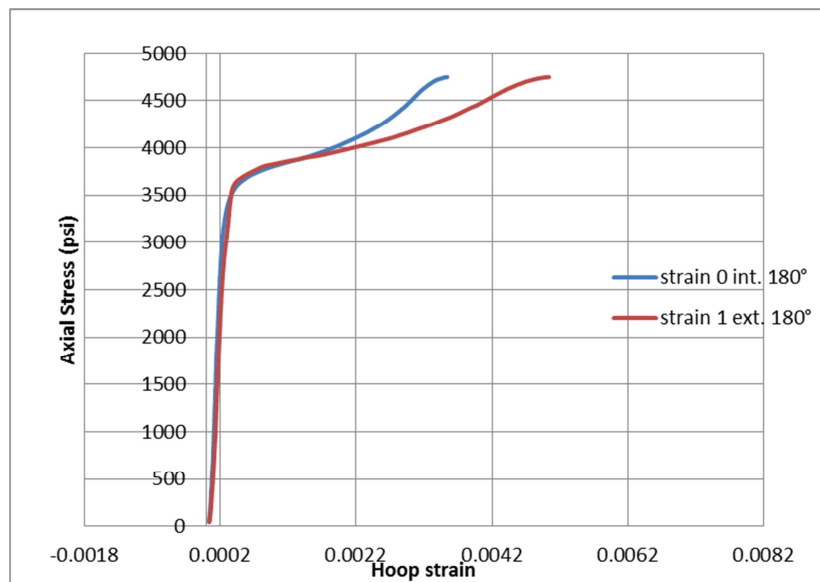
Figure 6.9 B2C1L2M failure mode

Figure 6.10 shows the values of axial stress versus hoop strain separated by location. Figure 6.10(a) shows the axial stress versus the hoop strain of the strains located in the left side of the overlap region. The strain values have similar values and shape until the unconfined compressive strength of the concrete is achieved. After that, the strain located in the interior (layer 1) was subjected to less strain compared to the strain measured in the exterior (layer 2). A similar phenomenon occurred at strain gages 0 and 1 as shown in Figure 6.10 (b). At this location opposite to the overlap region, the interior layer received less strain than the exterior layer. This behavior is opposite from the one observed in section 6.3.1 with the bidirectional GFRP. In Figure 6.10 (c) the gages showed opposite behavior; the exterior gage (strain 3) measured negative strain values before the GFRP jacket activated, suggesting that it received compressive strain. This situation may be due to the fact that strain gauge 3 was located on the failure surface of the GFRP confined system or as explained in section 6.3.1.1, due to volume expansion.

Once the GFRP confined system engaged, both gages (strain 3 and 5) measured the same rate of strain. Also is important to note that the interior gage (strain 3) engaged before the exterior one (strain5).



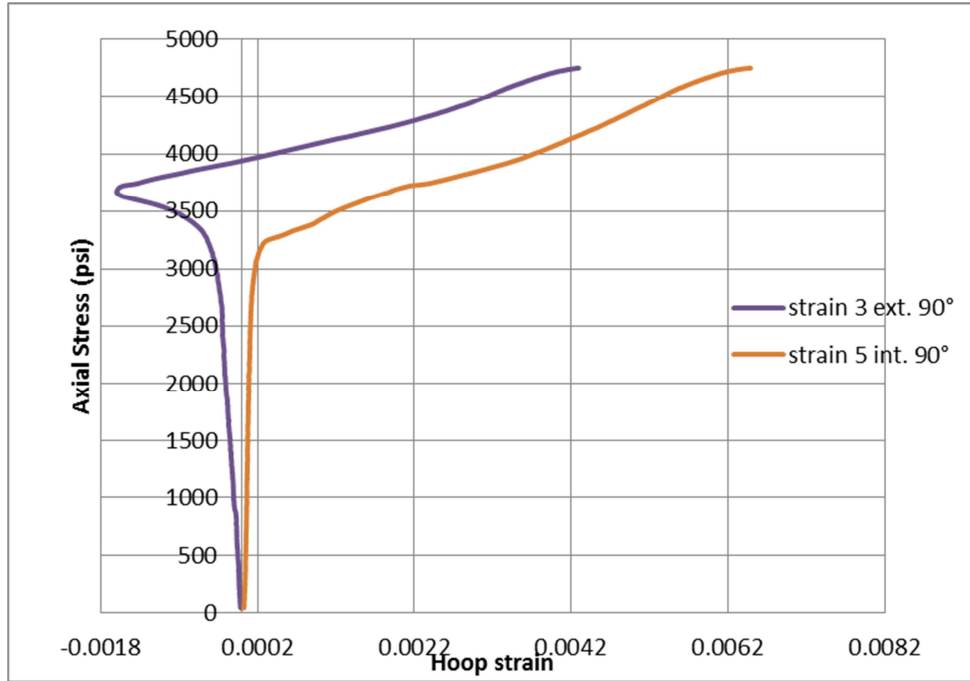
(a)



(b)

Figure 6.10 Axial Stress versus hoop strain for specimen B2C1L2M separated by location.

(a) left 90°. (b) middle 180°. (c) right 90°.



(e)

Figure 6.10 Continued

6.3.2.2 B2C2L2M

Specimen B2C2L2M axial stress versus hoop strain is shown in Figure 6.11. It can be observed that strain gages 0, 1, 4, and 5 showed a similar behavior up to the unconfined strength and then the shapes of the curves changed because strain was not shared uniformly throughout the GFRP wrap. Gage 2 also showed a similar behavior to the gages mentioned before with the only difference that it had an initial bump at the beginning of the test. The loss of strain observed at around 3750 psi for gage 1 can be attributed to the fact that it was on the failure area. Figure 6.12 shows the failure mode, strain gage 1 became a little detached from the specimen during testing.

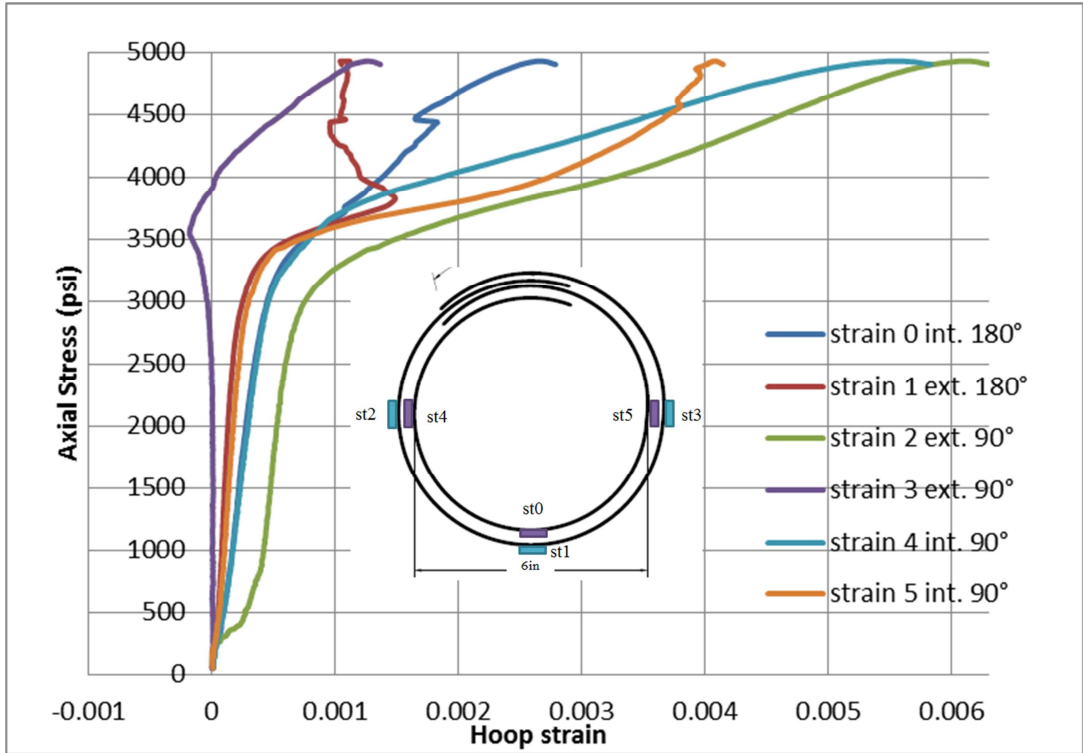


Figure 6.11 Axial Stress versus hoop strain for specimen B2C2L2M

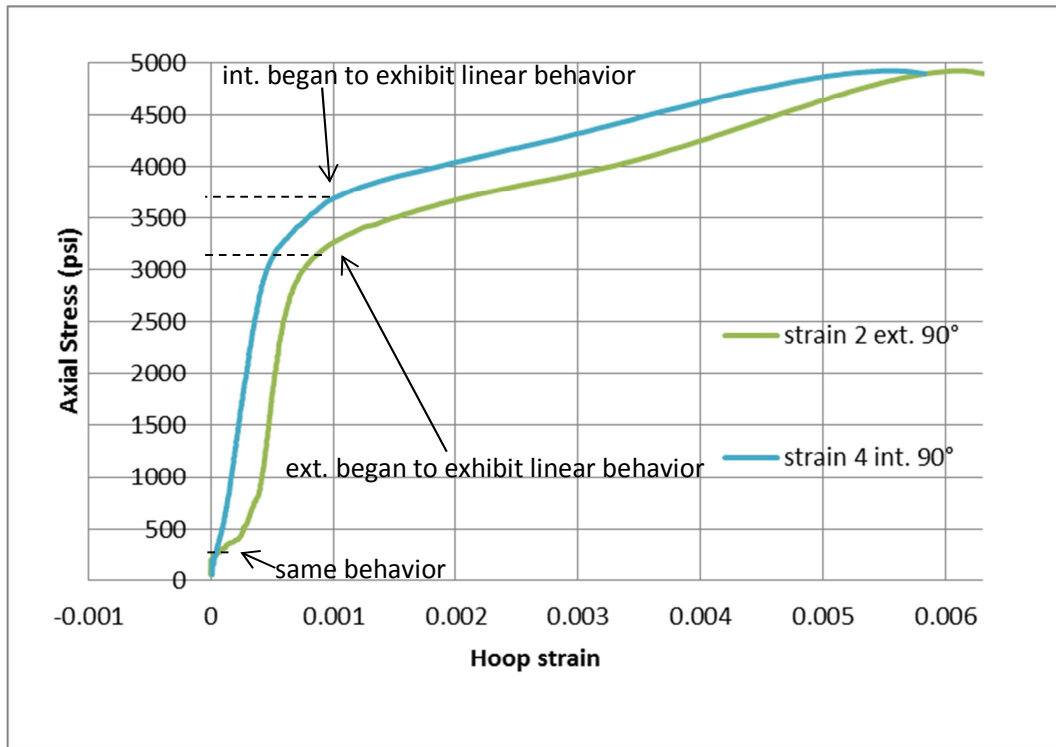


Figure 6.12 B2C2L2M failure mode

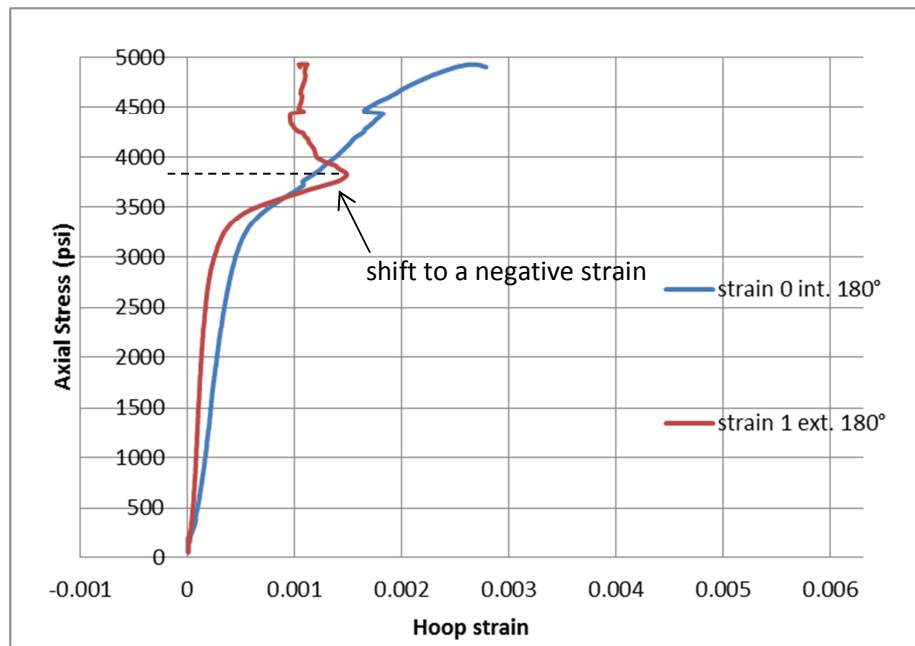
Figure 6.13 shows the values of axial stress versus hoop strain separated by location. Figure 6.13 (a) shows the axial stress versus the hoop strain measured by the

strain gages located on the left side of the overlap region. The strain gages had the same strain up to about the 250 psi mark, then there was a shift and the exterior strain gage gained more strain. This may be because strain gage 2 was near the failure of the GFRP jacket and the system activated earlier than in other zones. Except for the gap developed when the shift occurred, the strain values were similar in values and shape until the axial stress reached around 3100 psi. At this point, the FRP jacket became engaged in the area where the strain gage 2 (exterior) was placed and began to exhibit linear behavior dominated by the stiffness of the FRP-confined concrete. After that, at around 3600 psi, strain gage 4 (interior) began to exhibit this linear behavior. The interior gage (layer 1) is subjected to less strain compared to the gage located in the exterior (layer 2).

In Figure 6.13(b), it was observed that during the linear elastic period the interior wrap was taking more strain than the exterior one but as the wraps were just beginning to engage, the exterior gage was starting to take strain at a much higher rate until it reached around 3750 psi and gage 1 lost some strain because it was located near where the wrap was yielding. In Figure 6.13(c) the exterior layer gained very little strain and slightly lost strain prior to reaching f'_c . After that, when the GFRP jacket was activated, the exterior layer began to take tensile hoop strains but it never reached the same levels as the interior wrap.



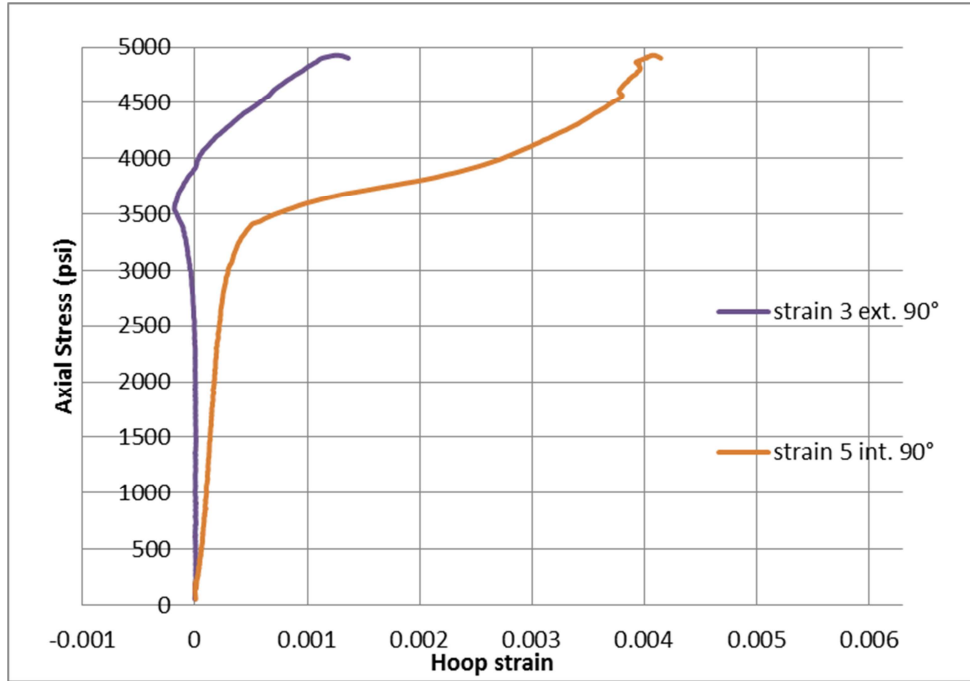
(a)



(b)

Figure 6.13 Axial Stress versus hoop strain for specimen B2C2L2M separated by location.

(a) left 90°. (b) middle 180°. (c) right 90°.



(e)

Figure 6.13 Continued

6.3.2.3 B2C3L2M

Specimen B2C3L2M axial stress versus hoop strain is shown in Figure 6.14. It can be observed that all the strain gauges recorded showed a similar strain behavior up to the unconfined concrete strength. At this point when the GFRP engaged, the shapes of the curves changed because the GFRP does not share strain uniformly throughout the wrap. As well, the shape of the stress-strain curve at strain gage 0 deviates from typical when this gage appears to fail at around 4900 psi. Figure 6.15 shows the failure mode of the specimen, strain gage 5 broke at the end of the test because it was on the failure area.

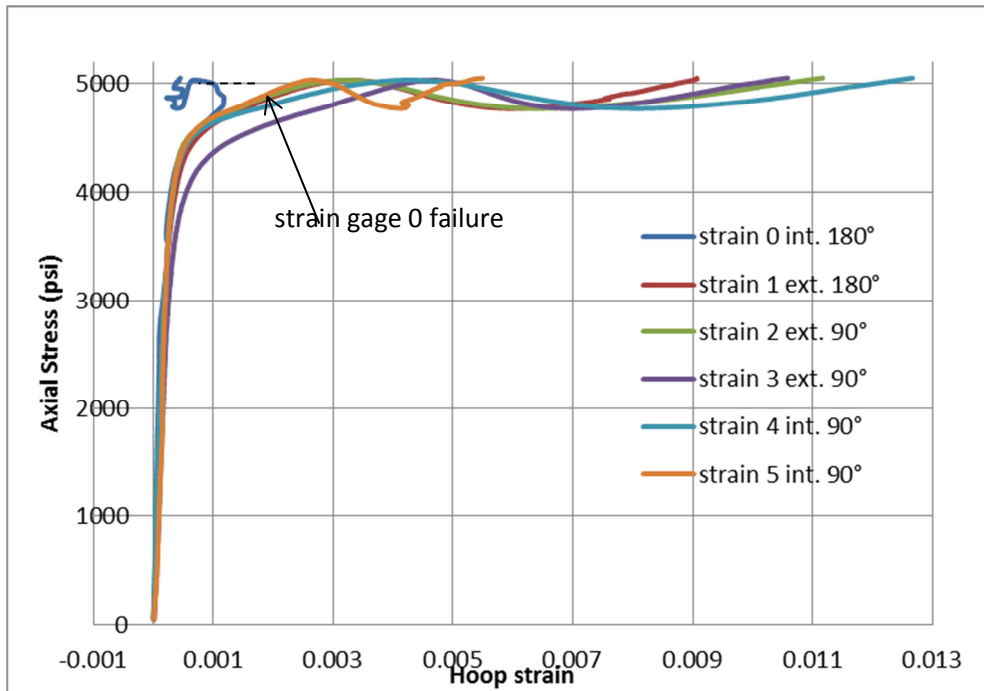


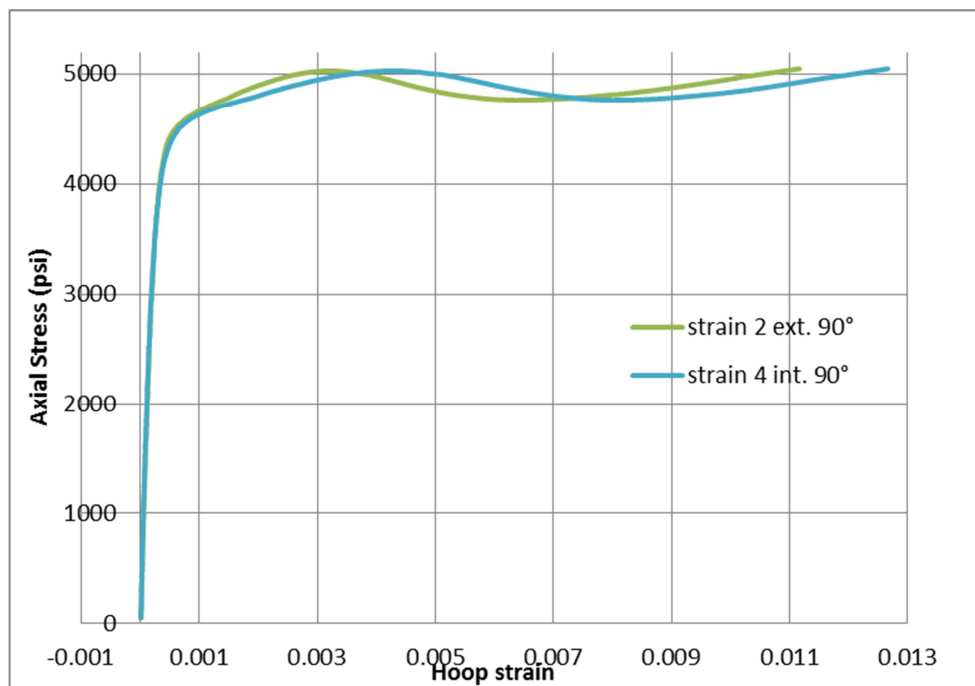
Figure 6.14 Axial Stress versus hoop strain for specimen B2C3L2M



Figure 6.15 B2C3L2M failure mode

Figure 6.16 shows the values of axial stress versus hoop strain separated by location. In Figure 6.16(a) the axial stress versus the hoop strain of the strains located in the left side are shown. The strain values are very similar, it can be assumed that both strain shared almost the same strain and shape except that after the GFRP jacket engaged,

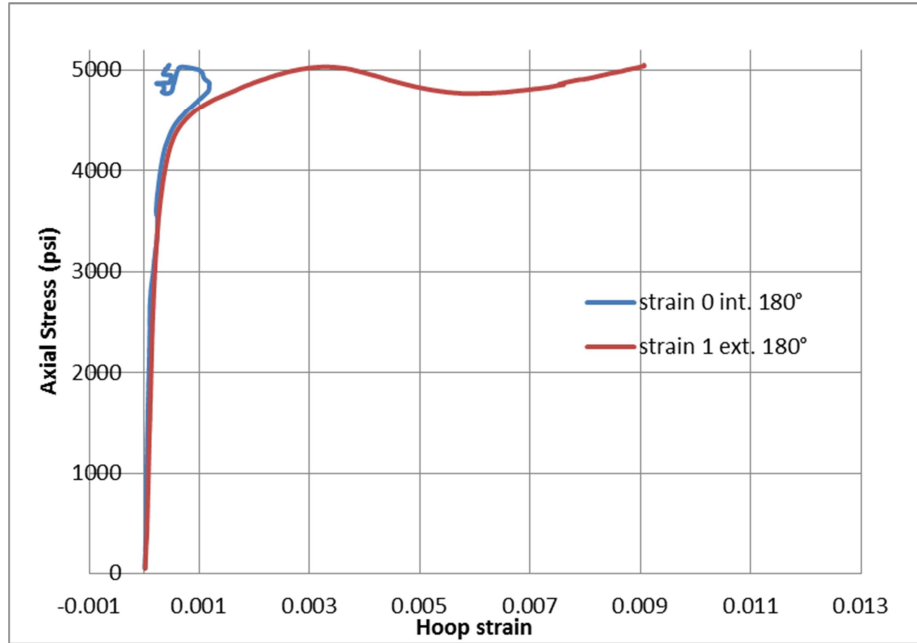
the interior layer consistently gained more strain than the exterior layer. It is important to note that this was the only part of the specimen where the interior layer carried more strain than the exterior layer. In Figure 6.16(b), strain gage 1 showed a similar behavior as strain gages 2 and 4 but strain gage 0 failed when it reached 4900 psi. The exterior layer was gaining strain more rapidly than the interior layer until the interior gage (strain 0) failed. In Figure 6.16(c) both strains showed similar behavior until the unconfined strength was reached, strain gage 5 received less strain because it was located in the failure zone.



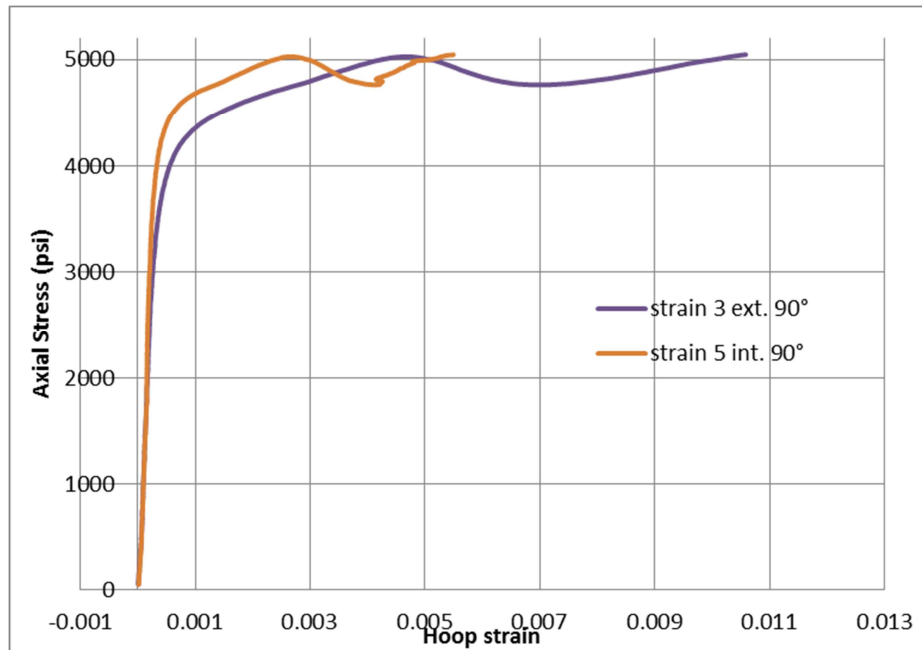
(a)

Figure 6.16 Axial Stress versus hoop strain for specimen B2C3L2M separated by location.

(a) left 90°. (b) middle 180°. (c) right 90°.



(b)



(c)

Figure 6.16 Continued

6.3.3 Summary of GFRP-Confined Concrete Cylinders with Two Layers

Section 6.3 discussed the results for GFRP-confined concrete cylinders with two layers. Specimens with bidirectional GFRP wraps exhibited a consistent trend where the exterior layer measured less strain than the interior layer and thus exhibited a greater stiffness versus the interior layer. This phenomenon may be because the interior layer was attached directly to the concrete and thus was the first to confine the deformations of the concrete receiving the axial stress.

Specimens with multidirectional GFRP wraps, however, exhibited the opposite trend versus the bidirectional wraps. The interior layer measured less strain than the exterior layer and thus exhibited the greater stiffness. This difference in behavior between different GFRP wraps may be due to the direction of the fabric. For specimens with multidirectional GFRP wraps, this trend was not consistent, with one out of the three sets of gages (interior and exterior gage on three different locations) for each specimen exhibiting the same behavior as bidirectional GFRP wraps where the exterior gage measured less strain than the interior gage. This deviation from the multidirectional strain sharing trend may be because those gages were located near a failure or because at some point in the test it received a negative volumetric strain.

6.4 GFRP-Confined Concrete Cylinders with Three Layers

Three cylinders of each type of GFRP (three layers of bidirectional or three layers of multidirectional) were tested while monitoring hoop strain and axial load. The results from specimen B1C2L3B were discarded due calibration of the DAQ system, this specimen reached a confined concrete strength of 4803 psi.

6.4.1 Three layer GFRP Bidirectional

6.4.1.1 B1C1L3B

Specimen B1C1L3B axial stress versus axial strain is shown in Figure 6.17. It can be observed that all the strains gages, except strain gage 2, showed a similar behavior up to the unconfined concrete strength, whereupon the stress-strain curves separated because the strain gages did not share the same amount of strain. It also can be observed that strain gage 0 (int. 90°) had greater strain values than the rest of the strain gages. This higher strain level may be because strain gage 0 was away from the rupture of the jacket and was able to achieve higher strain values.

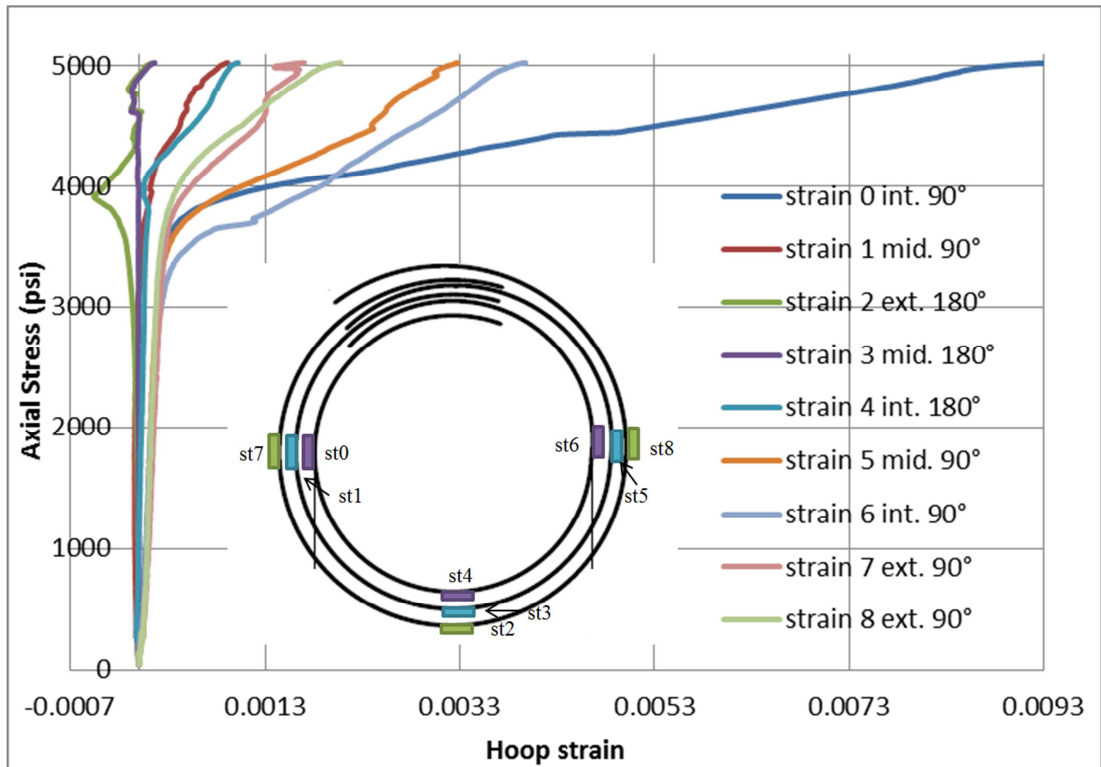
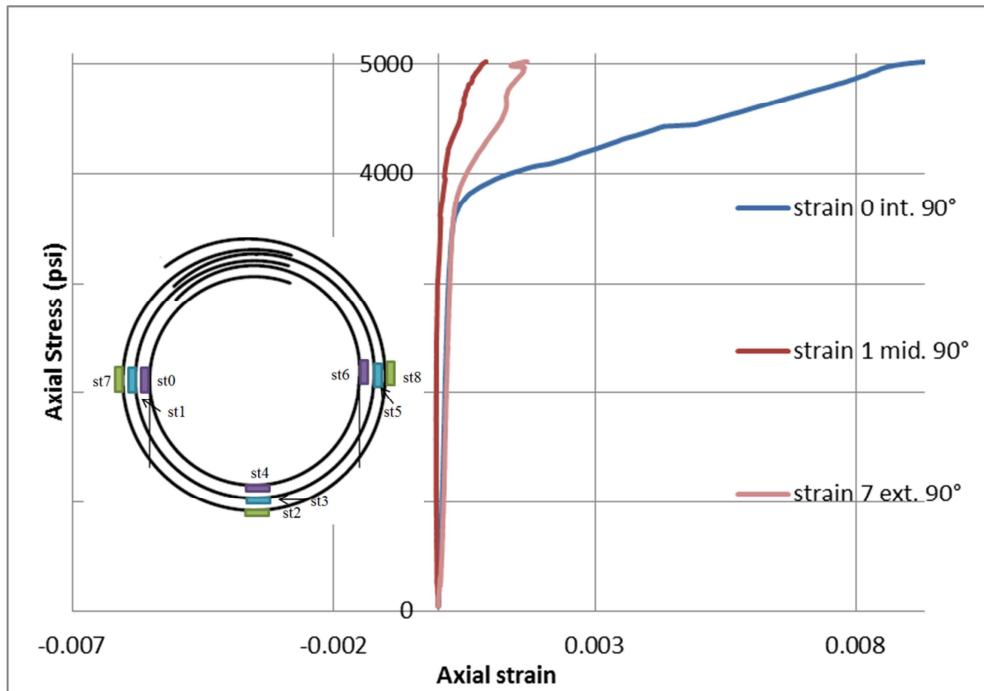
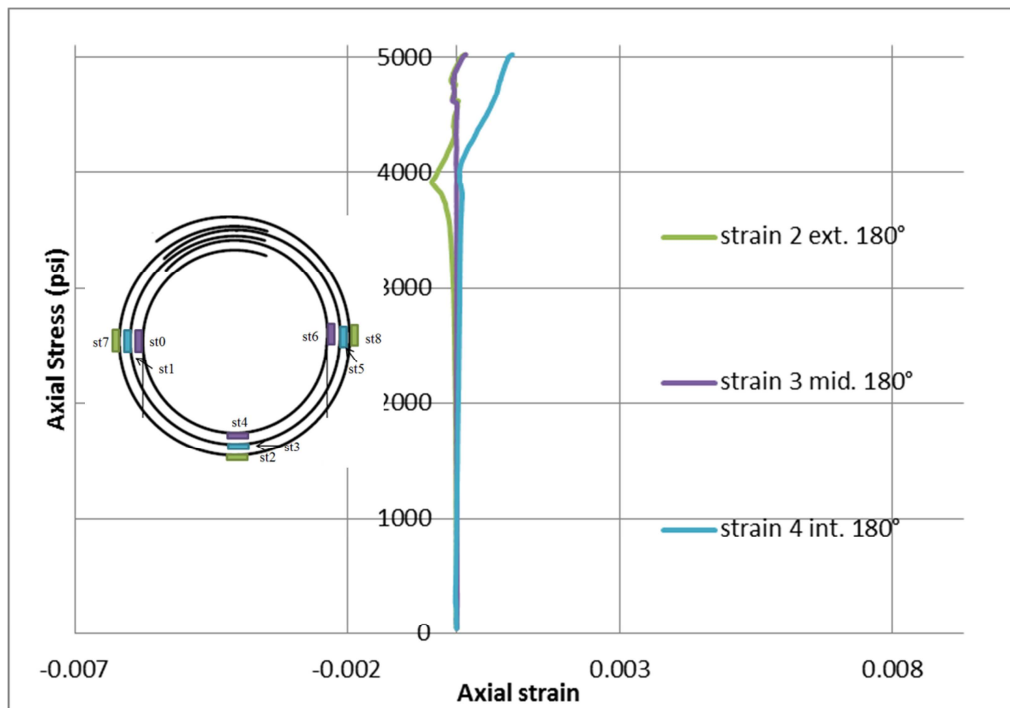


Figure 6.17 Axial Stress versus hoop strain for specimen B1C1L3B

Figure 6.18 shows the values of hoop stress versus hoop strain separated by location. In Figure 6.18(a) the axial stress versus the hoop strain measured by the gages located on the left side of the GFRP lap are shown. The strain values have similar values and shape until the unconfined compressive strength of the concrete is achieved. After that, gage 1 and 7 gained less tensile strain compared to the gage located in the interior (gage 0). This difference may be because the interior layer of FRP is the first to confine the concrete and thus might receive greater hoop strain. The middle layer received the least strain and while the outer layer had a little more strain, none of them were close to the failure of the GFRP jacket. Figure 6.18(b) shows that in this location there was very little strain recorded. Strain gage 2 had negative strain values when it reaches around 3600 psi, suggesting that it received compressive strain. As strain gage 2 was located near the failure of the GFRP confined system its proximity to the failure location could account for this unexpected reading. As mentioned before, a negative strain could also be due to the volume expansion called negative volumetric strain. Strain gage 3 almost did not receive any strain. It practically has a straight vertical line, suggesting that either the strain gage was placed incorrectly or this layer and location was relatively unaffected during the test. Strain gage 4 achieved the greatest strain of this location, although still only a modest tensile strain value for the test, suggesting again that gages in the interior layer received more strain. In Figure 6.18(c) the strain gages had similar shape and behavior but the interior layer attracted the greatest strain values and the exterior layer had the smallest strain values. In all of the locations (Figure 6.18a, b and c) the interior layer exhibited the highest strain values.



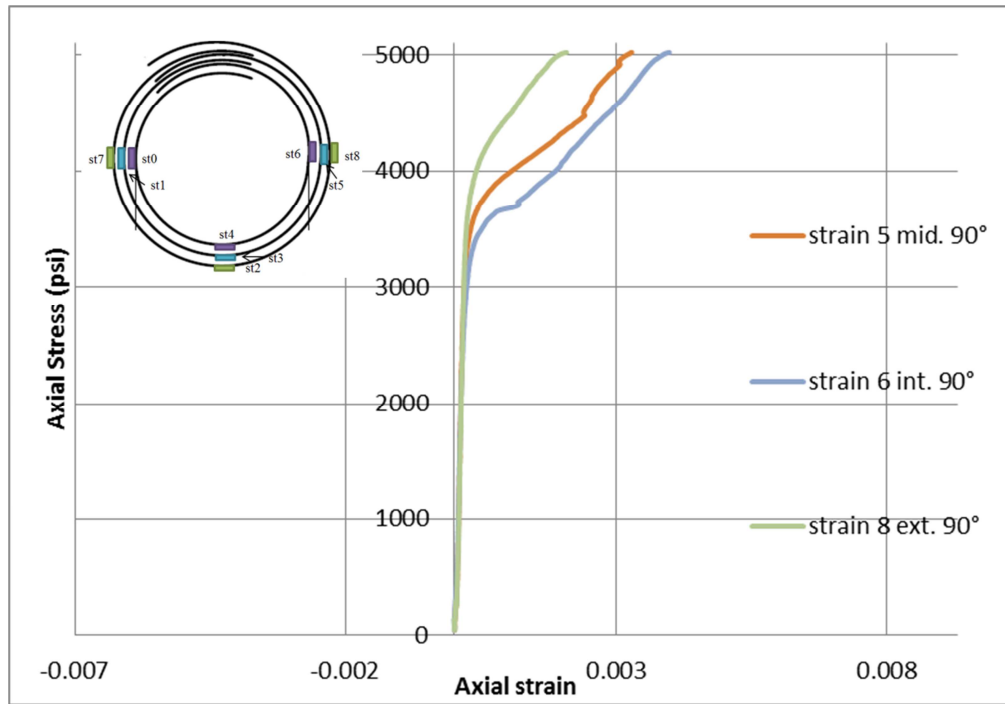
(a)



(b)

Figure 6.18 Axial Stress versus hoop strain for specimen B1C1L3B separated by location.

(a) left 90°. (b) middle 180°. (c) right 90°.



(c)

Figure 6.18 Continued

6.4.1.2 B1C3L3B

Results from specimen B1C3L3B are shown in Figure 6.19. At around 2200 psi, strain gage 4 measured a loss in tensile strain and then gained tensile strain again until about 4800 psi. At the 4800 psi point all of the gages showed a change in the stress-strain curves probably because the cylinder was going to fail but the FRP jacket stopped the failure. The rest of the gages had a similar stress-strain curve shape until it reached the unconfined compressive strength of the concrete at around 3400 psi. At this point the jacket activated and the strain readings changed for each gage. Strain gage 8 experienced the greatest strain, and this high strain reading may be because this gage was not near the failure of the jacket.

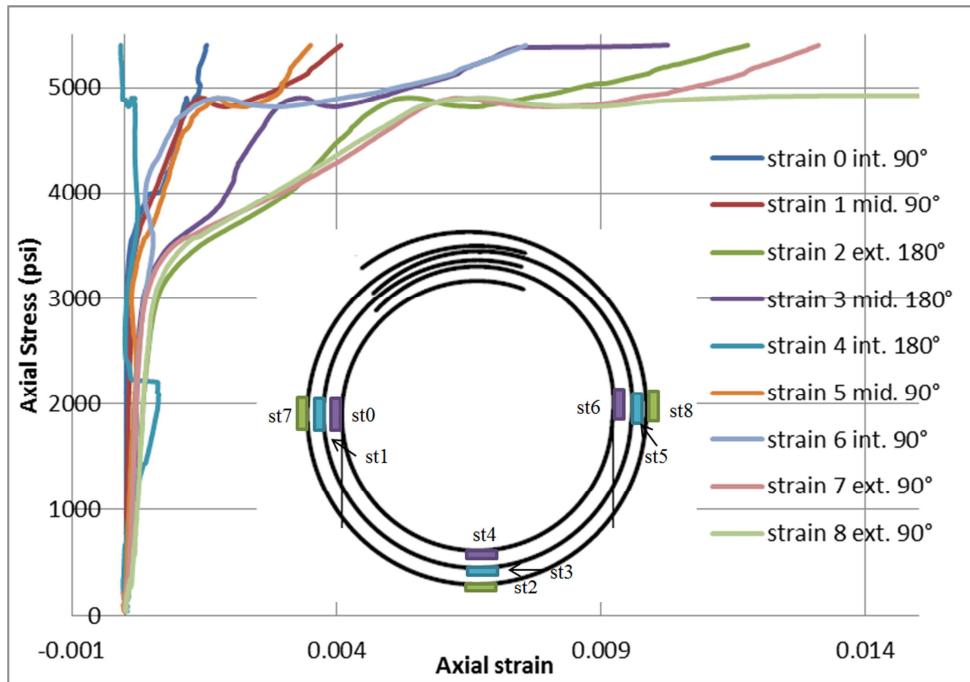
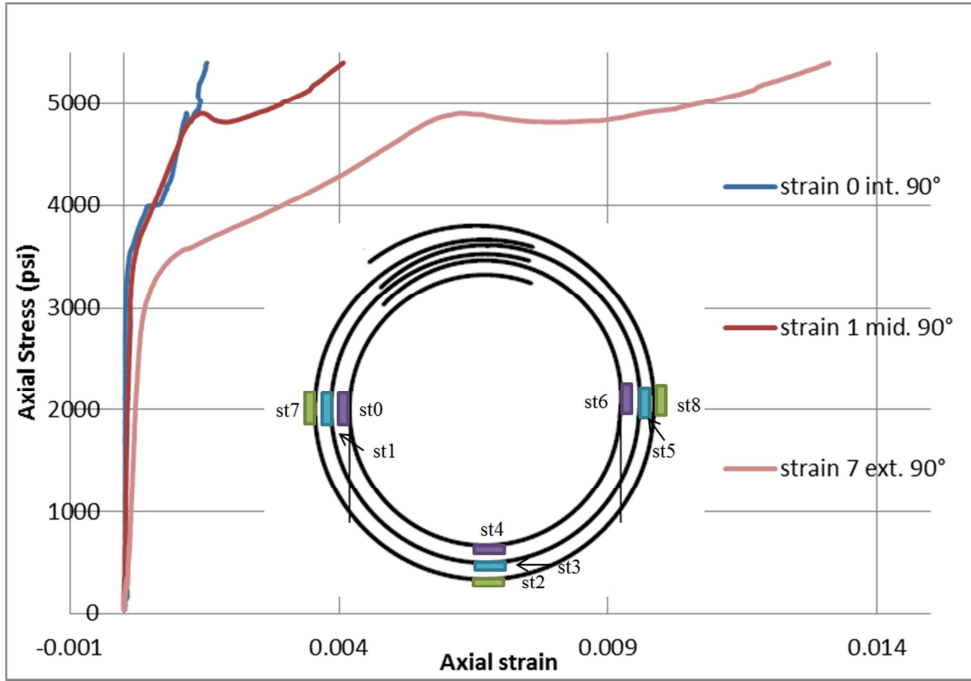
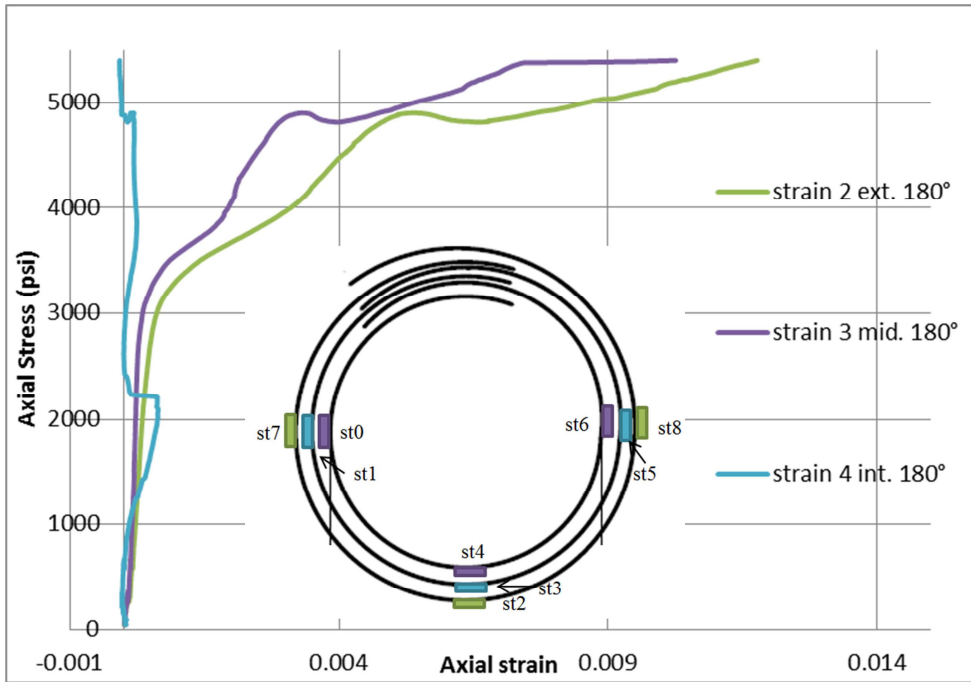


Figure 6.19 Axial Stress versus hoop strain for specimen B1C3L3B

Figure 6.20 shows the values of axial stress versus hoop strain separated by location. In Figure 6.20(a) the axial stress versus the hoop strain of the strains located in the left side are shown. Strain gage 0 was located near the failure and measured less strain compared to the other two gages. The exterior gage received the most strain at this location. In comparison with the last specimen, these gages showed the opposite behavior because the exterior layer had more strain than the interior one. Figure 6.20(b) shows the strain values opposite from the overlap region. This set of gages behaved the same way as the set on the left side: the interior layer measured less strain than the exterior one. It is also important to note that gage 4 did not have the typical strain-stress curve. Instead, it had more of a vertical straight line. The trend repeated again in Figure 6.20(c), with the middle layer gage measuring the least total tensile strain and the exterior gage measuring the greatest tensile strain.



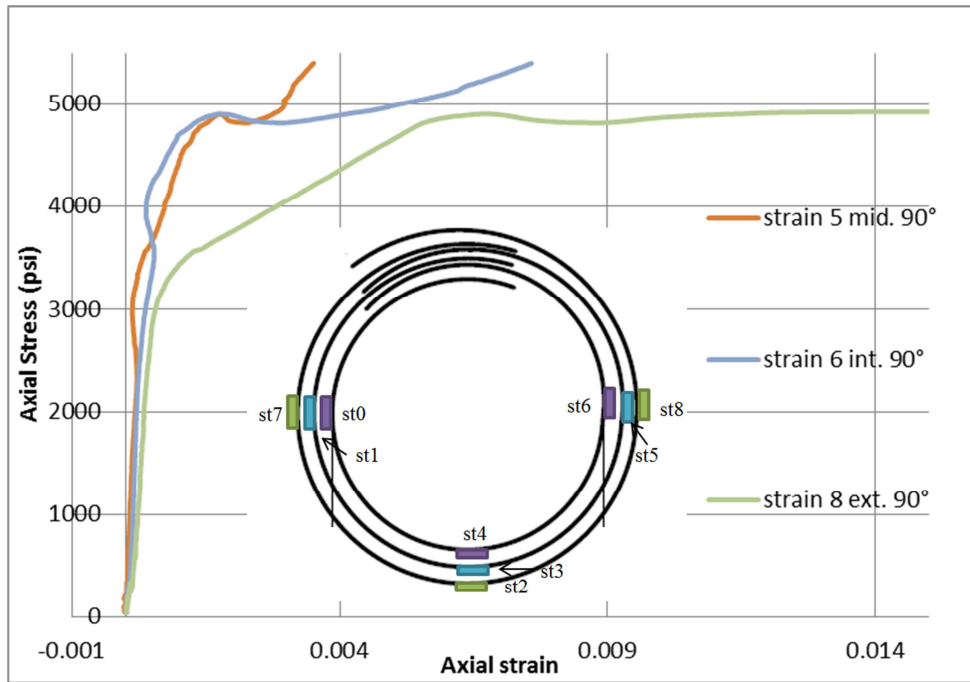
(a)



(b)

Figure 6.20 Axial Stress versus hoop strain for specimen B1C3L3B separated by location.

(a) left 90°. (b) middle 180°. (c) right 90°.



(c)

Figure 6.20 Continued

6.4.2 Three layer GFRP Multidirectional

6.4.2.1 B2C1L3M

Specimen B2C1L3M axial stress versus axial strain is shown in Figure 6.21.

Strain gages 4 and 6 measured a change in the stress-strain behavior that signaled the FRP wrap was engaged at those locations earlier than the other gages at around 2300 psi. Strain gage 6 also measured the greatest maximum tensile strain value. Gages 0, 2, and 8 indicated the FRP wrap had engaged at their locations around 2800 psi and the rest of the gages indicated FRP wrap engagement at 3400 psi.

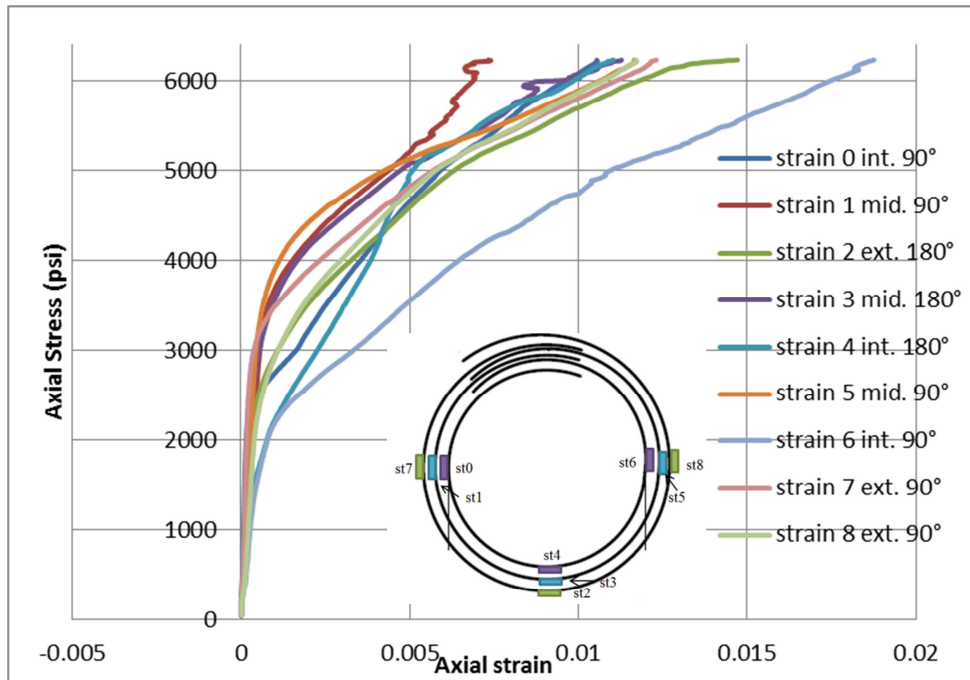
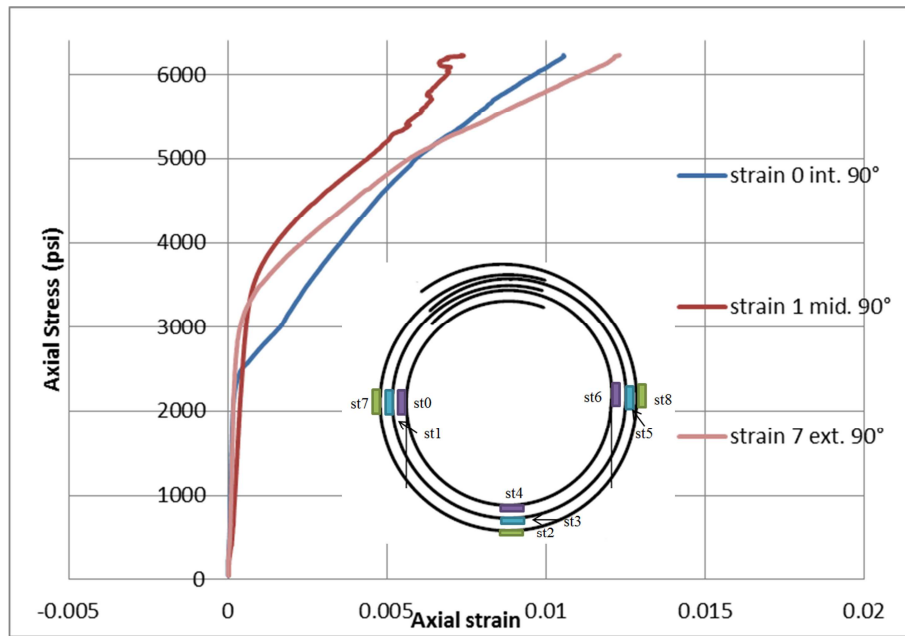


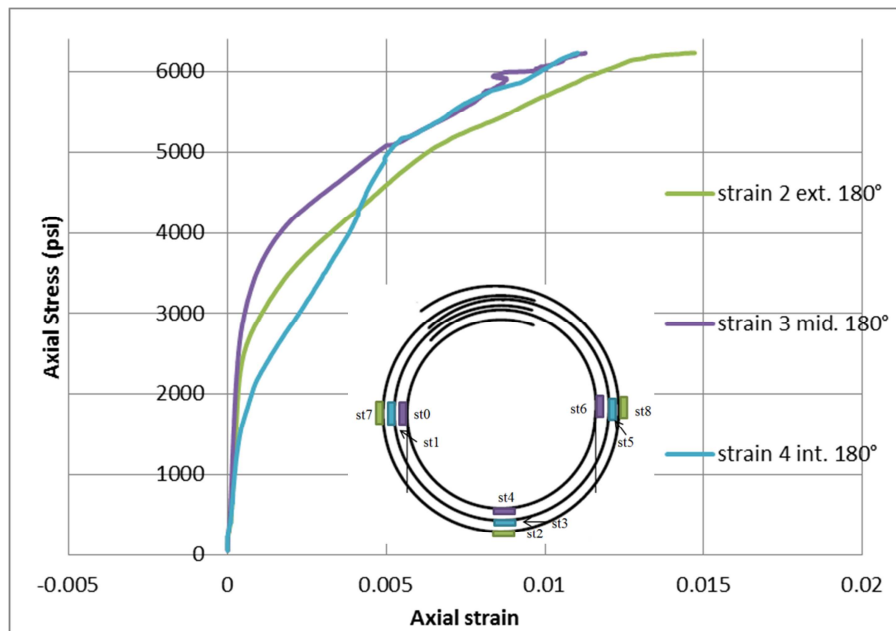
Figure 6.21 Axial Stress versus hoop strain for specimen B2C1L3M

Figure 6.22 shows the values of axial stress versus hoop strain separated by location. In Figure 6.22(a) is shown that interior layer of the FRP wrap monitored by strain gage 0 engaged earlier than at the other two gages. The exterior gage measured the greatest final strain and the middle layer gage recorded the lowest strain. This set of gages exhibit the same trend as specimen B1C3L3B. Figure 6.22(b) shows the strain values opposite from the overlap region. The strain sharing trend from Figure 6.22(a) was repeated here. The exterior gage measured the highest strain final strain although the interior layer of the FRP wrap engaged earlier. The middle and interior layers' gages measured almost the same final strain. In Figure 6.22(c) the trend shown was the opposite of figures a and b and therefore exhibited the same trend as specimen B1C1L3B. The interior layer measured the highest strain while the exterior and middle layers had the lowest final tensile strain. At the beginning, the exterior layer measured more strain than

the middle layer but at around 5500 psi they level up and ended with the same strain values.



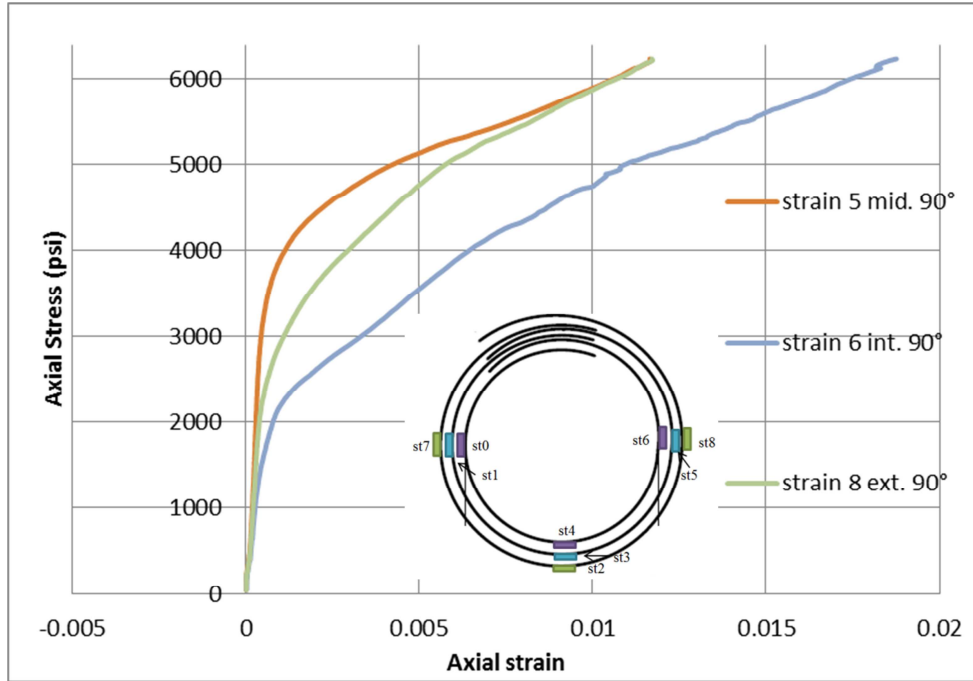
(a)



(b)

Figure 6.22 Axial Stress versus hoop strain for specimen B2C1L3M separated by location.

(a) left 90°. (b) middle 180°. (c) right 90°.



(c)

Figure 6.22 Continued

6.4.2.2 B2C2L3M

Results from specimen B1C3L3B are shown in Figure 6.23. Gages 0, 3 and 4 showed a different stress-strain curve than the rest of the gages. Gage 3 measured the lowest strain, this may be because this gage is located in the middle and as shown in previous specimens, the middle layer is receiving the less amount of strain. Gages 1, 3, 5 and 7 engaged around the same time (3000 psi). Gages 2, 6 and 8 engaged at around 2100 psi and gages 0 and 4 had a lower stiffness in the initial linear region and the FRP wrap at these locations on the interior layer engaged at around 5000 psi.

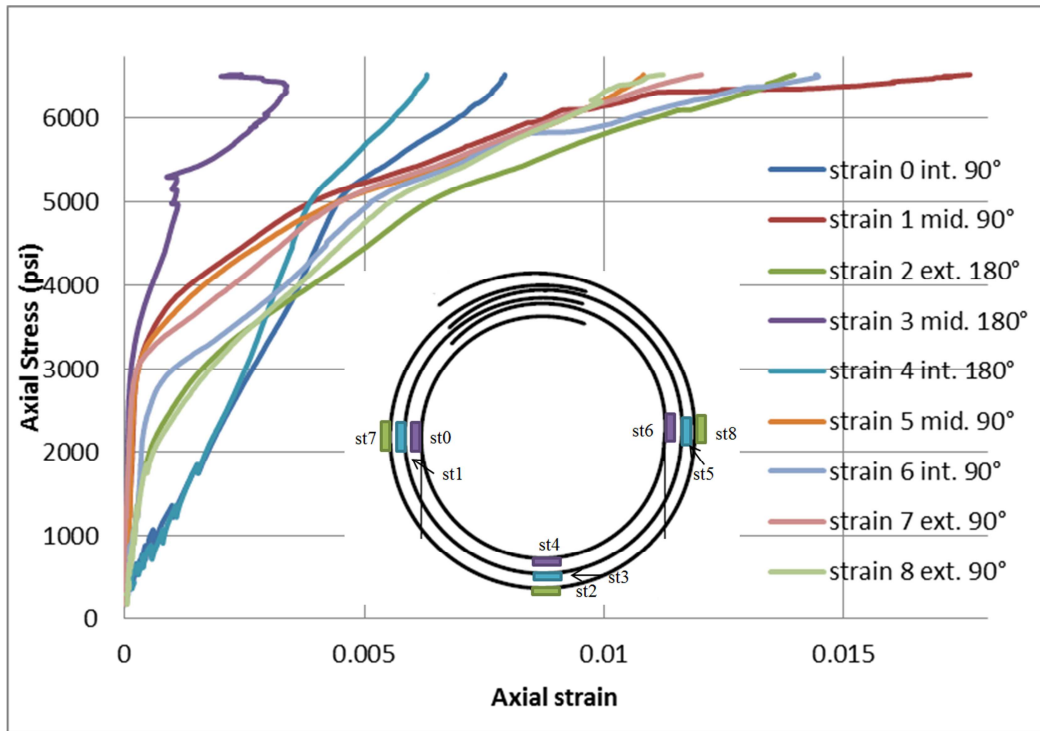
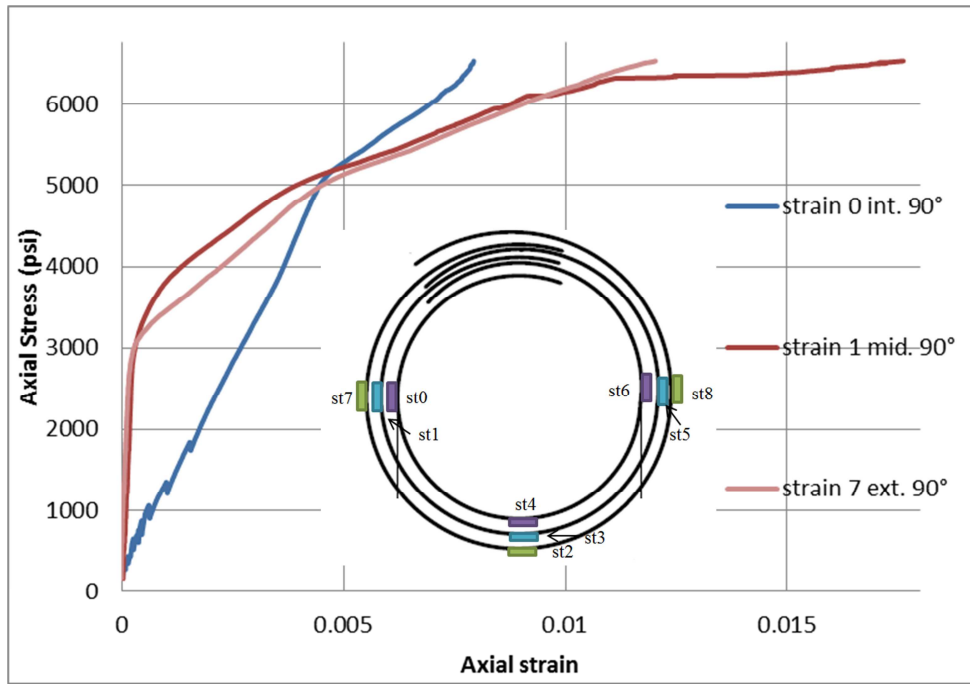


Figure 6.23 Axial Stress versus hoop strain for specimen B2C2L3M

Figure 6.24 shows the values of axial stress versus hoop strain separated by location. Figure 6.24(a) shows the axial stress versus the hoop strain of the strains located on the left side. The middle and exterior gages showed almost the same stress-strain curve although the middle gage recorded highest final tensile strain values. Strain gage 0 showed a very different stress-strain curve even though it wasn't located near the failure zone, in the first part is receiving more strain than the other gages and the line is steeper than the lines for the other two gages; then, when the GFRP jacket engaged, it showed a softer shift. Figure 6.24(b) shows very different shapes for each of the gages. The exterior layer exhibited the highest final strain values. The middle gage (strain 3) measured the lowest strain values and as observed before is becoming a trend. It is clearly observed that neither of these gages shared strain in equal proportion, strain 2 (exterior) exhibited the typical stress-strain curve and strain 3 and 4 exhibited a similar stress-strain

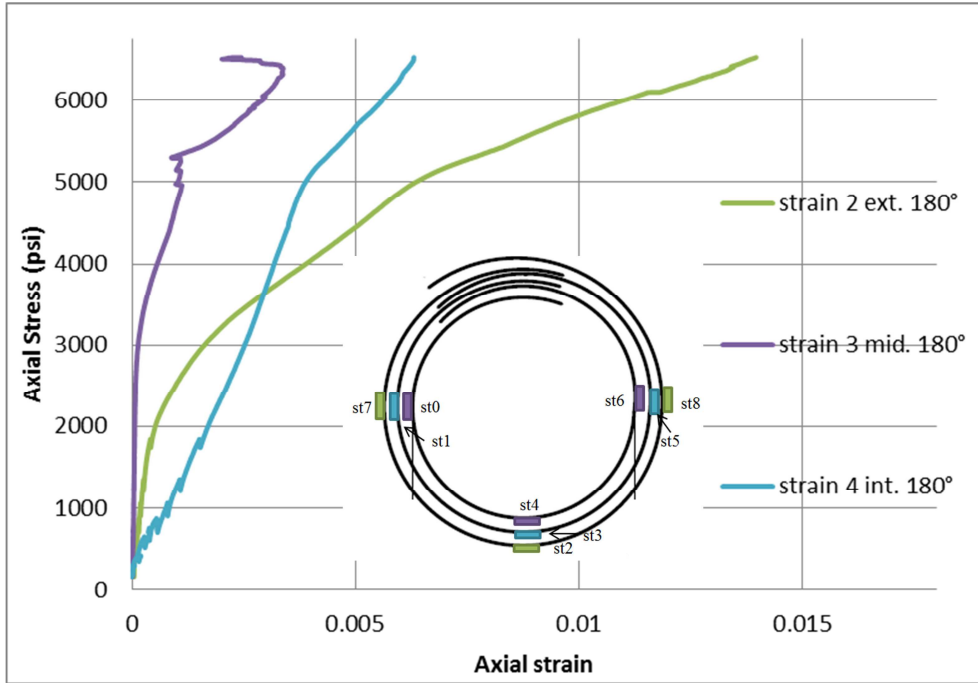
curve but not at the same level of strain. In Figure 6.24(c) the gages showed a similar behavior up until the GFRP jacket engages at around 2000 psi for the exterior gage. The interior gage measured the highest strain values at the end but the other two gages were close to each other. Again the middle layer measured the lowest strain.



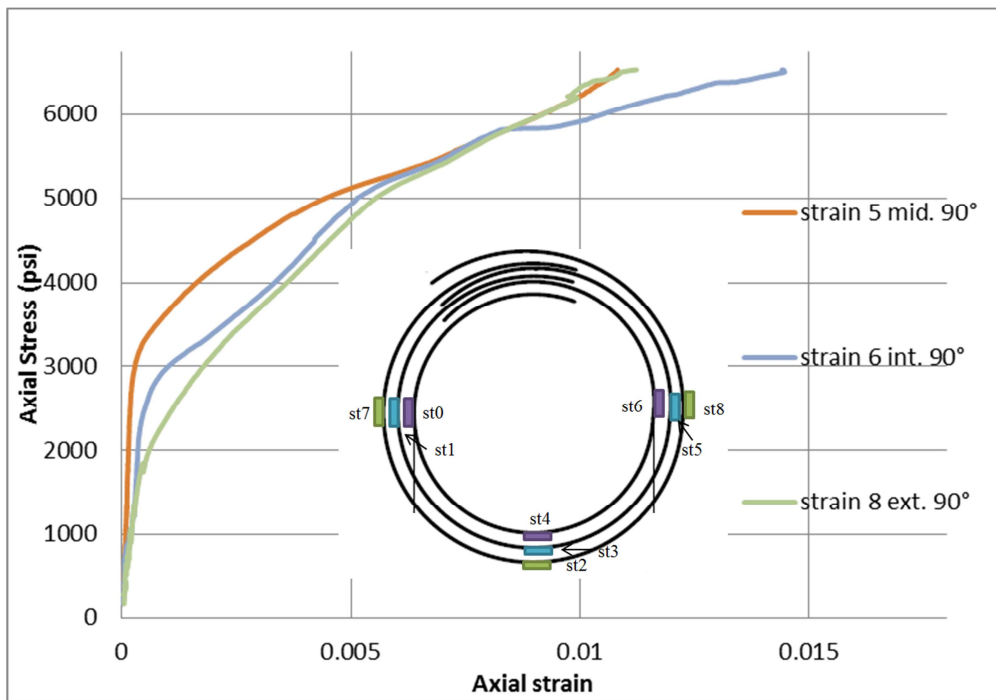
(a)

Figure 6.24 Axial Stress versus hoop strain for specimen B2C2L3M separated by location.

(a) left 90°. (b) middle 180°. (c) right 90°.



(b)



(c)

Figure 6.24 Continued

6.4.2.3 B2C3L3M

Results from specimen B2C3L3M are shown in Figure 6.25. Gages 2 and 4 are not shown because they didn't record adequate strains. All the gages except for gage 6, exhibited the same behavior until the unconfined concrete strength was reached at around 4000 psi. The highest recorded strain value was from gage 8. Gages 0 and 1 lost some tensile strain. The FRP wrap at gage 1 lost strain around 5100 psi but then it recovered the lost strain and gage 0 measured a strain loss at the time of failure.

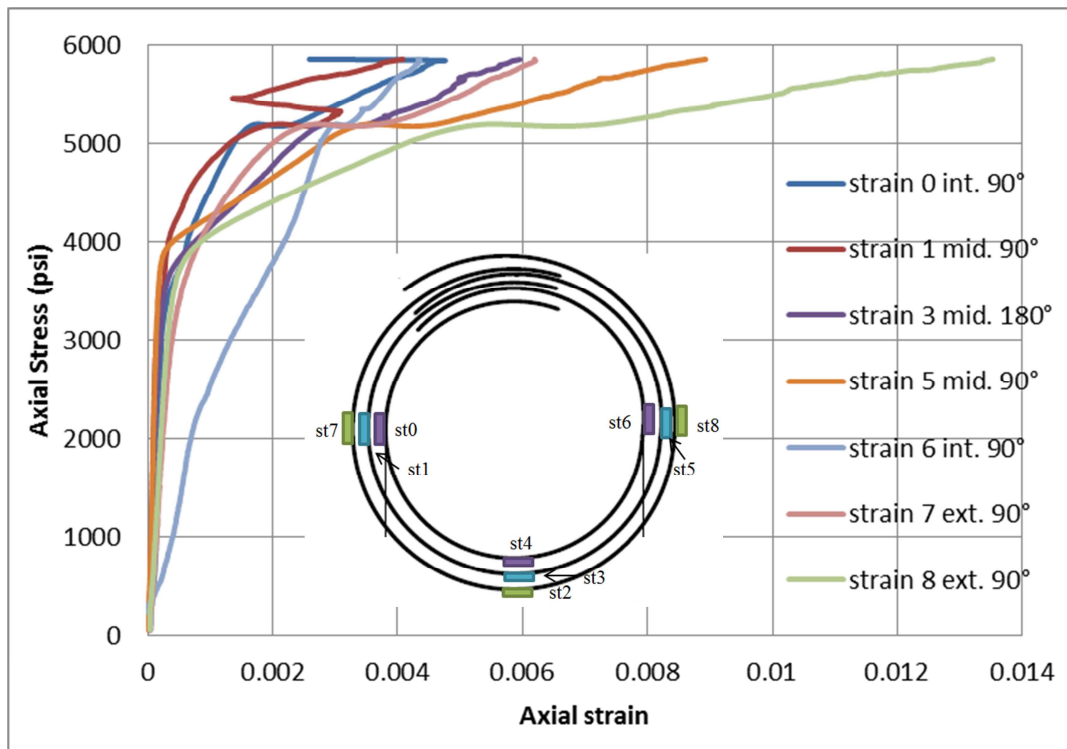
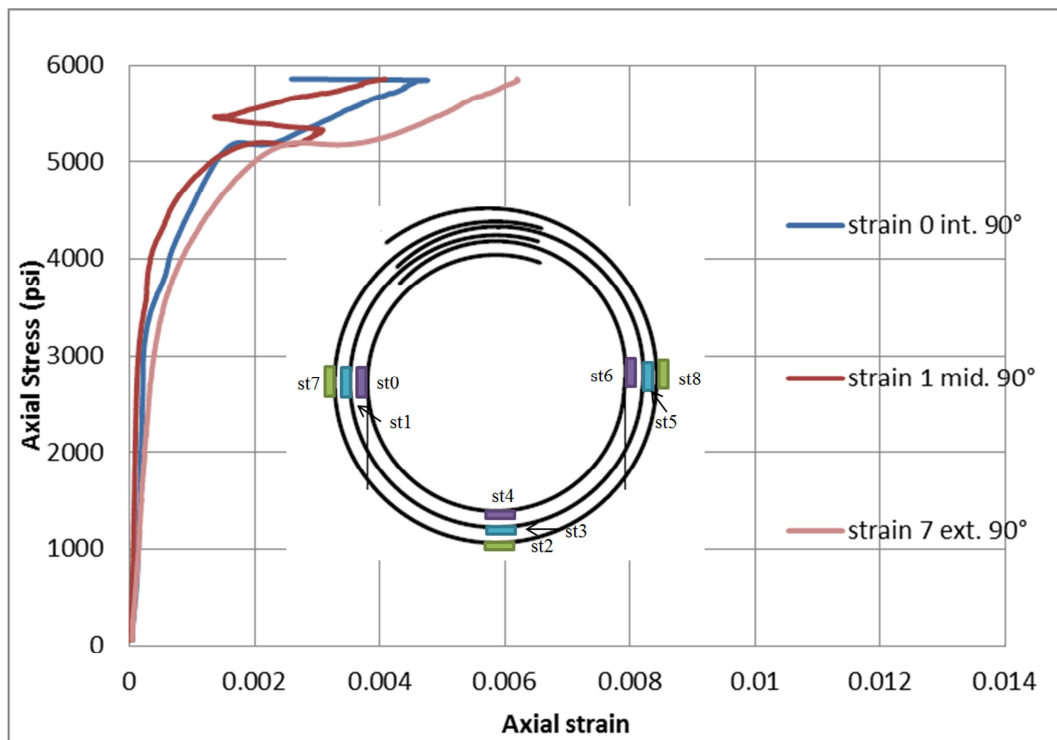


Figure 6.25 Axial Stress versus hoop strain for specimen B1C3L2B

Figure 6.26 shows the values of axial stress versus hoop strain separated by location. In Figure 6.26(a) it can be observed that the stress-strain curves were almost the same until around 5100 psi, whereupon strain gage 1 lost some strain. The exterior gage measured the highest final tensile strain. Figure 6.26(b) shows strain gage 3, as mentioned earlier strain gages 2 and 4 are not shown. Compared to the previous set of gages, the GFRP

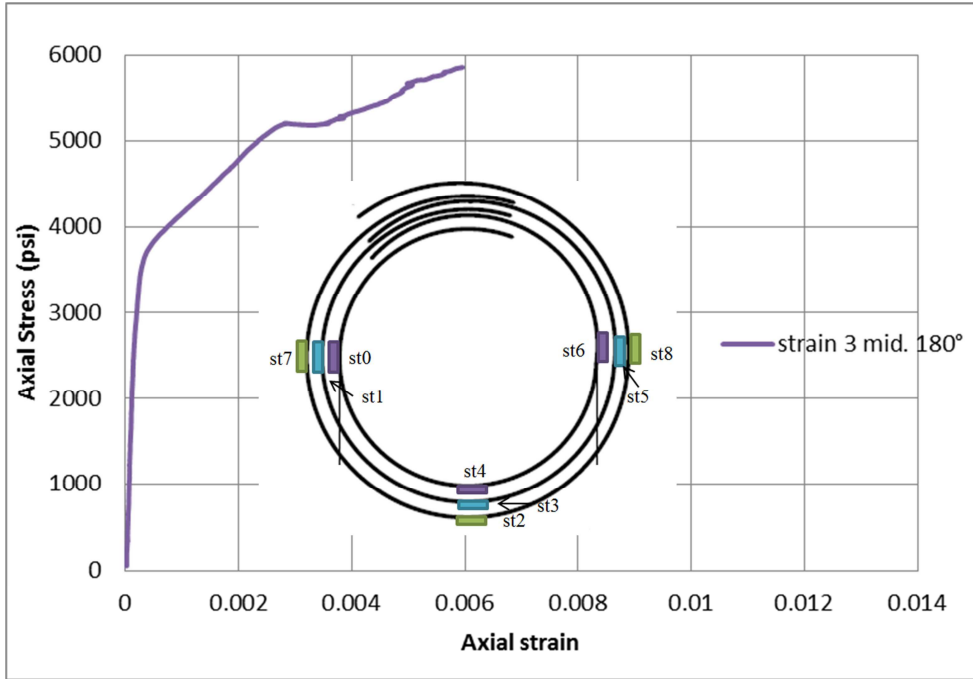
jacket engaged earlier at around 3900 psi. The trend repeated again in Figure 6.26(c), the exterior layer measured greater strain than the other two gages. Strain gage 5 and 8 behaved similarly but gage 6 had a different stress-strain curve. At the beginning of the test gage 6 had a low stiffness and therefore measured greater strain values in the first part of the curve.



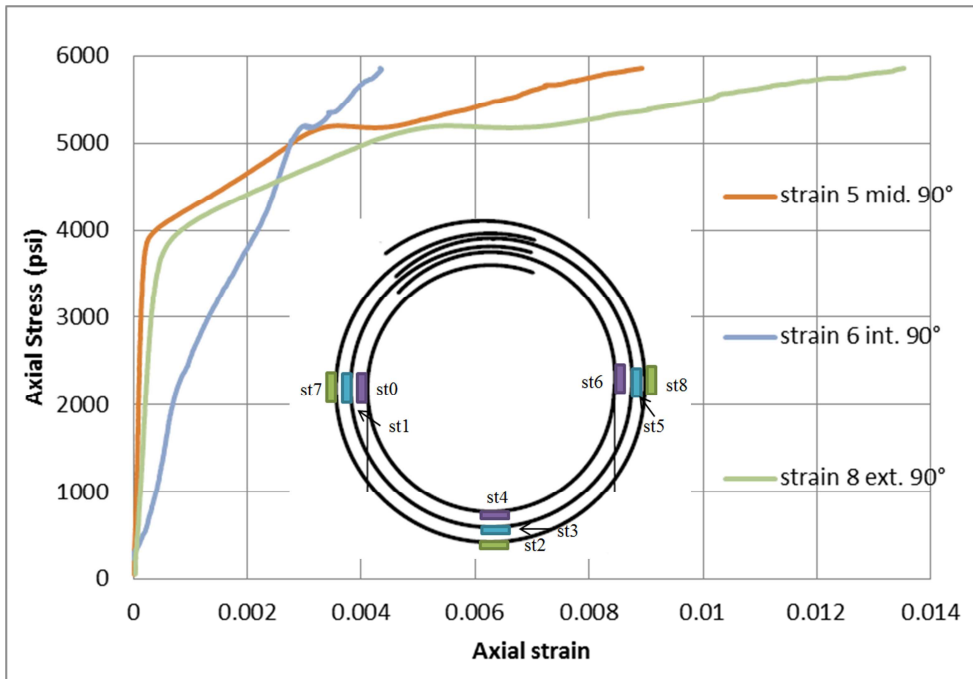
(a)

Figure 6.26 Axial Stress versus hoop strain for specimen B1C3L2B separated by location.

(a) left 90°. (b) middle 180°. (c) right 90°.



(b)



(c)

Figure 6.26 Continued

6.4.3 Summary of GFRP-Confined Concrete Cylinders with Three Layers

Section 6.4 discussed the test results for GFRP-confined concrete cylinders with three layers. Specimens with bidirectional GFRP wraps with three layers exhibited a similar trend where most of the specimens showed the exterior layer gaining greater tensile strains and thus had a lower stiffness and thus had a lower stiffness versus the interior and middle layers. The interior and middle layers typically measured similar strain values which indicated these layers had a similar stiffness. For most of the gages, the middle layers had the lowest tensile strain values. The exterior layer behaved more independently, suggesting that similar strain is shared between the closest layers to the concrete. This hypothesis needs to be verified with more three layer specimens and as well as with specimens that have more than three layers to support the theory. One of the sets (three gages with a location in the interior, middle, and exterior) showed the opposite behavior where the interior layer had greater strain values than the other two layers indicating the interior layer had the lowest stiffness, which was similar to what was observed for the bidirectional GFRP-confined concrete cylinders with two layers.

The three-layer specimens with multidirectional GFRP wraps exhibited the same trend as the bidirectional wraps. The exterior layer measured higher total tensile strain values than the interior and middle layers, which indicates that the exterior layer had the lowest stiffness. This trend suggests that for different types of GFRP fibers wrapped with three layers the fabric wraps behavior differences due to fabric may be mitigated and thus the specimens exhibited similar behavior and stress-strain curves. Additionally, as what happened in the bidirectional fabric, a couple of the gage sets measured the interior or

middle layer with higher total tensile strain values compared to the exterior layer, which indicate the exterior had the greatest stiffness at these locations.

6.5 Summary of FRP-Confined Concrete Cylinder Results

In this chapter a discussion of the test results for the share of strain of GFRP-confined concrete cylinders was made. Results from bidirectional and multidirectional GFRP wraps with one, two and three layers were reported and discussed.

Section 6.3 discussed the results for GFRP-confined concrete cylinders with two layers. Specimens with bidirectional GFRP wraps exhibited a consistent trend where the exterior layer exhibited a greater stiffness as measured by accumulating less total tensile strain than the interior layer. Specimens with multidirectional GFRP wraps, however, exhibited the opposite trend versus the bidirectional wraps. The interior layer exhibited a higher stiffness as indicated by measuring less total tensile strain than the exterior layer. This difference in behavior between different GFRP wraps appears to be a result of the direction of the fabric.

Section 6.4 discussed the test results for GFRP-confined concrete cylinders with three layers. Specimens with bidirectional and multidirectional GFRP wraps with three layers exhibited a similar trend regardless of fabric fiber weave, where most of the specimens showed the exterior layer exhibiting the lowest stiffness as it measured greater strains versus the interior and middle layers. The interior and middle layers exhibited similar stiffness as these layers measured similar total tensile strain values. For most of the gage sets, however, the middle layer had the lowest total tensile strain indicating some difference in interlayer stiffness. This consistent trend suggests that, differing from

what was observed for GFRP specimens with two layers, for different types of GFRP fibers once the specimen has been wrapped with three layers the fabric wraps exhibited similar behavior and stress-strain curves.

CHAPTER 7

CONCLUSIONS AND RECOMMENDATIONS

7.1 Summary of Research

For this thesis, an assessment of the current ACI 440.2R-08 design guidelines and an evaluation of hoop strain in GFRP-confined concrete were studied. An extensive database of GFRP and CFRP-confined concrete cylinders was compiled to evaluate the effectiveness of the ACI 440.2R-08 design guidelines to predict the confined concrete compressive strength in plain concrete cylinders strengthened by GFRP and CFRP wraps. In addition, GFRP-confined concrete cylinders compression tests were carried out to evaluate the share of hoop strain between different GFRP layers. GFRP-confined concrete cylinders were wrapped with one, two or three layers and two different kinds of GFRP were used: bidirectional and multidirectional. This chapter presents the conclusions reached in this study, and recommendations for further research.

7.1.1 Evaluation of ACI Design Guidelines

The confined concrete compressive strength, $f'_{cc \text{ predicted}}$, from Equation 2.2 was compared to the measured confined concrete strength, $f'_{cc \text{ measured}}$, from the database. For GFRP confined specimens it was shown that the current guideline Equation is unconservative over one third of the time and, therefore, it is not safe to use this Equation for designing GFRP-confined concrete cylinders. Additionally, the predicted confinement pressure, $f_l \text{ predicted}$, from Equation 2.3 was compared to the measured contribution of the GFRP jacket confinement, $f_l \text{ measured}$, in order to develop a better

design formula. With this comparison it was shown that Equation 2.3 fairly accurately predicts the additional capacity from GFRP jacket confinement. Therefore, for GFRP-confined concrete, the unconservativeness of Equation 2.2 appeared to be due to the factor of 3.3 in the design formula.

Equation 2.2 was then modified to replace the factor of 3.3 by a factor of 1.0 to develop a safer formula for design use in predicting f'_{cc} . This change resulted in the revised formula, Equation 5.1. The author urges the prompt integration of this modification into the current ACI design guidelines specifically for GFRP confined concrete so that design engineers following these guidelines produce safe and conservative structures.

The same procedure was used to evaluate the database for CFRP-confined concrete specimens. The confined concrete compressive strength, $f'_{cc \text{ predicted}}$, from Equation 2.2 was compared to the measured confined concrete strength, $f'_{cc \text{ measured}}$, from the database. For CFRP confined specimens it was shown that the current guideline Equation is conservative for 82% of the specimens, a higher percentage than for GFRP confined specimens. Also, as done with the GFRP confined specimens, the predicted confinement pressure, $f_l \text{ predicted}$, from Equation 2.3 was compared to the measured contribution of the GFRP jacket confinement, $f_l \text{ measured}$, in order to develop a better design formula. It was shown again that Equation 2.3 fairly accurately predicts the additional capacity from GFRP jacket confinement. The unconservativeness of $f_l =$

$$\frac{2E_f n t_f \varepsilon_{fe}}{D}$$

Equation Equation 2.3 again appeared to be due to the

factor of 3.3 in the design formula. Table 5.2 shows different factors and their percentage of conservative values. The author leaves it to the design professional to make the best

judgment and use the factor that best suits for the project. The author believes that using a 0.75 factor gives a good percentage of conservative values (93%) which is around the same percentage that GFRP confined specimens have with their 1.0 factor (94%) in Table 5.1. It is important to note that carbon and glass fibers should be treated separately and the design professional should use a different factor depending on the type of fiber. Additionally, Table 5.4 was presented for different modified reduction factors without changing the formula currently used as the ACI guidelines. For CFRP-confined specimens a modified reduction factor of 0.85 gives the same percentage of conservative values as Equation 5.3. These factors are just another option that design professionals can use if they do not feel comfortable using the new proposed formulas.

7.1.2 Evaluation of FRP-Confined Concrete Cylinders

For evaluating the share of hoop strain between different number of GFRP layers the results for each set GFRP-confined concrete cylinders were discussed. Specimens with bidirectional GFRP wraps with two layers exhibited a consistent trend where the exterior layer exhibited a greater stiffness as measured by accumulating less total tensile strain than the interior layer. Specimens with multidirectional GFRP wraps with two layers, however, exhibited the opposite trend versus the bidirectional wraps. For this fabric type the interior layer exhibited a higher stiffness as indicated by measuring less total tensile strain than the exterior layer. This difference in behavior between different GFRP wraps appears to be a result of the direction of the fabric. Specimens with bidirectional and multidirectional GFRP wraps with three layers exhibited a similar trend regardless of fabric fiber weave, where most of the specimens showed the exterior layer

exhibiting the lowest stiffness as it measured greater strains versus the interior and middle layers. The interior and middle layers exhibited similar stiffness as these layers measured similar total tensile strain values. For most of the gage sets, however, the middle layer had the lowest total tensile strain indicating some difference in interlayer stiffness. This consistent trend suggests that, differing from what was observed for GFRP specimens with two layers, for different types of GFRP fibers once the specimen has been wrapped with three layers the fabric wraps exhibited similar behavior and stress-strain curves. Future research needs to verify the last finding with additional three layer GFRP confined specimens with different fiber direction.

7.2 Conclusions

The key findings from this research are:

- The Equation from the ACI design guidelines for predicting the FRP-confined compressive strength is unconservative for both GFRP- and CFRP-confined specimens. This formula's unconservativeness results from the 3.3 factor. The safety of the ACI design guidelines formula for predicting the maximum confined compressive strength was improved by suggesting two new Equations, one for GFRP-confined specimens and another one for CFRP-confined specimens. The conservativeness of the design formula was improved to a 94% for the GFRP-confined specimens and to a 93% for the CFRP-confined specimens.
- Strain was not equally distributed between different numbers of GFRP layers in a single wrap. The strain amongst the GFRP layers was shared fairly equally only at the beginning of the compression test, when the concrete strength was dominating

specimen performance. When the GFRP jackets activated, as the specimens reached the unconfined concrete strength, the strain values separated and exhibited different final strain measurements. This unequal distribution of strain may be one of the reasons why FRP jackets do not achieve the same tensile strengths before failure as are predicted by results from coupon tests.

- Strain was shared differently between GFRP-confined concrete cylinders with two layers versus how the strain was shared in specimens with three layers. For the bidirectional GFRP-confined cylinders with two layers, the exterior layers exhibited greater stiffness than the interior layers. As such, they consistently had the lowest total tensile strain measurements. The multidirectional fiber showed the opposite behavior, with the interior layers having the greater stiffness so they had the lowest strain measurements. The specimens with three layers exhibited a different trend than the ones with two layers because for both bidirectional and multidirectional fibers, the exterior layer had the lower stiffness and hence measured the highest strains. These varying trends of strain sharing based on the number of layers or type of fabric may also be a reasons why FRP jackets do not achieve the same tensile strengths before failure as are predicted by results from coupon tests.

7.3 Recommendations for Future Work

The author recommends further testing to develop a model appropriate for the design of GFRP-confined high strength concrete. Also, a standardized testing technique for confined concrete needs to be developed in order to prevent errors in hoop strain

readings as cited by Teng et. al 2009 as sources of test result variation. This standardization should lead to the development of a more reliable database that should be examined to further revise the design guidelines. This standardized testing will also produce more reliable hoop strains readings. Hence, creating a better understanding of the strain behavior in FRP confined specimens and leading to the development of better maximum tensile strength predictions of the FRP when placed in the confined system.

REFERENCES

- American Concrete Institute. (2014). *The ACI Manual of Concrete Practice*. Farmington Hills, NI: American Concrete Institute.
- Arduini, M., Di Tommaso, A., Manfroni, O., Ferrari, S., & Romagnolo, M. (1999). Il confinamento passivo di elementi compressi in calcestruzzo con fogli di materiale composito. *Industria Italiana del Cemento*, 836-841.
- Berthet, J.F., Ferrier, E., & Hamelin, P. (2005). Compressive Behavior of Concrete Externally Confined by Composite Jackets. Part A: Experimental Study. *Construction and Building Materials*, 19, 223-232.
- Bouchelaghem, H., Bezazi, A., and Scarpa, F. (2011). Compressive behaviour of concrete cylindrical FRP-confined columns subjected to a new sequential loading technique. *Composites: Part B*, 42, 1987-1993.
- Campione, G., and Miraglia, N., "Strength and Strain Capacities of Concrete Compression Members Reinforced with FRP," *Cement and Concrete Composites*, V. 25, 2003, pp. 31-41.
- Chastre, C., and Silva, M.A.G. (2010). Monotonic axial behavior and modelling of RC circular columns confined with CFRP. *Engineering Structures*, 32, 2268-2277.
- Faella, C., Realfonzo, R., & Salerno, N. (2004, January). Sulla resistenza e deformazione di elementi in c.a. confinati con tessuti in FRP. In: *Proc. of the XI National Congress L'ingegneria Sismica in Italia*. Genova.
- Gharachorlou, A., & Ramezani pour, A.A. (2010, December). Durability of Concrete Cylinder Specimens Strengthened With FRP Laminates under Penetration of Chloride Ions. *International Journal of Civil Engineering*, 8(4), 327-336.

- Harries, K.A., Kestner, J., Pessiki, S., Sause, R. & Ricles, J. (1998). Axial behavior of reinforced concrete columns retrofit with FRPC jacket. Proceedings from ICCI '98: *Second International Conference on Composites in Infrastructure*. Tucson, AZ.
- Harries, K.A., & Kharel, G. (2003, June). Experimental investigation of the behavior of variably confined concrete. *Cement and Concrete Research*, 33(6), 873–880.
- Harries, K.A., and Carey, S.A., “Shape and Gap Effects on the Behavior of Variably Confined Concrete,” *Cement and Concrete Research*, V. 33, 2003, pp. 881–890.
- Hollaway, L.C., (2010). A Review of the Present and Future Utilization of FRP Composites in the Civil Infrastructure with Reference to their Important In-Service Properties. *Construction and Building Materials*, 24, 2419-2445.
- Karbhari, V., & Gao, Y. (1997). Composite Jacketed Concrete under Uniaxial Compression—Verification of Simple Design Equations. *Journal of Materials in Civil Engineering*, 9(4), 185–193.
- Karbhari, V.M., & Howie, I. (1997). Effect of Composite Wrap Architecture on Strengthening of Concrete Due to Confinement: II-Strain and Damage Effects. *Journal of Reinforced Plastics and Composites*, 16(11), 1039-1063.
- Karbhari, V.M., Rivera, J., & Dutta, P.K. (2000, November). Effect of Short-Term Freeze-Thaw Cycling on Composite Confined Concrete. *Journal of Composites for Construction*, 4(4), 191-197.
- Karbhari, V.M. (2002, February). Response of Fiber Reinforced Polymer Confined Concrete Exposed to Freeze and Freeze-Thaw Regimes. *Journal of Composites for Construction*, 6(1), 35-40.

- Lam, L., & Teng, J. (2003). Design-oriented stress-strain model for FRP-confined concrete. *Construction and Building Materials*, 17, 471-489.
- Lam, L., and Teng, J., "Ultimate Condition of Fiber Reinforced Polymer-Confined Concrete," *ASCE Journal of Composites for Construction J. Compos.*, V.8, No. 6, 2004, 539–548.
- Li, G. (2006, June). Experimental study of FRP confined concrete cylinders. *Engineering Structures*, 28(7), 1001-1008.
- Li, S.Q., Chen, J.F., Yu, T. and Teng, J. G, "Non-uniform stress distribution in FRP-wrapped circular concrete columns under uniform axial deformation," Sixth International Conference on FRP Composites in Civil Engineering, 2012, pp. 1-8.
- Lin, H.J., & Liao, C.I. (2004, August). Compressive strength of reinforced concrete column confined by composite material. *Composite Structures*, 65(2), 239-250.
- Micelli, F., and Modarelli, R. (2013). Experimental and Analytical Study on Properties Affecting the Behaviour of FRP-confined Concrete. *Composites: Part B*, 45, 1420-1431.
- Modarelli, R., Micelli, F., & Manni, O. (2005). SP-230-58: FRP-Confinement of Hollow Concrete Cylinder and Prisms. *ACI Special Publications*, 230(2), 1029-1046.
- Nanni, A., & Bradford, N.M. (1995). FRP Jacketed Concrete Under Uniaxial Compression. *Construction and Building Materials*, 9(2), 115-124.
- Ozbakkaloglu, T., & Lim, J.C. (2013, December). Axial Compressive Behavior of FRP-Confined Concrete: Experimental Test Database and a New Design-Oriented Model. *Composites Part B: Engineering*, 55, 607-634.

- Ozbakkaloglu, T., and Akin, E. (2012, August). Behavior of FRP-Confined Normal- and High-Strength Concrete under Cyclic Axial Compression. *Journal of Composites for Construction*, 16(4), 451-463.
- Pessiki, S., Harries, K.A., Kestner, J., Sause, R., and Ricles, J.M., “Axial Behavior of Reinforced Concrete Columns Confined with FRP Jackets”, *ASCE J. Compos. Constr.*, V. 5 , No. 4, 2001, pp. 237–245.
- Ramezaniapour, A. A., & Gharachorlou, A. (2009). Fracture optimization of RC beams strengthened with CFRP laminates with finite element and experimental methods.
- Realfonzo, R. & Napoli, A. (2011, June). Concrete Confined by FRP Systems: Confinement Efficiency and Design Strength Models. *Composites Part B: Engineering*, 42(4), 736-755.
- Sadeghian, P., Shekari, A.H., & Mousavi, F. (2008). Stress and Strain Behavior of Slender Concrete Columns Retrofitted with CFRP Composites. *Journal of Reinforced Plastics and Composites*, 28, 2387-2396.
- Saafi, M., Toutanji, H., & Li, Z. (1999). Behavior of concrete columns confined with fiber reinforced polymer tubes. *ACI Materials Journal*, 96(4), 500-509.
- Teng, J., Jiang, T., Lam, L., & Luo, Y.Z. (2009, August). Refinement of a Design-Oriented Stress-Strain Model for FRP-Confined Concrete. *ASCE Journal of Composites for Construction*, 13(4), 269-278.
- Toutanji, H., & Balaguru, P. (1998, February). Durability Characteristics of Concrete Columns Wrapped with FRP Tow Sheets. *Journal of Materials in Civil Engineering*, 10(1), 52-57.

- Toutanji, H.A. (1999). Durability of concrete columns confined with advanced composite materials,” *Composite Structures*, 44, 155-161.
- Weaver, A. (1999). Composites: Worldwide Markets and Opportunities. *Materials Today*. Retrieved from: <http://www.materialstoday.com/>
- Wu, G., Wu, Z. S., Lu, Z. T., & Ando, Y. B. (2008, June). Structural Performance of Concrete Confined with Hybrid FRP Composites. *Journal of Reinforced Plastics and Composites*.
- Xiao, Y., & Wu, H. (2000, May). Compressive Behavior of Concrete Confined by Carbon Fiber Composite Jackets. *Journal of Materials in Civil Engineering*, 12(2), 139–146.